SpinScope

Monitoring Bearing Health

Table of Contents

This project is made in collaboration with:

Funding:

INDUSTRIENS FOND

Executive Summary

DAMRC has identified an opportunity to potentially add value to Danish industry by evaluating and developing existing preventative maintenance technologies that diagnose machine spindles and bearings. The technologies currently available at DAMRC are SpinScope and SmartMeter. SpinScope is a program within the MetalMax family of software used for general data acquisition having additional sub-modules applicable to bearing and spindle diagnostics. SmartMeter is a handheld device developed specifically for measuring and diagnosing vibrations in rotating machinery. The objective of the SpinScope project is to evaluate these technologies and determine if they can be incorporated into a viable business case, with the expectation that at least one of these technologies can correctly detect differences in bearing condition and that there is a 90% consistency rate in data obtained from each machine tested.

Initial assessments of these technologies indicated that the capabilities of SmartMeter and SpinScope were severely constrained. It was found that while SmartMeter was technically ready for use in industry, the available options for signal processing and data sampling were severely limited. SpinScope, on the other hand, could only be used for general data acquisition and that diagnostic capabilities were blocked by licensing restrictions. It was therefore decided to continue the project focusing on developing and validating the analysis capabilities necessary to obtain meaningful diagnostic information from data measured with SpinScope. This work consisted of implementing spectral kurtosis and envelope spectrum analysis in python and validating these analysis methods in numerical simulations, empirical tests using a specially designed test rig, and a case study involving the DMU 80 T machining center at DAMRC.

These tests demonstrated that the augmented SpinScope software could reliably determine the condition of the bearing in the numerical simulations and custom test bench when comparing the resulting envelope spectra to expected fault frequencies. The results obtained from the custom test bench demonstrated that fault frequencies detected in the envelop spectra were consistent with theoretically expected fault frequencies, with the relative error between the theoretical and experimental results consistently having an upper bound of 3%. It was further found that these results improved with increasing accelerometer sensitivity.

However, performing the same type of diagnosis for real machine spindles is complicated if the bearing geometry is unknown. Diagnostics are also complicated by the potential for complex or distributed damage of the bearing and the need for more sophisticated signal processing methods to counteract, for example, the influence of other machine components on the resulting envelope spectrum or speed dependent dynamics. Furthermore, detecting bearing damage is only one part in providing a prognosis of the remaining useful life of a machine, which usually relies on collecting data over time to project trends into the future.

In the case study involving the DMU machining center, which has a history of heavy use, metrics were obtained potentially indicating bearing damage; however, these results have not been confirmed by inspection of the bearings themselves. The DMU case study demonstrated that identical test results could be consistently obtained for repeated trials with identical test conditions, but that the results (and therefore diagnostic information) varied as a function of spindle speed. These finding combined with the unknown status of the bearings in the DMU machining center

As a result of the activities of this project, nascent capabilities in bearing and spindle diagnostics were realized, and the infrastructure necessary to further mature this capability developed. The project can be considered a success as SpinScope augmented with envelope analysis met the success criteria of the project in both the numerical simulations and experiments with the custom test bench. However, additional testing is required to confirm that the success criteria were satisfied during the case study with the DMU. For this reason, as well as the fact that the infrastructure needed for further testing are already available, it is recommended to further advance these capabilities in a future R&D project. It is expected that the costs associated with a future project would be minimal due to the activities in the current project and that the potential benefits would be substantial.

1. Introduction

During the course of its business activities, DAMRC has received questions from industry about the possibility of applying tap test technology in the preventative maintenance of bearings. Currently, maintenance activities are typically done on a pre-defined schedule to prevent catastrophic failure without regard to the actual condition of the bearing. In this way, companies adopt an inefficient maintenance policy that has associated part, man-hour, and opportunity costs to avoid a more expensive outcome. With an estimated 60,000 CNC machines in the Nordic countries in 2020, there is an excellent opportunity for DAMRC to add value to clients and members by improving upon these inefficiencies in bearing maintenance. This can be done by expanding DAMRC's business offerings to include bearing diagnostics – determining the state of the bearings *in-situ* and predicting their effective lifespan to schedule maintenance activities more intelligently.

The objective of the SpinScope project is to evaluate technology possessed by DAMRC and apply it to bearing diagnostics if a feasible business case can be developed. DAMRC currently has two technologies that may be suitable for this purpose: SmartMeter and SpinScope. SpinScope is a program within the MetalMax family of software developed by Manufacturing Laboratories Inc. SpinScope is developed for general data acquisition and includes various modules tailored to specific applications, including evaluating the condition of spindles and bearings. SmartMeter is a handheld device developed by Test Products International Inc. specifically for vibration analysis and bearing condition monitoring. SmartMeter is used in conjunction with Vibtrend, an analysis software developed by the same company.

To advance the project, the status and features of the two software programs are to be evaluated in a series of tests involving a custom experimental setup and CNC machines available at DAMRC, with pertinent insights disseminated through usual channels.

This report aims to outline the scope, activities, and findings of the project, including conclusions and recommendations arising from the evaluation of the two technologies. This report is organized as follows: first, an outline of the pre-analysis supporting the project and an overview of the technologies to be evaluated is given in section 2; the structure of the project, in terms of hypothesis to be tested, formal success criteria, scope of work, and risk assessment, are presented in sections 3 – 6; the findings of the literature study supporting the activities of the project are given in section 7; the description, design, and procedures of experiments are given in section 8, while the results of such tests are presented and discussed in section 9; a discussion of the project is given section 10, while concluding remarks and recommendations are given in section 11.

2. Pre-analysis

2.1 Pre-Analysis from Project Application

In the project application, it is noted that DAMRC on a few occasions has received questions from industry about tap testing bearings. Dialogue with machining venders also demonstrates interest in being able to service machinery earlier instead of relying on specialists after a catastrophic event. The documented pre-analysis indicates that it should be possible to detect issues pre-emptively by utilizing the tap test hammer and accelerometer with the modal analysis capabilities provided by the SpinScope software.

2.2 Theory of Operations

2.2.1 Machine Tool Spindle Units

Machine tool spindle units are sub-assemblies within CNC machining centres that are responsible for rotating the tool (milling, drilling etc.) or workpiece (turning) in subtractive manufacturing processes. A section view of a spindle

unit is shown in Figure 1. As can be seen in the figure, modern spindle units are motorized, consisting of an electric motor that drives a central, rotating shaft that is connected to the tool and tool holder. The motor consists of a rotor and stator that induces an electromotive force which rotates the shaft. The shaft is supported by bearings placed on either side of the motor, and internal, liquid-based cooling is used to prevent thermal deformation. There are often separate coolant systems for the motor, bearings, and shaft, as well as an inner coolant supply for the cutting process. An assembly drawing showing the spindle unit in the context of a CNC machining centre is shown in Figure 2 and a more detailed discussion of machine tool spindle units can be found in [1].

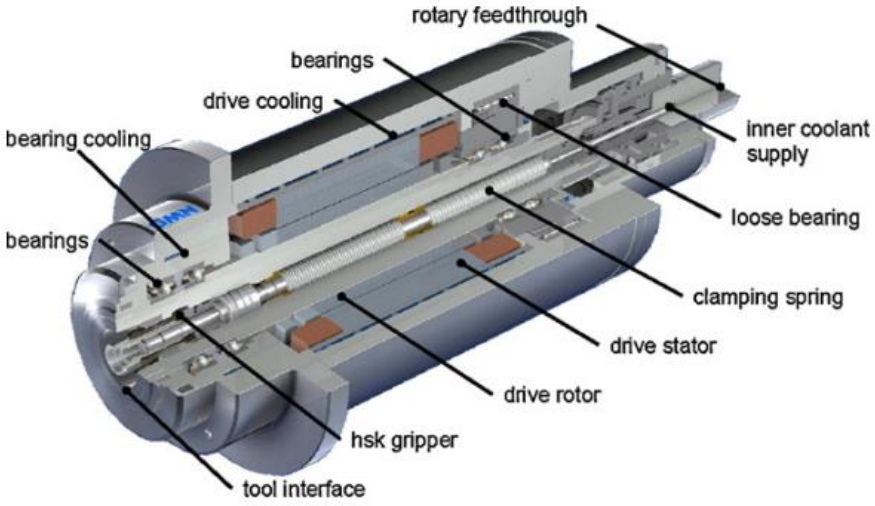

Figure 1: Section view of spindle unit [1].

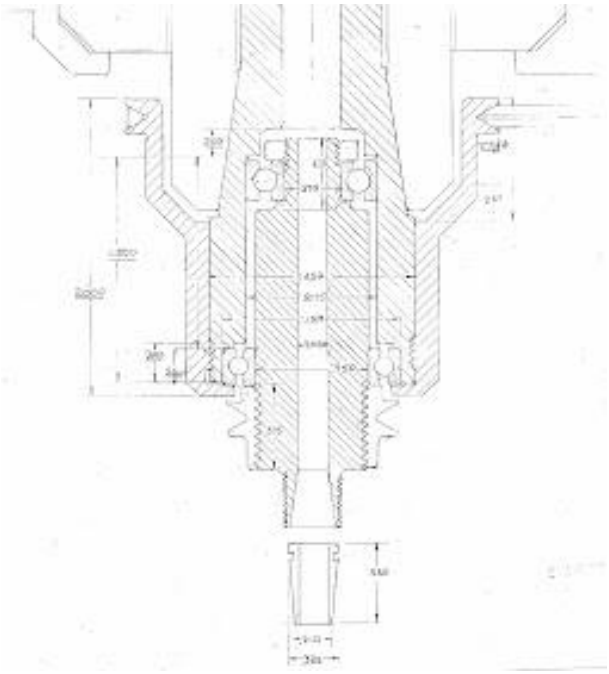

Figure 2: Assembly drawing of spindle unit [2]

2.2.2 SpinScope

SpinScope is a program within the MetalMax family of software developed by Manufacturing Laboratories Inc. SpinScope is developed for general data acquisition and includes various modules tailored to specific applications, including evaluating the condition of spindles and bearings.

After thoroughly testing the software for both the 32- and 64-bit Tap Test laptops, it was determined that the functionality of the SpinScope software (Figure 3) is severely limited by the software license possessed by DAMRC. With the current licenses, the 64-bit version of SpinScope is completely unusable, while for the 32-bit version of SpinScope all of the specialized modules, including spindle condition, are unusable so that it is only possible to use the software in “general data acquisition mode”. In general data acquisition, any transducer of choice is used with a data acquisition (DAQ) card to read measurement data into the PC in much the same way as is done for tap tests. The measured time-domain signal is provided by the software along with its frequency content. The software allows for four measurement channels to be used concurrently.

The software is capable of performing basic signal processing and generating advanced plots of the data, such as waterfall and short FFT plots, but does not perform any additional analysis. The signal processing capabilities are limited to numerical integration/differentiation of the measurement signal, and implementing predefined windowing functions and digital filters. The software does not provide any information about, for example, the condition of the bearing or spindle. Such knowledge must come from offline analysis of the data and expert knowledge.

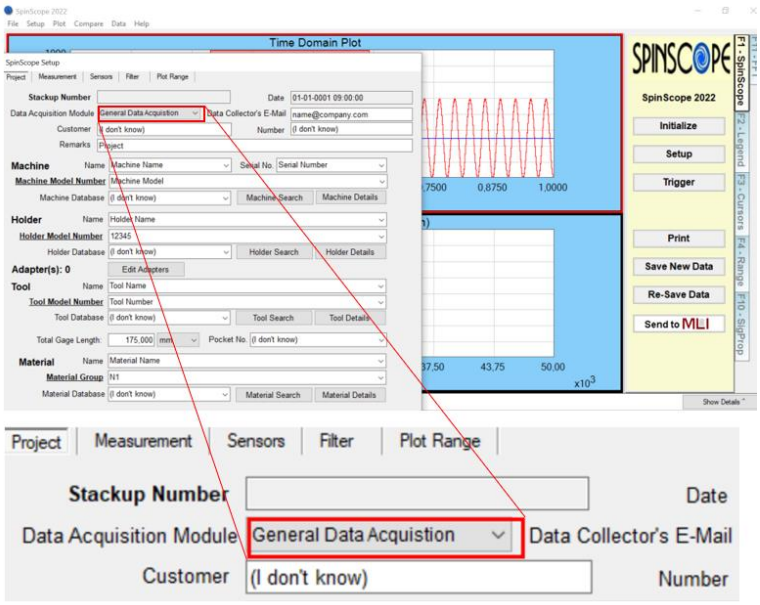

Figure 3: Setup window in the 64-bit SpinScope software. Licensing permitting, the data acquisition module could be changed to the more specific "Spindle Condition".

2.2.3 SmartMeter

SmartMeter is a handheld device for measuring vibrations in rotating machinery with an accelerometer and is used in conjunction with Vibtrend, an analysis software produced by Test Products International Inc. The SmartMeter device (Figure 4) is capable of measuring either peak-to-peak or RMS acceleration, velocity, and displacement data from measured vibrations, displaying the FFT of the measured vibrations, and presents vibration levels at integer multiples of the operating speed of the machine being tested. The SmartMeter also provides a metric for qualifying the severity of vibrations (referred to as Bearing Damage Units or ‘BDU’) and allows for vibration measurements to be uploaded to a PC for further analysis.

Bearing noise units or bearing damage units (BDU) is defined such that 100 BDU corresponds to 1g RMS vibration measured above 1 kHz, with higher quantities of BDU corresponding to a more damaged bearing. A commonly used heuristic is that 1 BDU is interpreted as a percentage of bearing wear, meaning the bearing is 100% worn or damaged and not usable at 100 BDU. The software also uses the measurement signal and the running speed of the motor to detect unbalance, misalignment, and looseness in the shaft. This is done by assigning the frequency band associated with the running speed of the motor and its harmonics to these faults, so that detecting a significant frequency

The Vibtrend software (Figure 5) developed by Test Products International Inc. facilitates the transfer of vibration measurements and allows for further analysis of the data. The Vibtrend software available to DAMRC is unlicensed; however, the free version of the software only limits the number of machines and the number of datapoints per machine that can be stored in the software concurrently. This is significant insofar as Vibtrend uses datapoints obtained from measurements taken over time (weeks, months) to project trends into the future and predict the remaining lifespan of the bearing. Otherwise, all of the features of the software are available. There does not appear to be a limit to how many workstations on which the software can be installed, and data can be exported and backed up to make room for additional machines.

The Vibtrend software provides some insight into the condition of the bearing and is able to extrapolate from existing trends to predict when the bearing will reach a critical status and what the state of the bearing will be at a specific point in time in the future. However, there is no option for numerical integration/differentiation or built in digital filters. While all of the features in Vibtrend are available for use, the ability to accurately predict the useful life of the bearing is limited by the number of datapoints that can be used concurrently in the free software. Another limitation is that the frequency content of signals obtained with the SmartMeter has a maximum resolution of 1.25 Hz, which may affect the quality of the measured data.

Figure 4: The SmartMeter from TPI Inc.

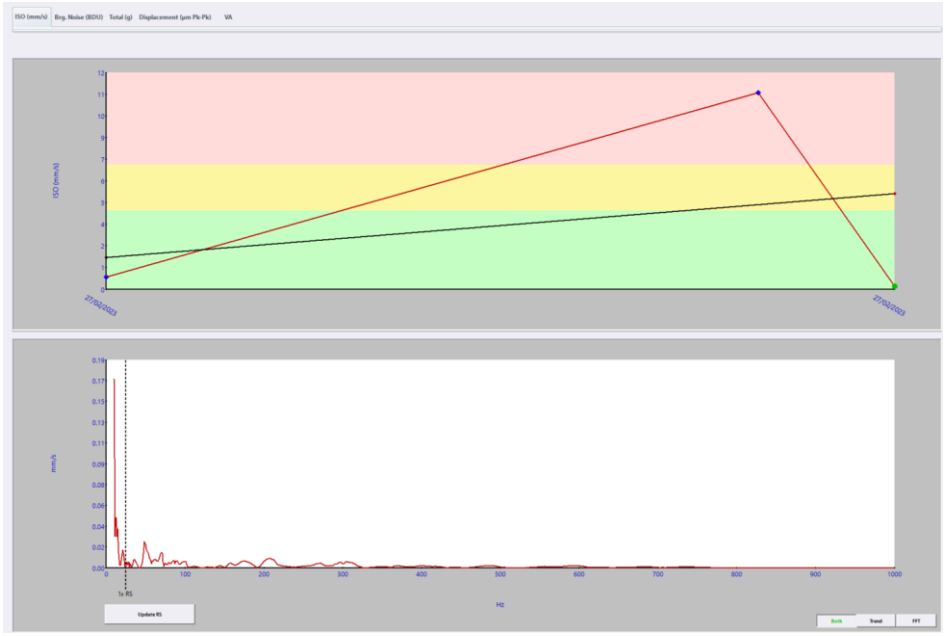

Figure 5: Representative window of the Vibtrend software. Top (red): time history of ISO (mm/s) alarm levels for the given machine with three discrete datapoints: top (black): linear trend line projected to the end of life of the bearing: bottom: frequency content of the selected datapoint in the top graph.

3. Hypothesis

The premise of the project is that SpinScope, included in the MetalMax suite of software, can be developed as a potential business offering to machining companies in Denmark for the purpose of detecting bearing faults in CNC spindles. The stated goal of the project is to test and evaluate the technologies detecting bearing damage currently available at DAMRC with regards to technical precision and value of insights for industry.

4. Success Criteria

The success criteria stated in the project application is:

- Minimum 1 of 2 tested bearing detection technologies (SpinScope and SmartMeter) can detect differences in wear in the bearings tested.
- 90% consistency in data for each machine tested (DMU80, Quaser, KUKA/Mazak QuickTurn + 2 case companies, etc.)

5. Project Scope/ description

The activities of the project are organized into 16 work packages, including one work package each for dissemination and project management activities. The remaining work packages involve preparing the bearing detection systems; testing the two systems on the KUKA robot and CNC-machines available at DAMRC; data analysis and report writing; evaluating the results of the first round of testing, the value of the corresponding insights, and the strength of the business case; testing the systems with and reporting to industrial partners.

According to the *Activity Plan* outlined in the project application, the scope of the project is limited to testing the bearing damage detection systems on the bearings and spindles in existing industrial robots and CNC machining centres. In other words, testing the bearing damage detection systems on custom experimental setups and running simulations or other theoretical work is outside the scope of the project. Similarly, the allocated "machining hours" are only for running CNC machining centres and industrial robots during testing and do not include any machining of parts or components to be used in testing. Project hours have been allocated for data analysis, but it is understood that the purpose of the project is test the bearing damage detection systems and these hours do not include the development of additional software or algorithms to augment the functionality of the systems to be tested.

6. Risk Analysis

To validate the data from the bearing damage detection systems, the data must be compared with expected results. This necessitates knowing the condition of the tested bearings beforehand and obtaining theoretical results that are independent of the SpinScope and SmartMeter systems. Testing the systems on "old" machines with suspected bearing damage is insufficient if the exact failure mode of the bearing, and therefore the expected result, is unknown. Without creating a purpose made experimental setup that would be outside the scope of the project, this would require acquiring an already-validated detection system from a third party (potentially rendering the current project moot) or disassembling machining centres to assess the condition of the bearings by visual inspection which is also outside the scope of the project besides being prohibitively expensive. Without such measures, there is a non-trivial risk that test results obtained with the incumbent bearing diagnosis technologies would lead to false negative or false positive results, or otherwise erroneous diagnoses.

It was determined during early testing of the bearing damage detection systems that the functionality of the SpinScope software is limited by its existing license. This means that while it can be used for general data acquisition in conjunction with offline analysis, it is currently unsuitable for online condition monitoring, for example during field visits to members' facilities. Similarly, the number of measurements, or data points, that can be used by the SmartMeter/Vibtrend system is limited by a restricted license. This reduces the robustness of the useful life predictions, which are based on obtaining data points to project trends into the future. These factors affecting SpinScope and SmartMeter present potential barriers and risks to the success of the project.

Moreover, practical constraints must be considered when conducting tests involving CNC machining centers, especially when utilizing these technologies for industry. For example, it must be possible to safely access the workspace in CNC machining centres during testing considering the length of the data cables used with SmartMeter and SpinScope. Furthermore, the following risks and uncertainties associated with the project have been identified in the project application:

- It is uncertain whether the CNC machines available at DAMRC's technology center is having dislocations in their bearings - why it will be uncertain if detection of abnormality can be detected. Therefore, tests will be made on both an old and a new CNC machine in order to see if any differences in the old and new bearings can be detected.
- Validity of the two bearing wear technologies to be tested

Additionally, it is expected that the safety risks associated with testing the bearing damage detection systems will be negligible as a physical safety barrier will be present between the workspace of the machine and the operator of the bearing test technologies. However, specific environment, health, and safety (EHS) assessments should be performed for each test as required.

7. Literature Study

7.1 Introduction to Literature Study

Rolling element bearings (REB) are used extensively in machine assemblies to support loads experienced by shafts while allowing relative motion between the rotating (shaft) and supporting (housing) components, as shown in Figure 6. Rolling-element bearings consist of an inner and outer race (or ring), the rolling elements themselves, and a cage (also known as a retainer). The rolling elements allow for low-friction relative motion between the outer and inner race while the cage maintains proper spacing between the rolling elements. The rolling elements themselves can have either a spherical or cylindrical geometry and may or may not be tapered. Rolling-element bearings can support radial or axial loads, or a combination of both, depending on the specific design of the bearing and its rolling elements. Different types of bearings are shown in Figure 7.

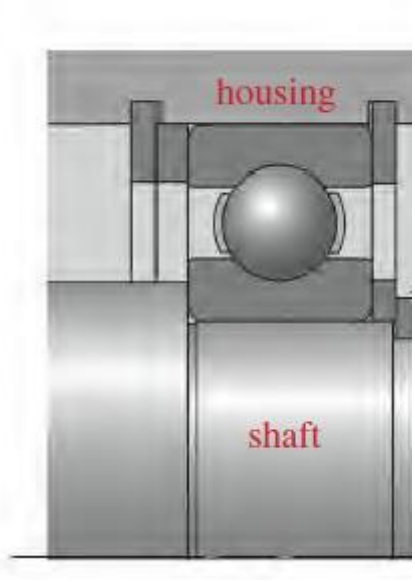

Figure 6: Detailed view of a REB in the context of a machine assembly. The inner race rotates with the shaft, while the outer race and housing do not. The rolling elements of the bearing allow for relative motion between the inner and outer races [3].

Rolling-element bearings are usually rated for a life span consisting of a number of hours of rotation at some design speed but sometimes fail prematurely due to a number of factors and failure modes. The defects that lead to failure may be localized or distributed about the circumference of the bearing depending on the nature of the defect and the load distribution. A sample load distribution is shown in Figure 8. Common failure modes include pitting, spalling or flaking of the bearing races or roller elements (due to cyclic loading and fatigue damage), corrosion and/or surface wear (due to foreign particles or liquids entering the contact area), plastic deformation (due to excessive loading when the bearing is stationary or rotating at low speeds), and brinelling (regularly spaced indentations over the whole raceway circumference due to excessive static/shock/vibration loads).

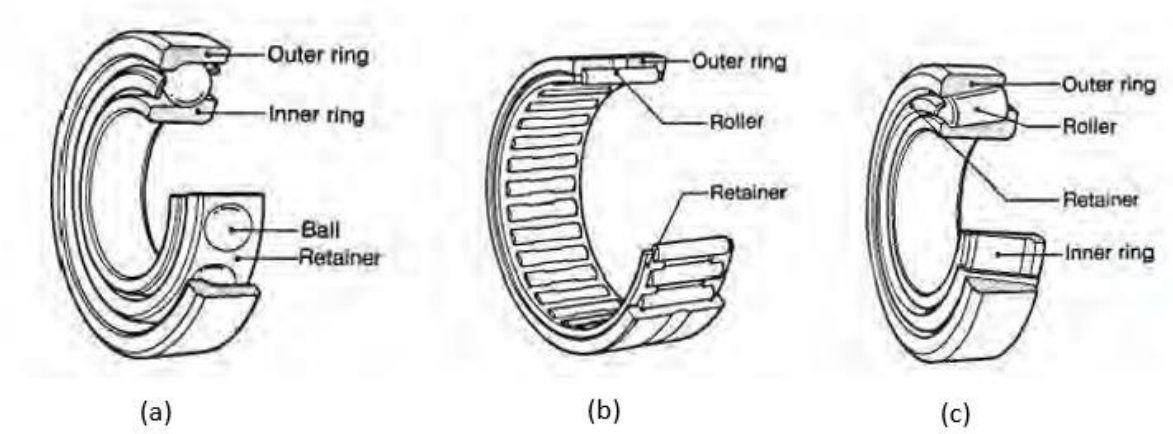

Figure 7: Different types of rolling-element bearings. (a) Angular contact ball bearings. (b) Needle roller bearings. (c) Tapered roller bearing [3].

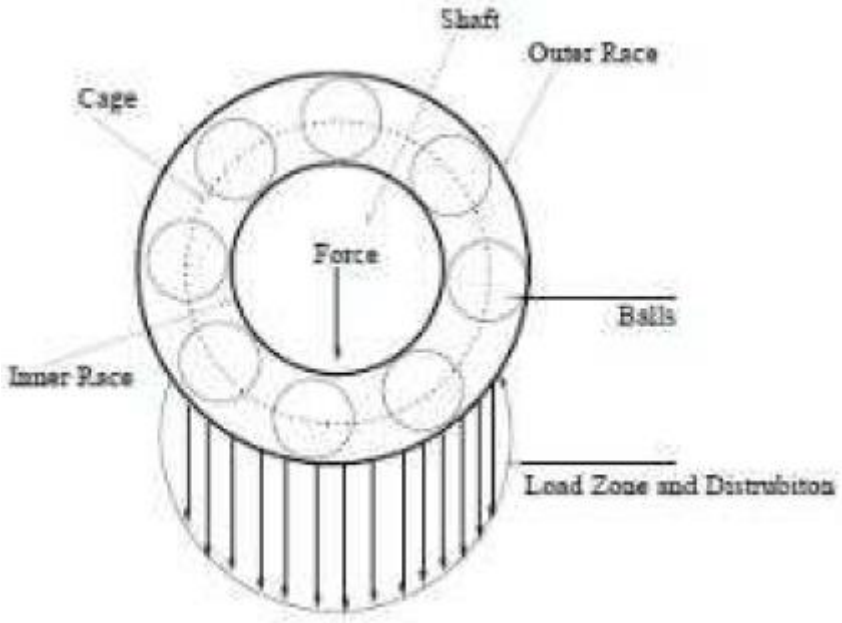

Figure 8: Sample load distribution in a REB. The unequal radial load distribution may depend on, for example, the weight distribution and orientation of the shaft [4].

Bearing diagnostics are typically done by the analysis of vibration signals or acoustic emissions, or also by measuring spindle current signals to observe vibrations indirectly. Rantatalo et. al [5] used non-contact, magnetic excitation to analyse the lateral vibrations in milling machine spindles, while Lu et al. [6] used a microphone and highspeed camera to implement fault detection under variable speeds. It has been proposed that analysis based on a zero-rpm tap test can be used, but studies [5] [6] [7] suggest that this would be inadequate due to speed dependent dynamics or speed dependent stiffness of the bearings.

7.2 Vibration Signals

Vibration signals (which can be measured by accelerometers) arise due to the repeated impacts between a local surface defect and the rolling elements of the bearings, as shown in Figure 9. The repetition frequency of each component of the bearing (i.e., outer race ball-passing frequency, inner race ball-passing frequency, roller spin speed, and cage speed) can be determined from kinematic analysis using the speed of rotation and geometry of the

REB, and bearing faults can be diagnosed by matching measured vibration frequencies with these theoretical rotational frequencies. These frequencies are given as [8]

$$BPFO = \frac{nf_r}{2}\left\{1 - \frac{d}{D}\cos\varphi\right\} \quad 1$$

$$BPFI = \frac{nf_r}{2}\left\{1 + \frac{d}{D}\cos\varphi\right\} \quad 2$$

$$FTF = \frac{f_r}{2}\left\{1 - \frac{d}{D}\cos\varphi\right\} \quad 3$$

$$BSF = \frac{D}{2D}\left\{1 - \left(\frac{d}{D}\cos\varphi\right)^2\right\} \quad 4$$

Where equations 1 and 2 give the outer and inner race ball pass frequency, respectively, equation 3 is the fundamental train frequency (cage speed), and equation 4 is the ball spin frequency. *D* and *d* are respectively the pitch and rolling element diameters, *n* is the number of rolling elements, f_r is the shaft speed, and φ is the contact angle of the rolling element (defined as the angle of the load from the radial plane).

However, in reality the load on (and rolling diameter of) a rolling element depends on the local loading and hence its circumferential position so that each rolling element tends to roll at different speeds but are all constrained by the cage of the bearing. Therefore, random slip occurs that fundamentally changes the vibration signal; the vibration signals from bearing defects then have a stochastic component, are not strictly periodic, and can also be contaminated with ambient frequency from other machine components which complicates the analysis. However, the underlying rotational frequency of the REB component is periodic, and the vibration signals can be considered cyclostationary [8].

A number of techniques have been proposed and tested to extract meaningful diagnostic information from measured vibration signals. Adaptive Noise Cancelation (ANC), signal decomposition, and power cepstrum have been used [9] [10] [11], as has envelope analysis or "high frequency resonance technique" [8]. The wavelet transform [12] and pattern recognition techniques [13] have also been presented as viable options. Analytical models have been presented for vibrations due to distributed defects [14]; however, many frequencies from distributed defects coincide with frequencies from local defects, hence why it has been suggested that both the amplitudes and frequency of spectra be studied [15]. In any case, the general aim of these methods is to increase the "impulsivity" of the signal that exists due to the periodic impacts of the localized faults so that characteristic signal properties of faulty bearings are more apparent in measured data.

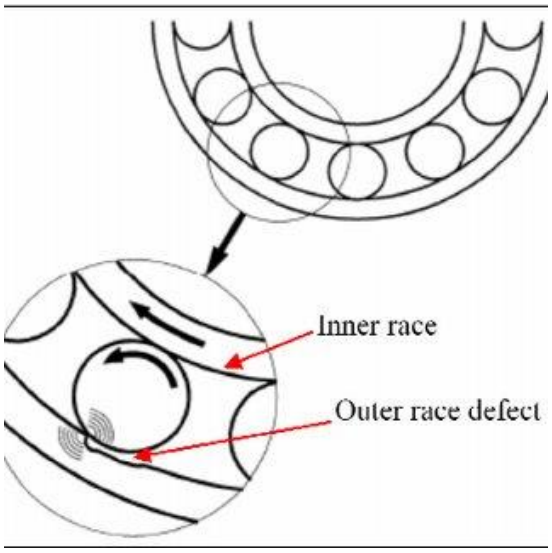

Figure 9: Illustration of an impact between rolling element and defect in the outer race.

Envelope analysis, one of the more popular techniques, is based on the principle that more diagnostic information can be obtained from envelope signals (Figure 10) than from the raw vibration signals. This is because in the raw signal, low harmonics of the repetition frequency are easily masked by other frequency components and, when random slip is accounted for, the higher frequencies are “smeared” over one another so that key frequency signatures typical for bearing faults are lost, whereas the repetition frequency can be identified in the envelope spectra [8]. The general procedure for envelope analysis is to bandpass filter the measurement signal in a high frequency band in which the fault impulses are amplified by structural resonances, and then amplitude-demodulate the signal to produce the envelope signal. The signal can be frequency-modulated to account for the rate at which the fault passes through the load zone or measurement point. A detailed discussion of envelope analysis is given in [8] and an approach for selecting an optimal demodulation band is presented in [16].

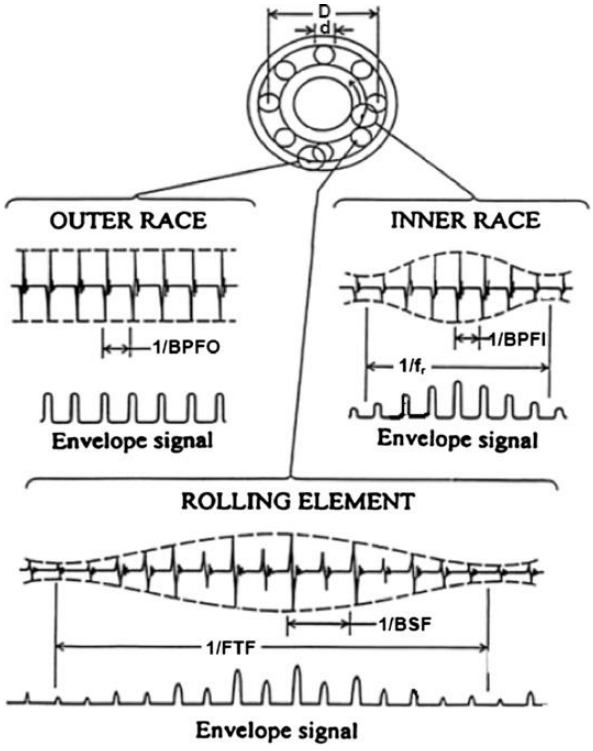

Figure 10: Sample envelope Signals for different localized defects [8].

7.3 Acoustic Emissions and Noise

Acoustic emissions (AE) refer to the phenomenon of transient elastic wave generation due to the rapid release of strain energy caused by structural alterations due to mechanical or thermal stress [17]. These emissions are measured using specialized AE sensors that are typically placed on the housing or casing of the spindle or gearbox, much like a doctor's stethoscope. Characteristic parameters, such as ringdown counts, number of events, and peak amplitude, that are present in the measured AE signal are analysed to diagnose the bearings. A typical acoustic emission burst signal is shown in Figure 11, and the general methodology is discussed in more detail in [17]**.** Acoustic noise, which must be distinguished from AE, can also be measured using microphones and similarly analysed. Research work has been done to measure AE in combination with novel filtering or signal processing techniques for bearing diagnostics [18], [19]. It is a requirement to isolate the noise resulting from defective bearings from ambient sound when using sound pressure or sound intensity to diagnose bearings.

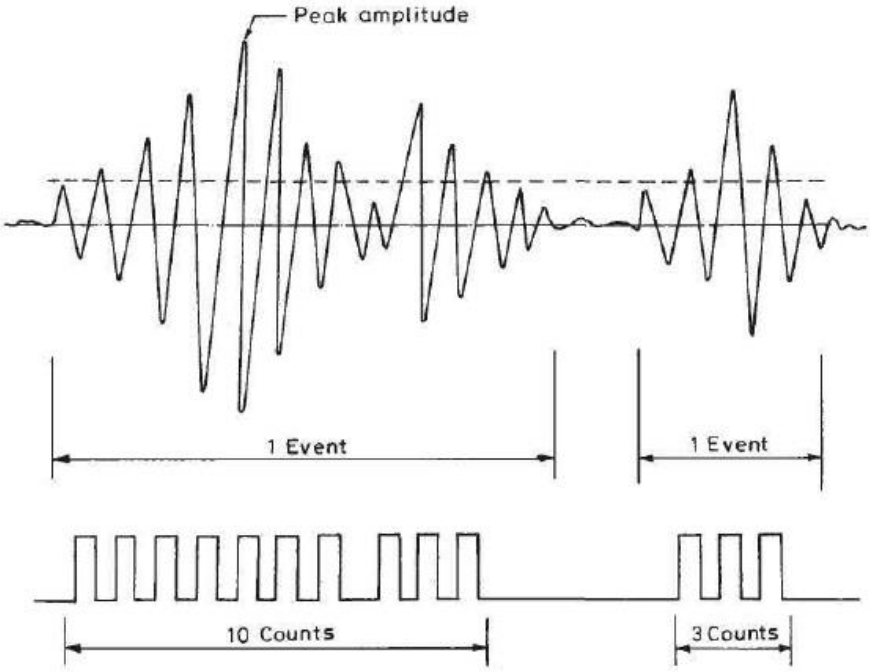

Figure 11: Typical AE burst signals

7.4 Conclusion of Literature Study and Pre-Analysis

A comparison of the pre-analysis performed before the launch of the project, a 'post-analysis' after the start of the project of the technology (SpinScope, SmartMeter) available at DAMRC, and available scientific literature reveals significant discrepancies between the means necessary to analyse and diagnose spindle bearings and DAMRC capabilities. It is clear from the scientific literature that bearing diagnostics are not normally performed with impact hammers and any attempt to do so is highly experimental, requiring a significant allocation of resources and time spent performing basic research that has not been allocated for the project. Existing documentation for the (spindle condition module of) SpinScope and SmartMeter technologies are clear that they utilize accelerometers only. As such, these technologies are well suited for the analysis of bearings by the measurement of vibration (acceleration) signals (section 7.2), and it is therefore unnecessary to investigate other diagnostic methods.

Initial testing and analysis of the technology available at DAMRC indicates that the SmartMeter is already suitable for use in industry, despite some limitations arising from being unlicensed software. Indeed, the

SmartMeter has already been used in industry in conjunction with the vibratory stress relief (VSR) treatments provided by DAMRC to industrial partners. The SpinScope software is also unlicensed. However, the resulting limitations are much more severe; as stated previously, the 64-bit version of SpinScope can only be used in 'read-only mode,' while the 32-bit version can only be used for general data acquisition. As a result, 32-bit SpinScope can theoretically be used to capture acceleration signals from spindle units in industry, but, as was seen in 7.2, additional analysis is necessary to derive meaningful results from bearing test measurements. Consequently, the 32-bit version of SpinScope is also unsuitable for use in industry unless additional development activities are carried out to build up the necessary analysis capabilities.

8. Experiment Design:

8.1 Introduction

After communicating the limitations of the SpinScope software (as summarized in 7.4) to management, the decision was made to proceed with the project and carry out the work necessary to make SpinScope usable in industry. This work consisted of implementing the algorithms described in [8] and [20] necessary to perform envelope analysis on the measured acceleration signals. Additionally, the planned experiments of the project were reorganized into two categories: (1) experiments to validate the newly developed envelope analysis capabilities, and (2) the originally planned experiments to compare the performance of SmartMeter and SpinScope on various new and old machine spindles. The first set of experiments are performed on a specially designed test rig similar to what has been used in the literature, which allows for a more thorough comparison of experimental and theoretically expected results. The design of both sets of experiments are discussed in the following sections.

8.2 Experimental Test Design

8.2.1 Design of Experiments Validating Envelope Analysis

To facilitate the testing and validation of the results obtained with envelope analysis, a test bench based on the mechanical installation shown in Figure 12 is created. The test bench consists of an electric motor that acts as the prime mover for a drive belt that transfers motion to the test bearings as shown in the detail view of the figure. The motor output (and therefore the shaft speed seen by the bearings) is controlled with a variable frequency drive (Siemens Sinamics G120C PN), whose output is determined by custom software developed during the P901 - Elforsk VSR project. The open-loop control is facilitated by the schematic shown in Figure 13.

The experimental setup shown in the figures is designed to facilitate the rapid exchange of test bearings, which is designated as "bearing 1" in Figure 12. The test bearings alternate between healthy and damaged bearings between tests depending on the needs of the specific experiment being conducted, where the damaged bearing is simulated by drilling a 1-millimeter fault into the outer race. The resulting vibrations (or lack thereof) are then measured with one of the accelerometers included with the MetalMAX (SpinScope) equipment.

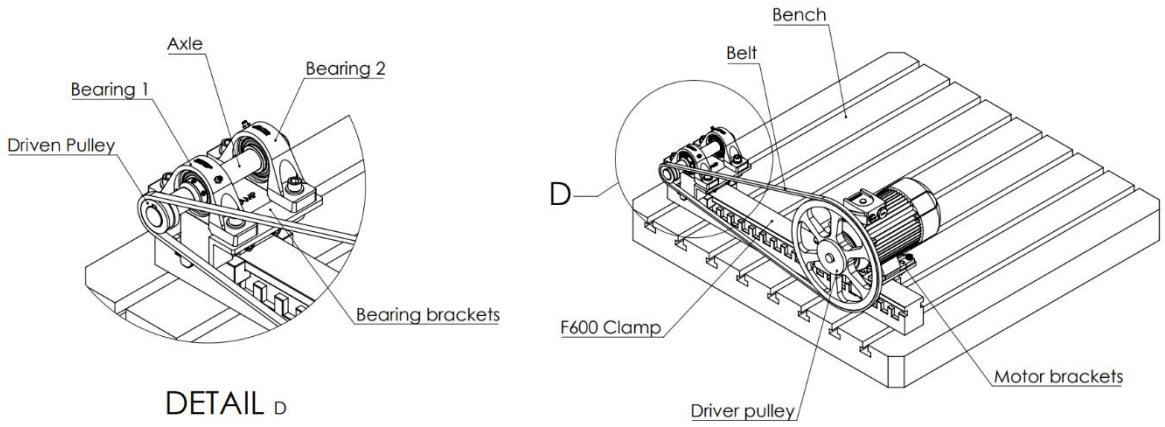

Figure 12: Overview of mechanical installation

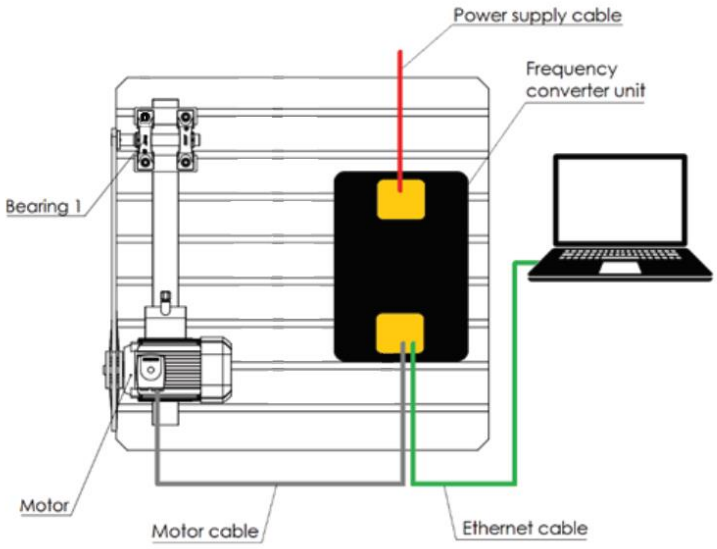

Figure 13: Schematic diagram of the experiment

8.2.2 Design of Experiments Comparing SpinScope and SmartMeter

To compare the performance of SpinScope and SmartMeter, the same experiment as described in the previous section is performed with the addition of an extra accelerometer connected to the SmartMeter. In this way, a “baseline” comparison between SpinScope and SmartMeter can be established for both healthy and faulty bearings.

Additional tests of the two technologies are carried out on the spindle units of actual CNC machines to further compare their capabilities and simulate actual conditions when performing tests in industry. These tests consist of placing two accelerometers (one for SpinScope and one for SmartMeter) on the spindle of the CNC machine. The accelerometers should be placed as close together as possible so that differences in the acceleration signals resulting from the nonuniform load distribution on the bearing and differences in the transmission path between the (potential) bearing fault and the accelerometer is minimized. With the

accelerometers so placed, the spindle is run at predetermined speeds and a prescribed number of measurements are taken at each speed. The associated acceleration data is saved for offline analysis.

8.3 Equipment for the Test

8.3.1 Equipment for Validation of Envelope Analysis

The items outlined in the bill of materials in Table 1 are necessary to perform the first set of experiments described in section 8.2.1

Table 1: Bill of materials/list of required equipment for the first experiments in section 8.2

Description	**Qty.**
Electric Motor (1LE10010EA022AB4)	1
Frequency converter unit	1
Motor control and power cable	1
Ethernet cable	1
Laptop with DAMRCVSR software running	1
Power supply cable	1
Axis	1
Healthy bearing (UCP 206)	2
Fail bearing (UCP 206)	1
Motor brackets	2
Bearing brackets	2
Mechanical hardware kit	1
SmartMeter, incl. magnetically mounted accelerometer and data cable	1
32-bit MetalMax laptop running SpinScope Software	1
Data Acquisition Card for MetalMax Laptop	1
Accelerometer and data cable for MetalMax Laptop	1
32-bit MetalMax license dongle	1

8.3.2 Equipment for Comparison Tests between SpinScope and SmartMeter

The items outlined in the bill of materials in Table 2 are necessary to perform the second set of experiments described in section 8.2.2. Since these tests are performed on spindle units in real CNC machines, only the equipment associated with the SpinScope and SmartMeter technologies are required.

Table 2: Bill of materials/list of required equipment for the second experiments in section 8.2

Description	Qty.
SmartMeter, incl. magnetically mounted accelerometer and data cable	1
32-bit MetalMax laptop running SpinScope Software	1
Data Acquisition Card for MetalMax Laptop	1
Accelerometer and data cable for MetalMax Laptop	1
32-bit MetalMax license dongle	1

8.4 Material for the Test

Since the prescribed tests of the project involve collecting acceleration data from spindles and bearings, the consumption of additional stock material is not required.

8.5 Test Procedure

8.5.1 Validation of Envelope Analysis

Acceleration signals from bearing #1 are measured using the 32-bit MetalMAX laptop and DAQ card to assess the capabilities of the SpinScope software. Two tests of the software are performed, one in which bearing #1 is healthy and one where it is damaged as indicated above. For each test, six separate trials are conducted in which a distinct acceleration signal that is between 20 and 30 seconds is captured with SpinScope. An extract of a representative measurement signal is presented in Figure 14. These measurement lengths are chosen to account for unexpected settling time of the signal that was observed in the beginning of the measurement. The experiments are run using an output (bearing side) shaft speed of approximately 1100 RPM, which is independently measured with a handheld tachometer (Diesella 107-B6322TD). The resulting data was then exported to a .txt file and analysed with a custom, purpose-specific python script. The results of the subsequent analysis are discussed in the next section 9. The procedure for the experiment can be stated as follows:

1. Prepare the MetalMax equipment and SpinScope software for use, placing the accelerometer on the test bearing.
2. Obtain a steady-state shaft speed using the VSR software and variable frequency drive.
3. Use the SpinScope software to obtain acceleration data from the test bearing.
4. Import the acceleration data to the desired PC for offline envelope analysis.

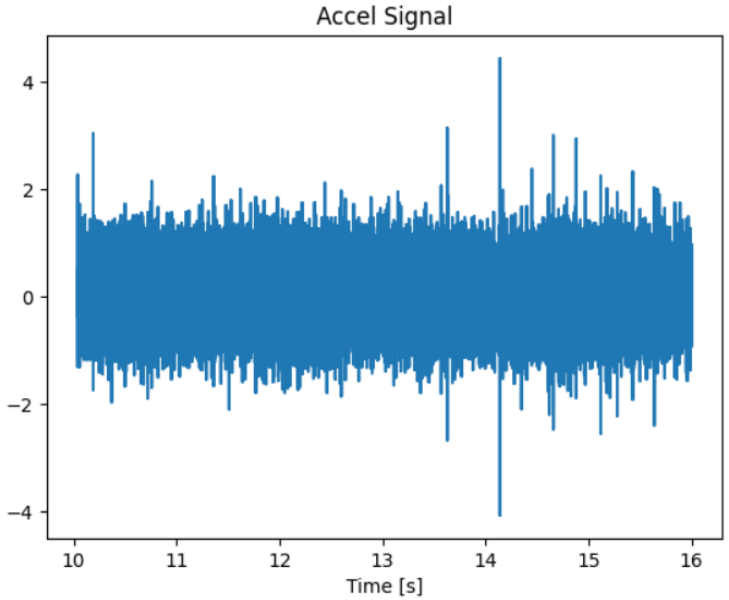

Figure 14: Extract of one of the acceleration signals obtained during the test with the healthy bearing.

8.5.2 Test Procedures for Comparing SpinScope and SmartMeter

The test procedure for comparing the performance of SpinScope and SmartMeter on a real CNC machine or using either technology in a case study with an industrial partner, consists of setting up the SpinScope and/or SmartMeter equipment, placing the accelerometer(s) on the spindle, and measuring the resulting acceleration as the spindle runs. The procedure is therefore the same as that stated in the previous section, with the addition of a second accelerometer for SmartMeter placed on the test bearing and/or CNC spindle.

9. Test Results and Data Analysis

9.1 Introduction to Test Results

As stated in section 7.2, the vibration signals arising from REBs tend to be cyclostationary[1], due in part to random slip of the rolling elements, and additional analysis is required to obtain meaningful diagnostic information. While many options are available, this project implements a method adapted from [8] and [20] to inform the required envelope analysis. This method is implemented in a python script with the aim of performing this analysis offline. The analysis is then validated in a numerical study before being used in experiments as described in section 8.2.1 In this section, the details of the implemented analysis method, which is applied to all results obtained by SpinScope, are outlined. The following sections present the results of the numerical study and physical experiments.

In [8], a four-step process for the diagnosis of REBs is discussed after introducing the issues mentioned in section 7.2. This process consists of:

[1] A signal that is *nth order cyclostationary* is one whose nth order statistics are periodic, with higher order statistics being non-periodic [7].

1. Order tracking
2. Separation of bearing signals from discrete frequency noise
3. Enhancement of the bearing signal
4. Envelope Analysis

The third step of enhancing the bearing signal can be further divided into two separate stages, Minimum Entropy Deconvolution (MED) and Spectral Kurtosis (SK), to arrive at a five-step process. Order tracking (step 1) refers to a procedure for establishing the order of cyclostationarity of the signal and has applications in compensating for variations in shaft speed and making the second step of the above process possible in difficult cases. The second step refers to the process of separating the frequency signature of the bearings from other frequency components, for example from gear mesh frequencies or frequencies associated with other machine components. A range of methods are available to achieve this separation, such as Self-Adaptive Noise Cancelation (SANC), Discrete/random separation (DRS), and time synchronous averaging (TSA) [8].

Even after this separation, the final diagnosis of the REM is improved by enhancing the bearing signal. This can be done first by MED (step 3a), which seeks to account for the transmission path between the bearing fault and measurement device, which is achieved by finding an inverse filter to compensate for the transfer function associated with the transmission path. The bearing signal can be further enhanced after this compensation by bandpass filtering the measurement signal in a range of frequencies such that the impulses associated with the bearing fault are amplified by structural resonance, which is a central component of Envelope Analysis. SK (Step 3b) is used to determine the optimal filter parameters to achieve this amplification. Finally, in the last step of the process, the diagnosis of the bearing is performed by applying Envelope Analysis. Envelope Analysis (step 4) consists of first bandpass filtering and then modulating the bearing signal. The effect of applying Envelope Analysis to REB diagnostics is shown in Figure 15.

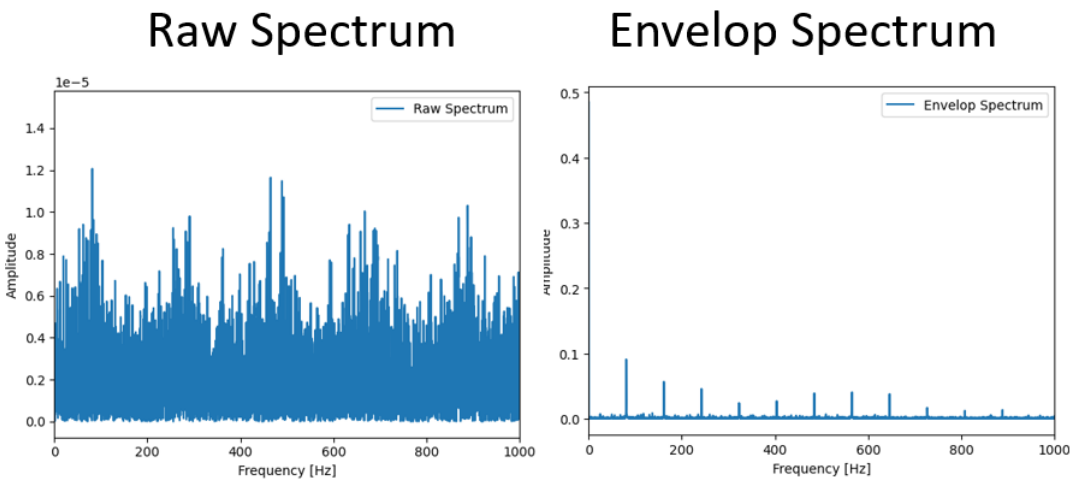

Figure 15: frequency spectrum of the same acceleration signal of a REB with (right) and without (left) envelope analysis. As shown in the figure, the frequency components in the spectrum of the REM signal are smeared and it is hard to distinguish bearing fault frequencies.

A minimalist version of the above procedure is implemented in python due to the constraints placed on the project. The abridged algorithm consists only of calling a modified version of the .m function in [21] to generate the kurtogram (a 2D colour map showing spectral kurtosis as a function of filter central frequency and filter bandwidth), and then using the resulting optimal filter parameters for Envelope Analysis. A more

detailed and theoretical treatment of SK and Envelope Analysis is given and in [8] [22] [23], while a flowchart illustrating the algorithm implemented in python is given in Figure 16.

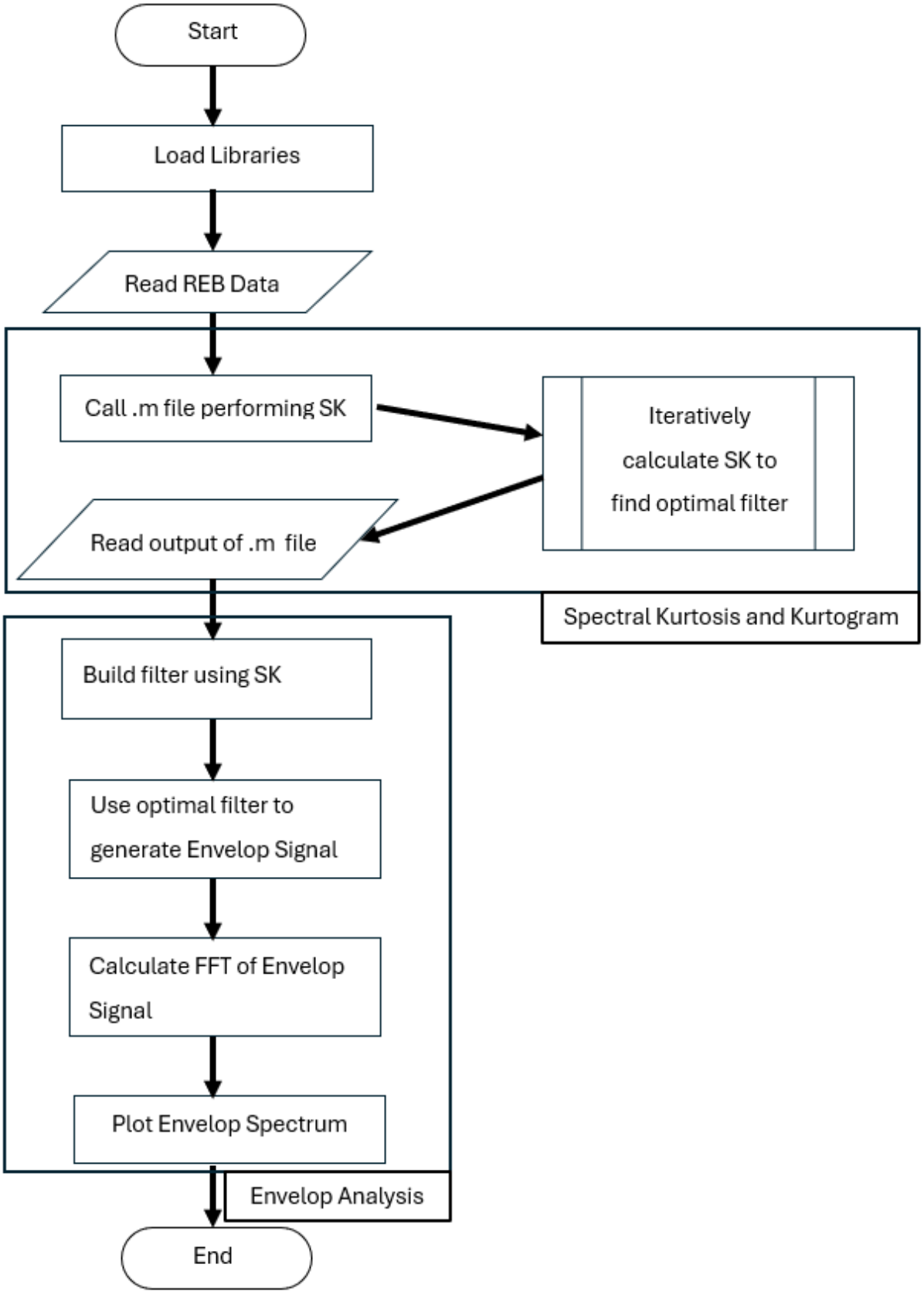

Figure 16: Flowchart illustrating the operations performed in the python script

9.2 Numerical Simulation

The implemented algorithm discussed in the previous section is tested in numerical simulations using test data obtained from [24]. Test data for three cases (a healthy bearing, a bearing with inner race fault, and a bearing with outer race fault, as shown in Figure 17) are used to evaluate the algorithm by way of comparison with the examples in [25], which use the same test data. The results of these three numerical case studies are presented in the following subsections.

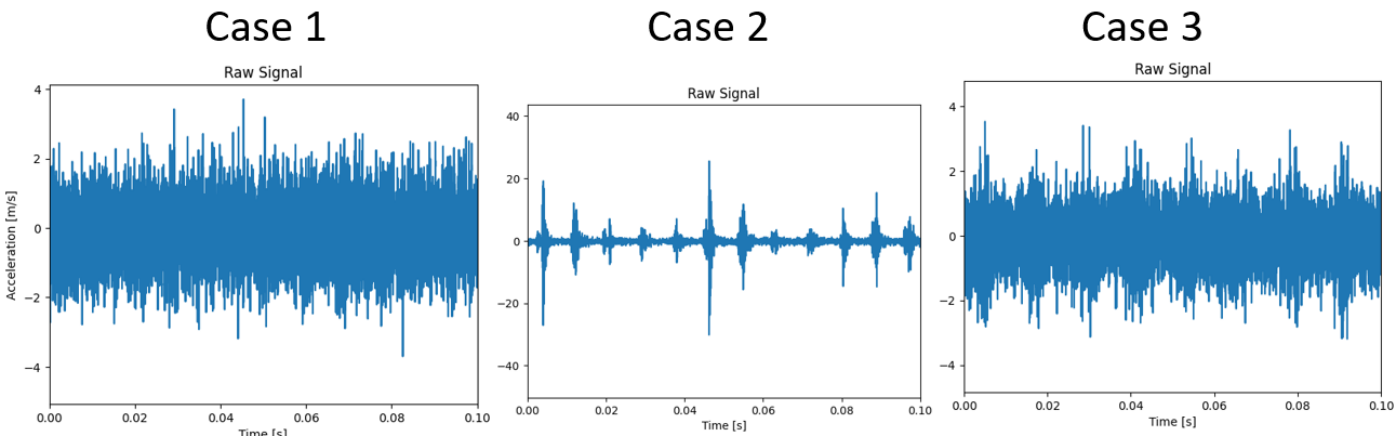

Figure 17: Vibration signals from three case studies representing: healthy bearing (left), inner race fault (middle), and outer race fault (right)

9.2.1 Case 1: Healthy Bearing

The first case simulating a healthy bearing is studied using the file 'baseline_1.mat' from the 'Three Baseline Conditions' group. The data in the .mat file is obtained from a custom test rig using healthy bearings having a roller diameter of 0.235 inches, pitch diameter of 1.245 inches, 8 rolling elements, and contact angle of 0 degrees. The data was collected for 6 seconds at sampling rate of 97,656 Hz while the 270 lbs of load was applied when the input shaft speed was 1500 RPM.

The resulting Kurtogram is presented in Figure 18. The Kurtogram shows that the frequency spectrum of the baseline data exhibits a spectral kurtosis that is maximum in a frequency band centred at 12207 Hz with a bandwidth of 24414 Hz. This information is then used to define the window length and central frequency of the bandpass filter used in envelope analysis. The result of the envelope analysis is shown in Figure 19. The figure indicates that there are no noteworthy frequency components in the baseline data after envelope analysis, and that this is true for both the analysis implemented in python as well as in the MATLAB example [25]. In this case, all of the frequency spectra presented in the figure are indistinguishable from that of a noisy signal.

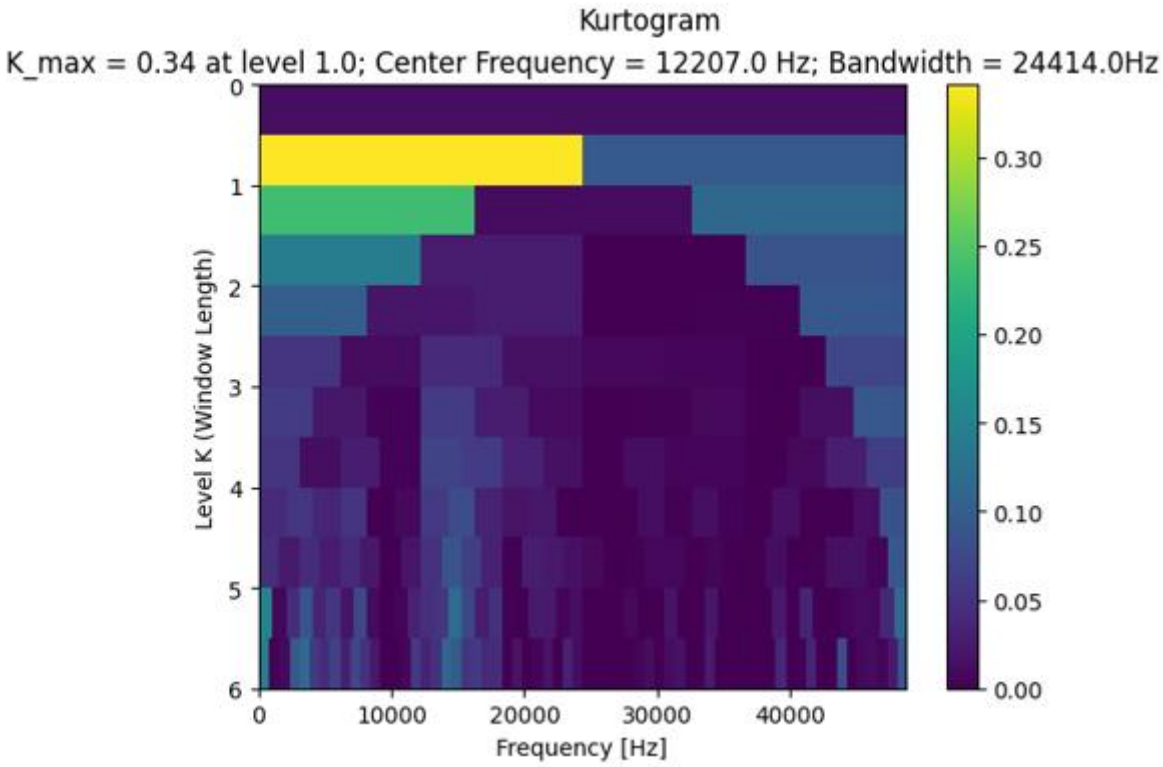

Figure 18: Kurtogram for the simulated healthy bearing

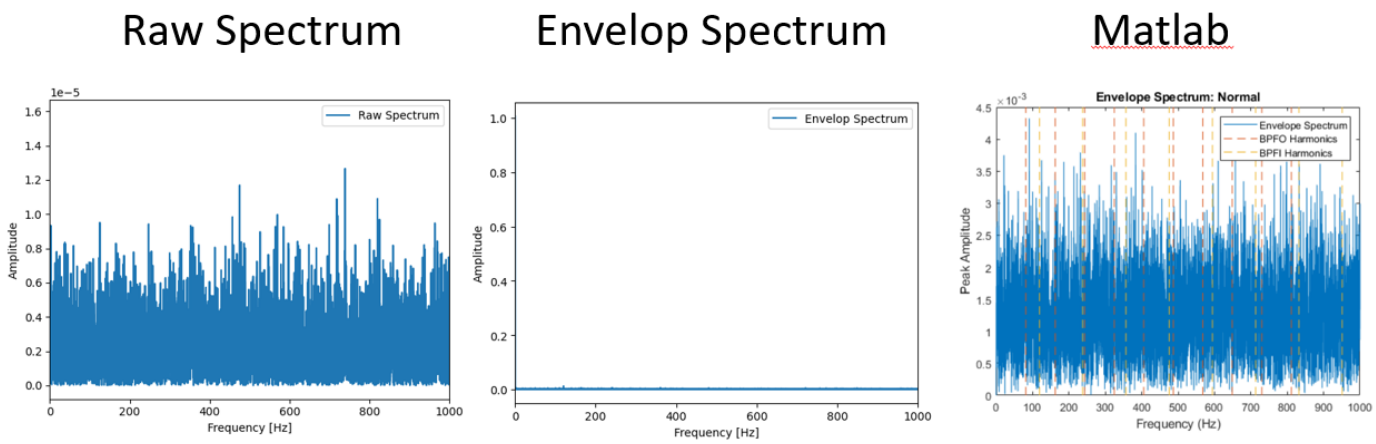

Figure 19: End results of the first case study. Frequency spectra of baseline data without envelope analysis (left), results of the envelope analysis of the baseline data (middle), and comparable results from MATLAB example in [25] (right).

9.2.2 Case 2: Inner Race Fault

The case for an inner race fault is studied using the file 'InnerRaceFault_vload_1.mat' from the group 'Seven Inner Race Fault Conditions.' The data in this .mat file is obtained in a similar manner as in the previous case using the exact same bearings, with the exception that an unspecified fault has been introduced into the inner race. The vibration signal was measured for 3 seconds at a sampling rate of 48,828 Hz when the shaft speed was 1500 RPM and loading was 0 lbs.

The resulting Kurtogram is presented in Figure 20. The Kurtogram shows that the frequency spectrum of the inner race fault data exhibits a spectral kurtosis that is maximum in a frequency band centred at 13732 Hz with a bandwidth of 1017 Hz. This information is likewise used to define the window length and central frequency of the bandpass filter used in envelope analysis. The result of the envelope analysis is shown in Figure 21. The figure indicates that distinct frequency components corresponding to the fault impact frequency are present in the envelope spectrum generated with python, and that comparable results are obtained in the MATLAB example. When envelope analysis is not used, however, it becomes more difficult to distinguish between fault impact frequencies and frequencies deriving from other sources, as these tend to 'smear' into each other.

The results obtained from the analysis implemented in python and in MATLAB are qualitatively compared, and it is observed that, while the predicted impact frequencies are consistent, there are discrepancies between the amplitudes of the resulting frequencies. This discrepancy likely arises from slight differences in the implementation used in python compared to MATLAB. Since only the frequency itself, not the corresponding amplitude, is needed to characterize the type of fault, this discrepancy does not affect ability to diagnose REBs. However, the discrepancy in amplitude may have adverse implications for assessing the severity of damage associated with the fault, and therefore predictions of the remaining useful life of the bearing is also affected.

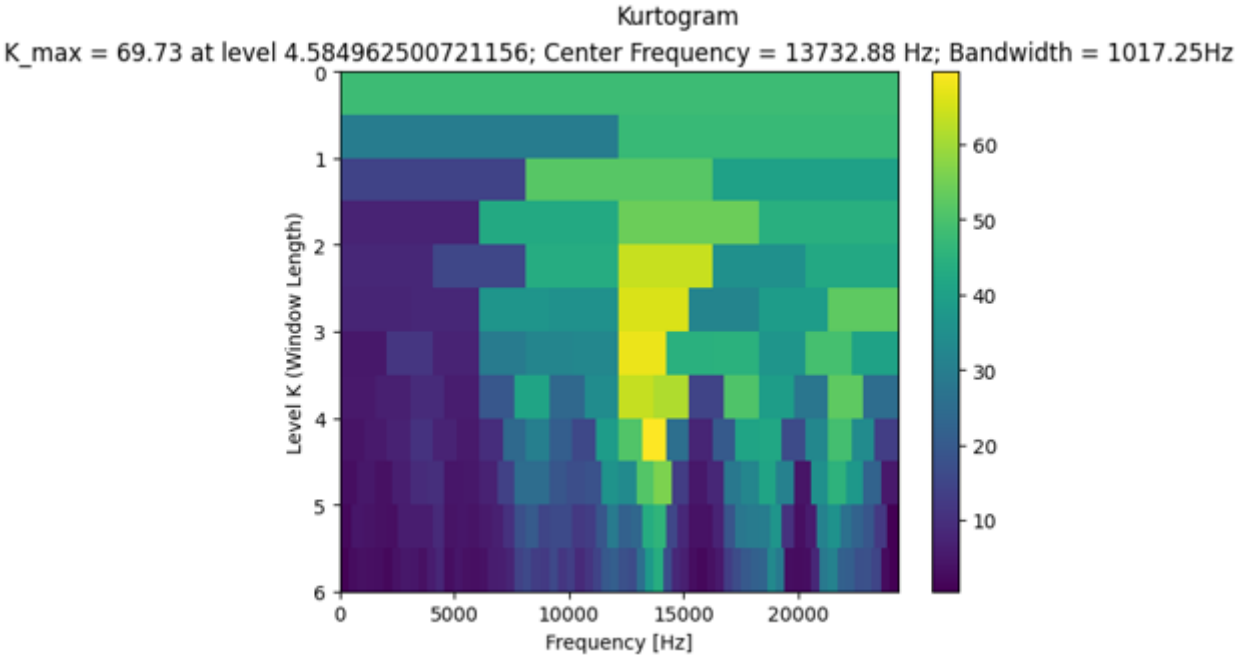

Figure 20: Kurtogram for the simulated inner race fault.

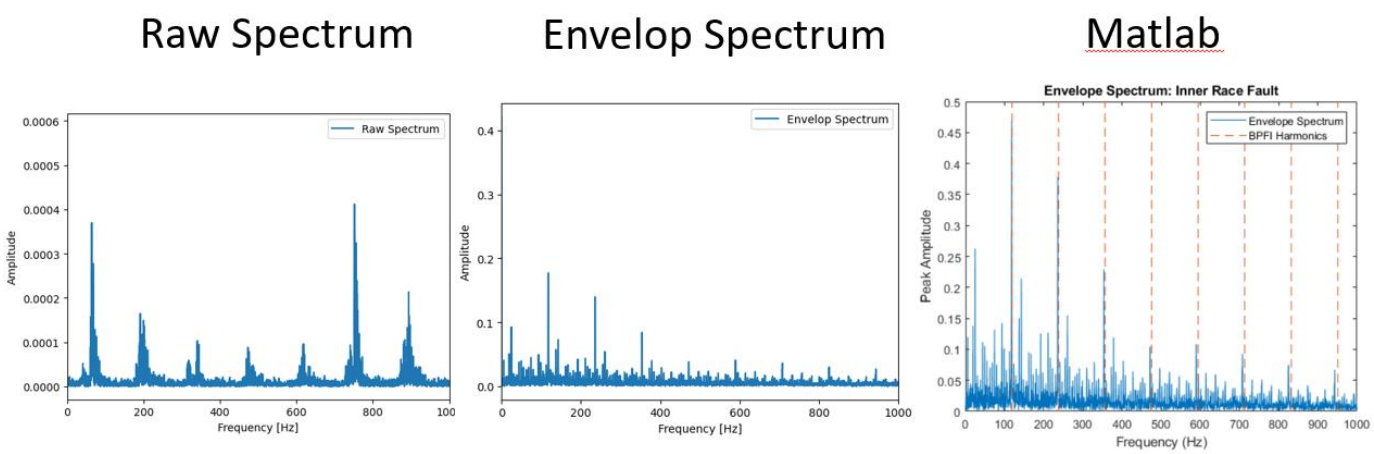

Figure 21: End results of the second case study. Frequency spectra of inner race fault data without envelope analysis (left), results of the envelope analysis of the inner race fault data (middle), and comparable results from MATLAB example in [25] (right).

9.2.3 Case 3: Outer Race Fault

The case for the outer race fault is studied using the file 'OuterRaceFault_2.mat' from the group 'Three Outer Race Fault Conditions.' The data in this .mat file is obtained in a similar manner as in the previous case studies using the exact same bearings, with the exception that an unspecified fault has been introduced into the outer race. The vibration signal was measured for 6 seconds at a sampling rate of 97656 Hz when the saft speed was 1500 RPM and the loading was 270 lbs.

The resulting kurtogram is presented in Figure 22. The kurtogram shows that the frequency spectrum of the outer race fault data exhibits a spectral kurtosis that is maximum in a frequency band centred at 2670 Hz with a bandwidth of 763 Hz. This information is likewise used to define the window length and central frequency of the bandpass filter used in envelope analysis. The result of the envelope analysis is shown in Figure 23. The figure indicates that the distinct frequency components corresponding to the fault impact frequency in the frequency spectrum are present, and that comparable results are obtained in the MATLAB example. When envelope analysis is not used, however, the resulting frequency spectrum becomes indistinguishable from a noisy signal, similar to the 'raw' spectrum obtained in the first case study for healthy bearing. Then in this case an incorrect diagnosis of the bearing (in this case a false negative) can be made if envelope analysis is not implemented. The same conclusions regarding the resulting frequencies and their amplitudes can be made as was done for the second case study (for the inner race fault).

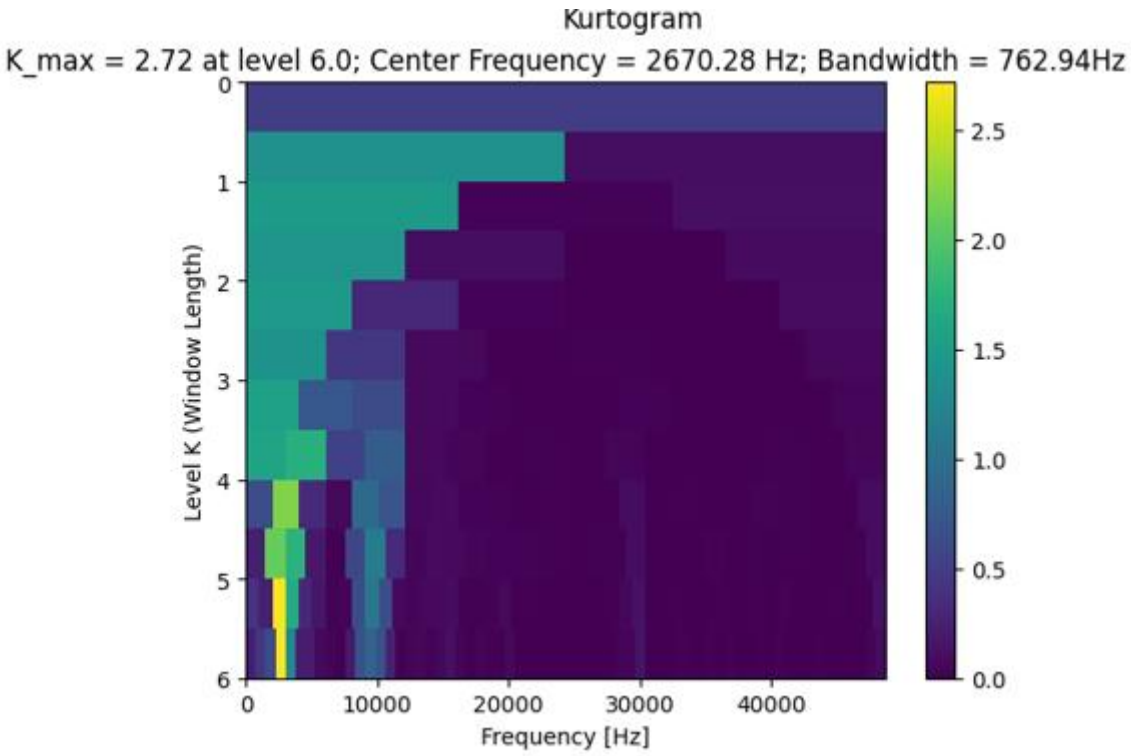

Figure 22: Kurtogram for the simulated outer race fault

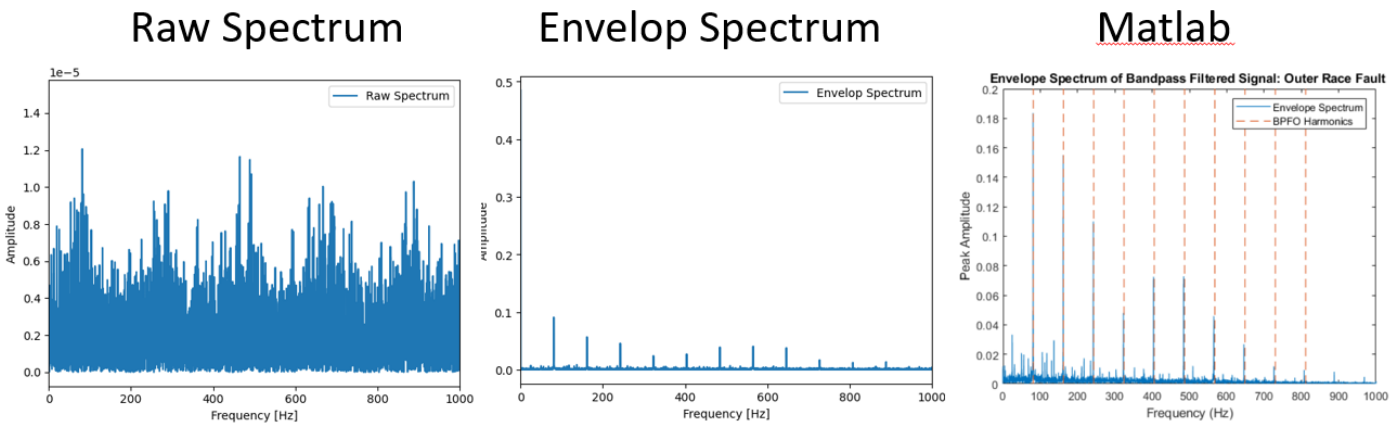

Figure 23: End results of the third case study. Frequency spectra of outer race fault data without envelope analysis (left), results of the envelope analysis of the outer race fault data (middle), and comparable results from MATLAB example in [25] (right).

9.3 Preliminary Experimental Results with Envelope Analysis

The spectral kurtosis and envelope analysis tested in the numerical case studies of the previous section was further validated with recorded vibration signals obtained from tests using the custom test rig at DAMRC shown in Figure 24. The tests consisted of placing the 'large' accelerometer (PCB model 352O68) from the 32-bit MetalMax equipment on the test bearing and recording the resulting vibration signals while the shaft was running at a prescribed speed controlled by the variable speed drive. Six recordings of 30 seconds are obtained each for the healthy bearing and for a damaged bearing. The shaft speed is regulated to operate at approximately 1100 RPM, with some degree of speed fluctuation expected, and measured independently of the control system depicted in Figure 13 using the tachometer.

As seen in the numerical simulations of the previous section, only a few seconds are needed for the envelope analysis; however, it was observed that the accelerometer signal obtained with SpinScope needed additional time to settle after the beginning of the experiment. Further, it is hypothesized that the data obtained during a longer sampling period might be beneficial for a latter study on related topics. Therefore, accelerometer data is recorded for 30 seconds at a sampling frequency of 65,536 Hz for each individual measurement, and then a portion of the resulting data, approximately 6 seconds in duration, is exported for subsequent Envelope Analysis.

Figure 24: The test rig used at DAMRC to verify the implemented envelope analysis

For brevity, the results of the fourth trial for the healthy and faulty bearing test are presented here, while the results obtained for the other trials are provided in appendix 13.1. The truncated acceleration signals obtained during the fourth trials are shown in Figure 25. The figure shows that the amplitude of the acceleration obtained from the damaged bearing is much greater than that of the healthy bearing, but no information about the source of the underlying vibrations is provided, necessitating additional analysis. Furthermore, it is difficult to establish a “threshold” amplitude level that be consistently applied to all potential bearings and CNC machines.

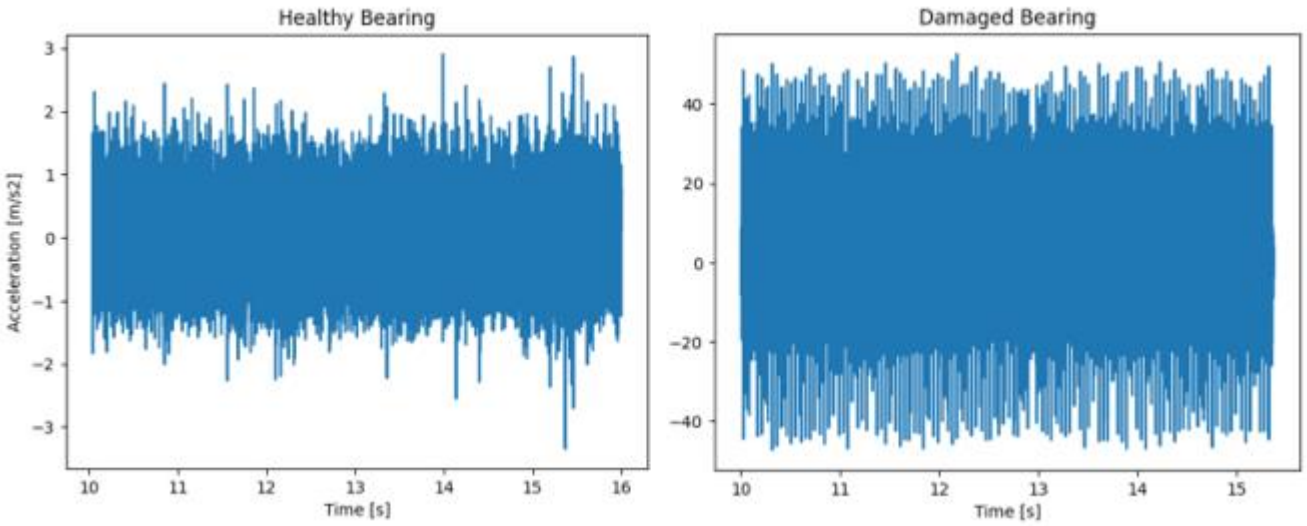

Figure 25: Truncated acceleration signal obtained during the fourth trial for both the healthy (left) and damaged (right) bearing

The kurtogram for the healthy and damaged bearing are shown in Figure 26 and Figure 27, respectively. From the results obtained in section 9.2 and as reported in the literature, it is generally expected that when a bearing fault is present spectral kurtosis is maximal in a narrow frequency band centred at a high frequency associated with the dynamics of the machine structure that amplifies the impact between the bearing fault and the rolling elements. These results are therefore expected to be present in the kurtograms shown in the figures below.

The kurtogram for the healthy and damaged bearing are shown in Figure 26 and Figure 27, respectively. Comparing the results in the two figures, it is observed that the kurtogram for both bearings present a maximal spectral kurtosis in a similarly sized frequency bandwidth of approximately 1024 Hz. However, the central frequency of this frequency band is much higher for the damaged bearing than it is for the healthy bearing (24,063 Hz for the damaged bearing compared to 1,537 Hz for the healthy bearing). Similarly, the maximum spectral kurtosis for the healthy and damaged bearing are reported as 2.17 and 20.73, respectively. Therefore, the resulting maximum spectral kurtosis and central frequency for the healthy and damaged bearing presented in Figure 26 and Figure 27 are consistent with expected results, while the bandwidth for the healthy bearing was expected to be wider than that for the damaged bearing.

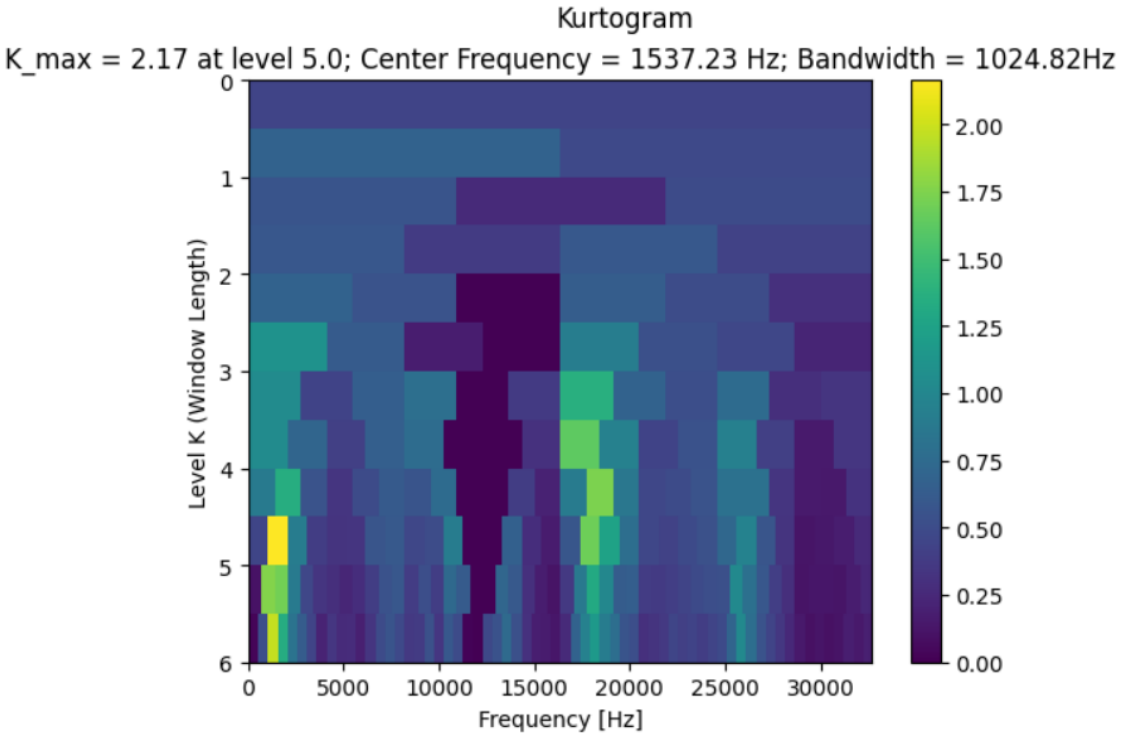

Figure 26: Kurtogram generated during trial 4 for the healthy bearing

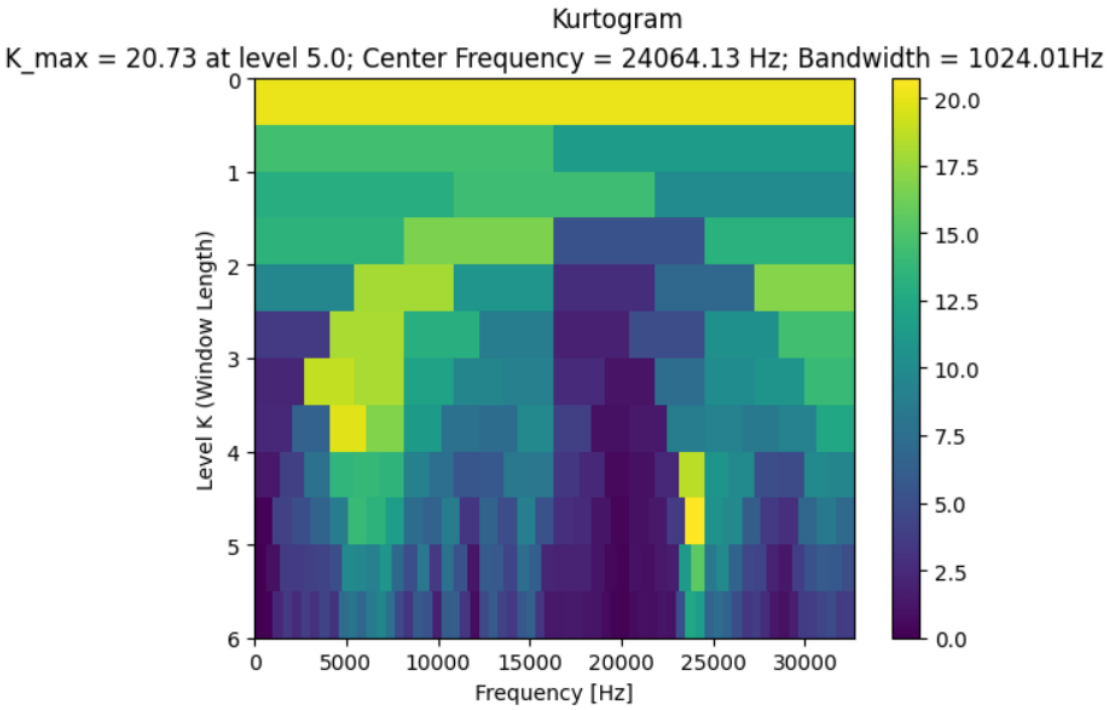

Figure 27: Kurtogram generated during trial 4 for the damaged bearing

The envelope spectrum for the healthy and damaged bearing are presented in Figure 28 and Figure 29, respectively, which highlight the frequency component with the maximum amplitude. As expected, the results for the damaged bearing clearly exhibit a frequency component associated with the impact frequency of the bearing fault and its harmonics, which experimentally is found to occur at 68 Hz

compared to the theoretically predicted 70 Hz. The maximum frequency component for the healthy bearing, on the other hand, is barely distinguishable from noise and is approximately an integer multiple of the shaft rotation frequency. This is expected since there is no damage in the healthy bearing to detect. The experimental results for both the healthy and damaged bearing are therefore consistent with theoretical expectations.

Considering the results for the damaged bearing, the relative error between the experimental and theoretical impact frequency is calculated to be on the order of 2%, where the experimental impact frequency is taken as the fundamental frequency detected in the envelope spectrum and the theoretical frequency is calculated according to equation 1 in section 7.2. The resulting relative error is largely consistent across all trials as shown in Table 3.

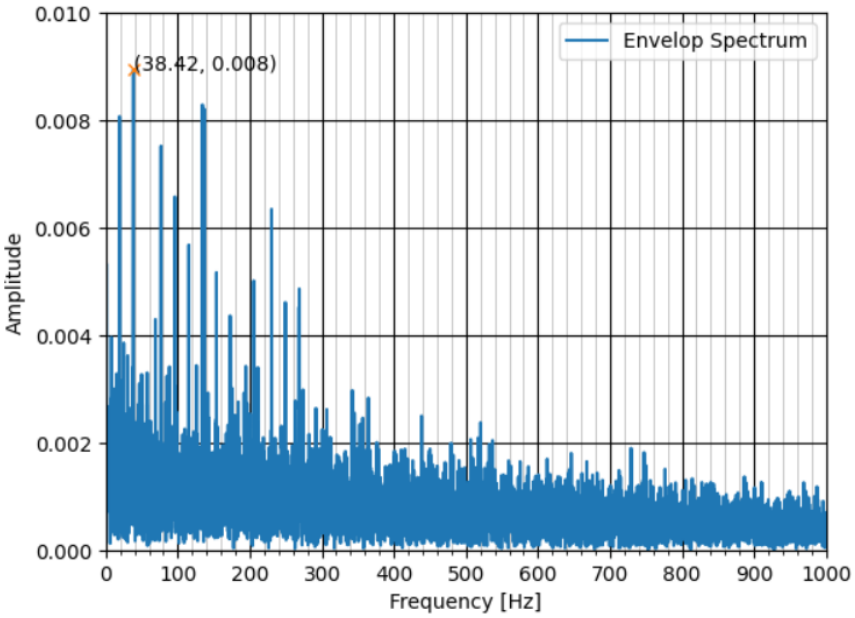

Figure 28: Envelope spectrum for the healthy bearing

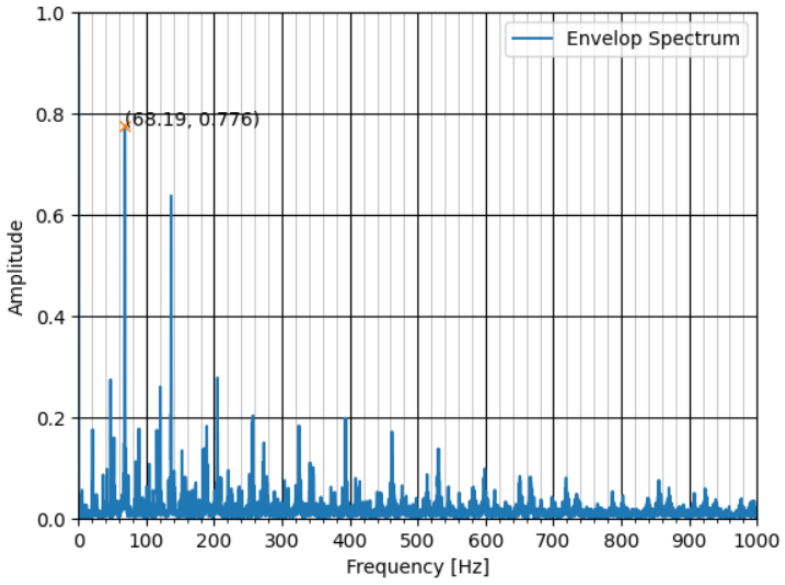

Figure 29: Envelope spectrum for the damaged bearing

The results in Figure 28 and Figure 29 show that an interpretation of the relative magnitude can be useful for determining the health of the bearing. Given the fact that it is not usually feasible to have a 'baseline' to compare to when testing bearings in industry, and that results for the healthy bearing in the other trials produced a maximum frequency component consistent with the impact frequency in the damaged bearing, best results in bearing diagnosis are obtained when the fundamental frequency and amplitude are used together with the results from the kurtogram in a holistic diagnosis methodology. These results further reinforce the concept that both frequency and amplitude, as suggested in [15], need to be studied.

The success criteria given in section 4 and the project application include the statement that there should be "90% consistency in the data obtained for each machine," and so a measure of this consistency of the empirical results are also given in Table 3. Consistency is taken to be equal to 1 minus the coefficient of variation of the data, expressed as a percentage, where the coefficient of variation is a common statistical measure defined as the ratio between the standard deviation and the mean, σ/μ . The coefficient of variation approaches 0 with decreasing standard deviation (or decreased "spread" or higher "consistency") and increases in the opposite case. For this reason, consistency in the results is given as 1 minus the coefficient of variation. This definition of consistency is reported for the test results in the following sections and sample calculations are given below

$$x = \{64.65, 67.95, 67.65, 68.19, 67.84, 67.92\}$$

$$\mu = \frac{1}{n}\sum_{i=1}^{n} x_i = 67.36$$

$$\sigma = \sqrt{\frac{1}{n}\sum_{i=1}^{n}(x_i - \mu)^2} = 1.34$$

$$\text{"Consistency"} = \left(1 - \frac{\sigma}{\mu}\right) \times 100\% = 98.01\%$$

Table 3: Summary of the preliminary test results for all trials of the damaged bearing

Parameter	Trial 1	Trial 2	Trial 3	Trial 4	Trial 5	Trial 6
Measured Shaft Speed [RPM]	1075	1100	1100	1108	1104	1104
Theoretical Ball Pass Frequency - Outer Race [Hz]	68.08	69.67	69.67	70.17	69.92	69.92
Experimental Ball Pass Frequency - Outer Race [Hz]	64.65	67.95	67.65	68.19	67.84	67.92
Max Spectral Kurtosis	1009	22	23	21	20	22
Difference in Peak Amplitude [m/s2?]	0.029	0.013	0.848	0.694	0.197	1.013
Relative Error (Ball Pass Frequency) [%]	5.04%	2.46%	2.89%	2.83%	2.97%	2.86%
Consistency in Experimental BPFO	98.01 %					

9.4 Preliminary Experimental Results using SpinScope and SmartMeter

The experiments presented in the previous section to validate the envelope analysis are repeated with minor alterations to compare the performance of SpinScope and SmartMeter. These changes consist of placing two accelerometers, one each for SpinScope and SmartMeter, on the test bearing as shown in Figure 30. The “XLG” accelerometer (PCB model nr. 393A03) is used with the SpinScope system, while an accelerometer from TPI Inc. (model nr. A9012) is used with the SmartMeter. The data obtained with SpinScope is acquired with a sampling rate of 65,536 Hz while the default settings are used with the SmartMeter. Acceleration data is recorded for three trials each for the healthy and damaged bearing.

Both SmartMeter and SpinScope are used simultaneously for each of the trials. Acceleration data of 30 seconds in duration is obtained with SpinScope as was done for the previous test. The SmartMeter, however, is only able to obtain 0.08 seconds of data at a time. While the SmartMeter has not exhibited the same issue regarding settling time as SpinScope, this shorter sampling period adds complexity to both the analysis using SmartMeter/Vibtrend and comparing the results obtained with SpinScope. For this reason, the data obtained with SmartMeter is by design made to coincide with the halfway point of the of the acceleration signal obtained with SpinScope; however, this timing was not precisely controlled.

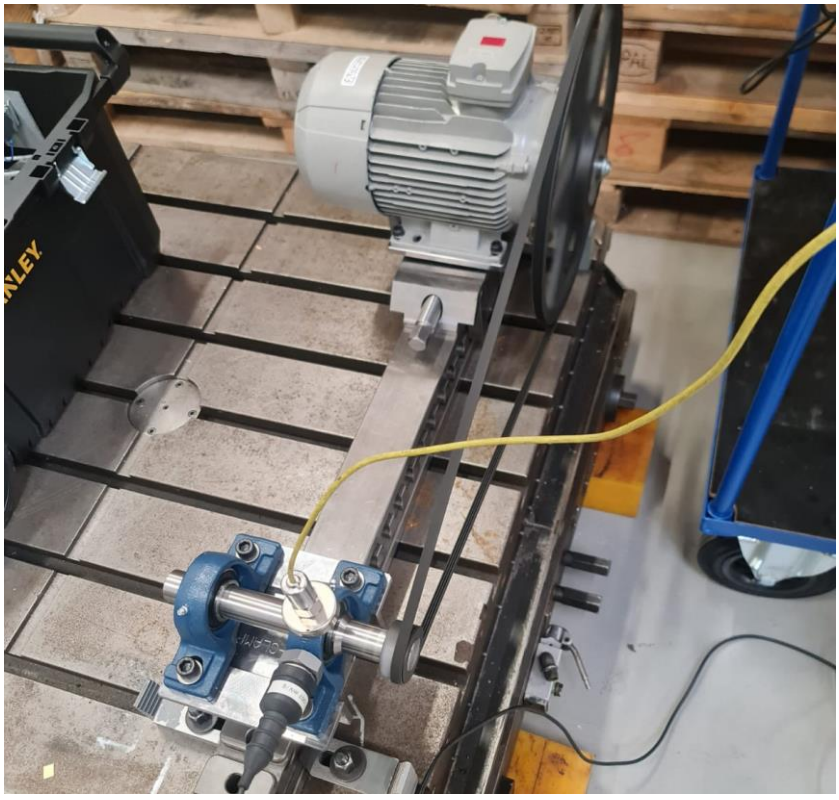

Figure 30: The custom test rig used compare the performance of SpinScope and SmartMeter. Two accelerometers, one for each system, is placed on the test bearing as shown

For brevity, the results of the third trial for the healthy and faulty bearing test are presented here, while the results obtained for the other trials are provided in appendix 13.2. The acceleration signals obtained by SpinScope are presented in Figure 31, while those obtained by SpinScope are shown in Figure 32. As in the previous test, the figures show that the amplitude of the acceleration signals are significantly higher for the damaged bearing, as was the case for the experiments presented in section 9.2. For the signals obtained by SpinScope, there is approximately a seven-fold increase in the vibration amplitude for the damaged bearing compared to the healthy bearing, while with SmartMeter the increase is observed to be on the order of 20.

The data obtained with the SmartMeter, which was sampled at approximately 27 kHz, also exhibits the characteristic embedded impulse associated with the impact between the race fault and the rolling element in the bearing. Close inspection of the data in Figure 32 shows that this impulse occurs approximately every 0.015 seconds (or 66.66 Hz) and that the amplitude of the decayed impulse is approximately equivalent to the vibration amplitude for the healthy bearing. More will be said about this apparent impact frequency below.

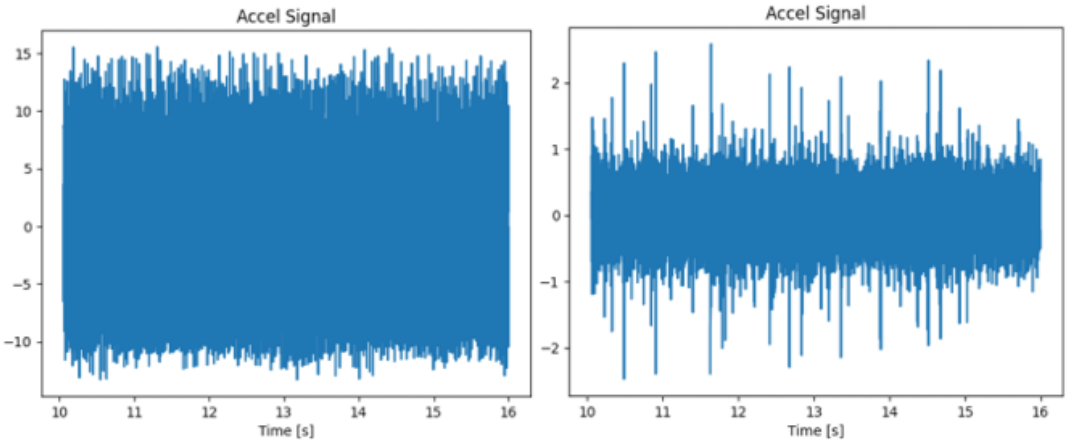

Figure 31: Truncated acceleration signal obtained from SpinScope during the third trial for both the damaged (left) and healthy (right) bearing.

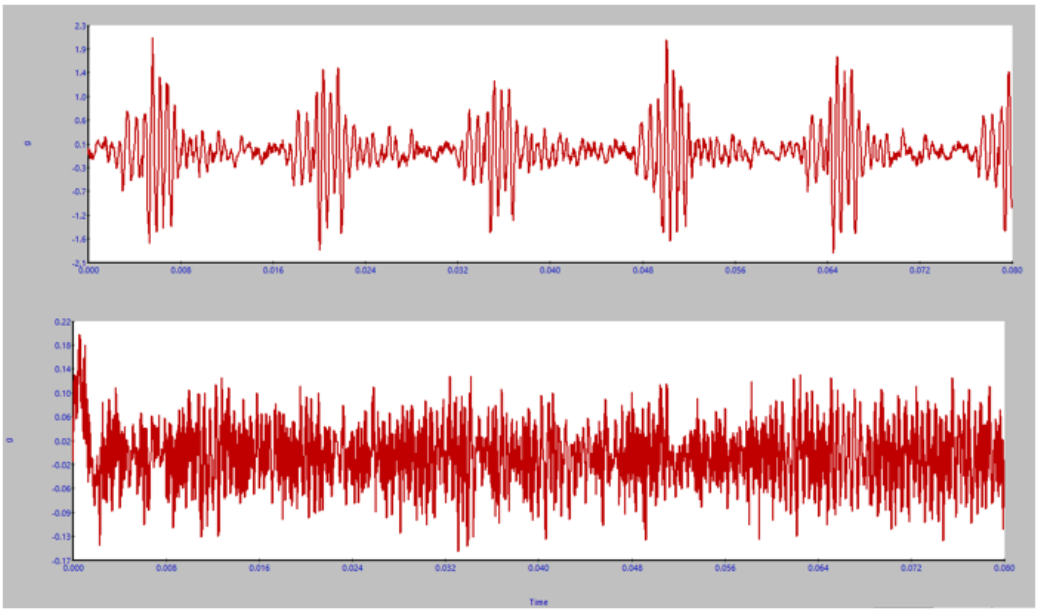

Figure 32: Acceleration signal obtained from SmartMeter during the third trial for both the damaged (top) and healthy (bottom) bearing.

The kurtogram for the damaged and healthy bearing are shown in Figure 33 and Figure 34, which only treat the data obtained with SpinScope. Comparing the kurtograms in the two figures, it is observed that the relative difference between the results obtained for the damaged and healthy bearing follows the same pattern observed for these results obtained in section 9.3, in which the kurtogram for the damaged bearing presents a larger maximum spectral kurtosis in a frequency band with a higher central frequency. Surprisingly, the optimal window length for the healthy bearing is smaller than for the damaged bearing,

which reinforces the concept that no single metric from the kurtogram can be used to determine the state of the bearing, but all of them together can be used together in conjunction with the envelope spectrum as part of a holistic diagnostic approach.

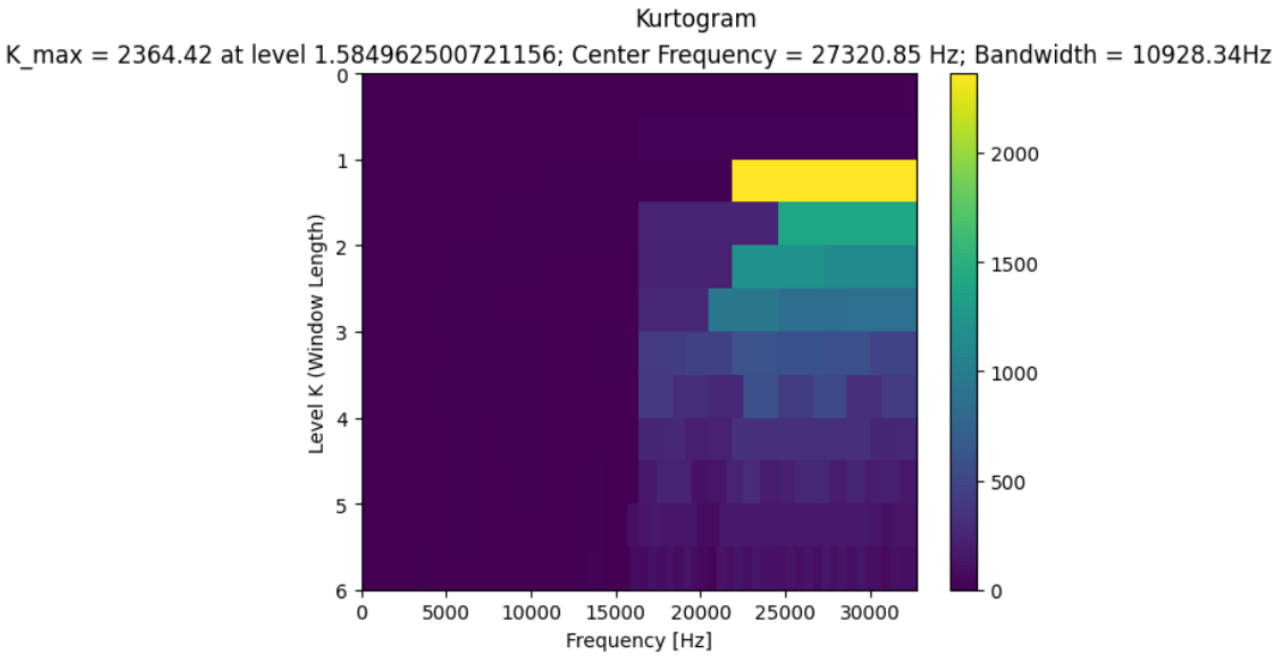

Figure 33: Kurtogram generated during trial 3 for the damaged bearing.

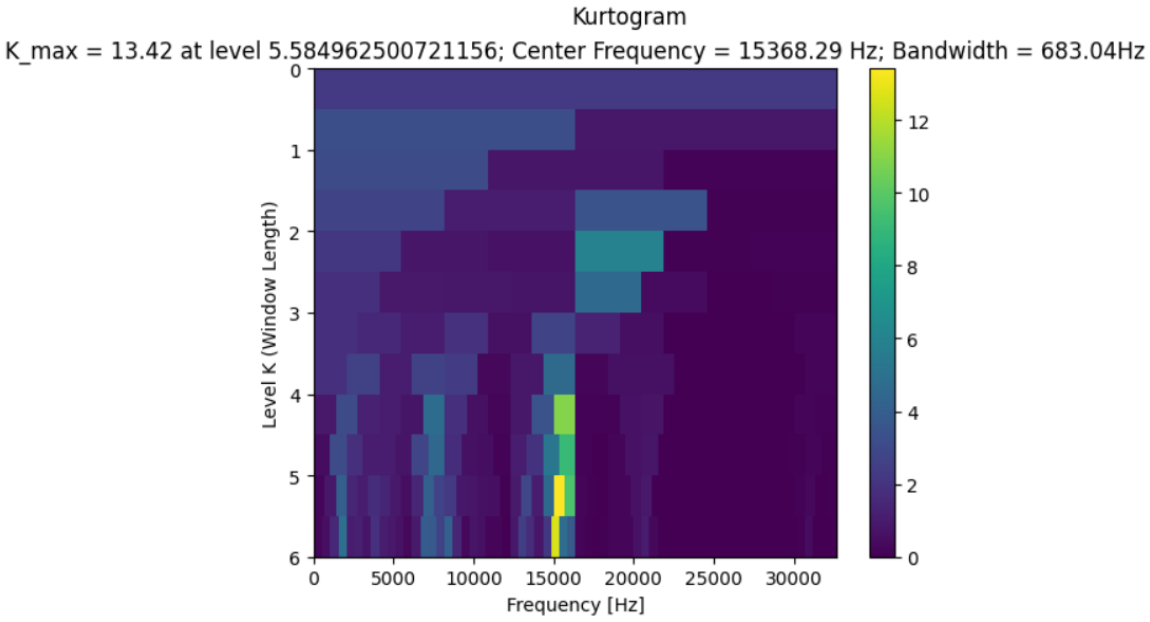

Figure 34: Kurtogram generated during trial 3 for the healthy bearing.

The envelope spectra for the damaged and healthy bearing are presented in Figure 35, while the unprocessed frequency spectra obtained by SmartMeter are shown in Figure 36. As expected, the results obtained by SpinScope for the damaged bearing exhibit a frequency associated with the bearing impact

frequency, which experimentally is found to occur at 71 Hz, that is amplified and clearly distinct from other frequency components (i.e. no “smearing” effect). The envelope spectrum for the healthy bearing, on the other hand, has characteristics similar to the envelope spectrum of the healthy bearing in section 9.3, providing no useful information about the bearing.

The “raw” frequency spectra obtained by SmartMeter (Figure 36) show the same fault impact frequency as the frequency presented in Figure 35 (represented by the red cursor in Figure 36) as well as the shaft rotational frequency (represented by the cursor labelled as ‘1x RS’ in Figure 36), and furthermore a similar difference in amplitude shown in Figure 35 is also observed in the spectra obtained with SmartMeter. However, as can be observed in the results in Figure 36, the bearing fault impact frequency (reported as 67.5 Hz by SmartMeter) is not the most dominant component, which occurs at approximately 406 Hz. This frequency happens to approximately coincide with the 6th harmonic of the fault impact frequency reported by SmartMeter. It may be that this 6th harmonic is so prominent in the spectrum while the lower harmonics are not because the 6th harmonic coincides with a structural resonance frequency as discussed in section 7.2. Similar results are obtained with SpinScope when Envelope Analysis is not used, with some differences compared with the spectrum obtained by SmartMeter. These differences are likely due to the differences in sampling rate and FFT resolution.

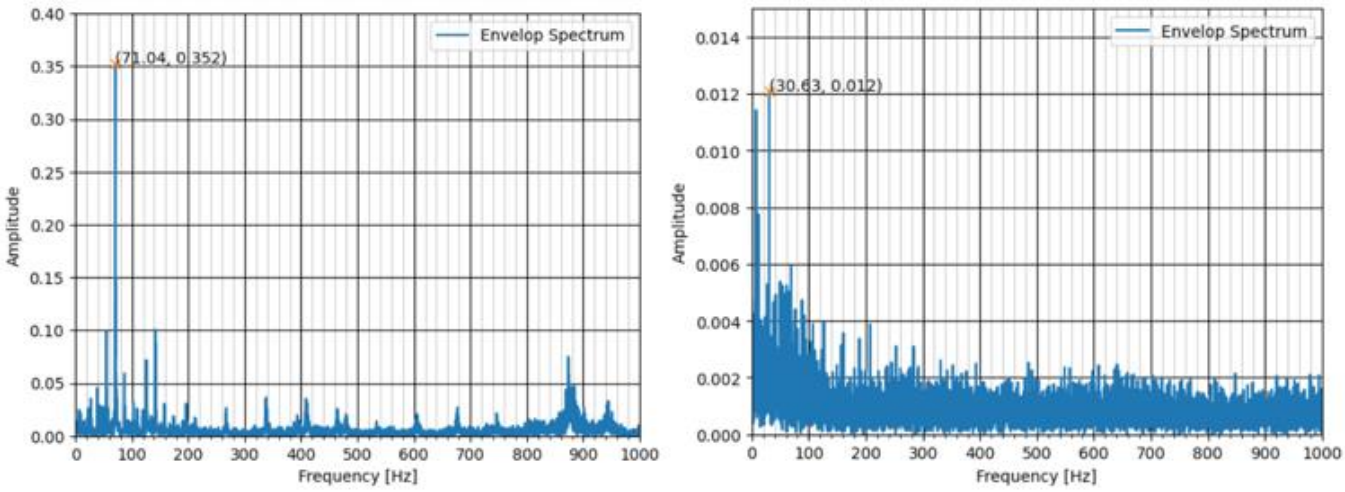

Figure 35: Envelope spectrum for the damaged (left) and healthy (right) bearing.

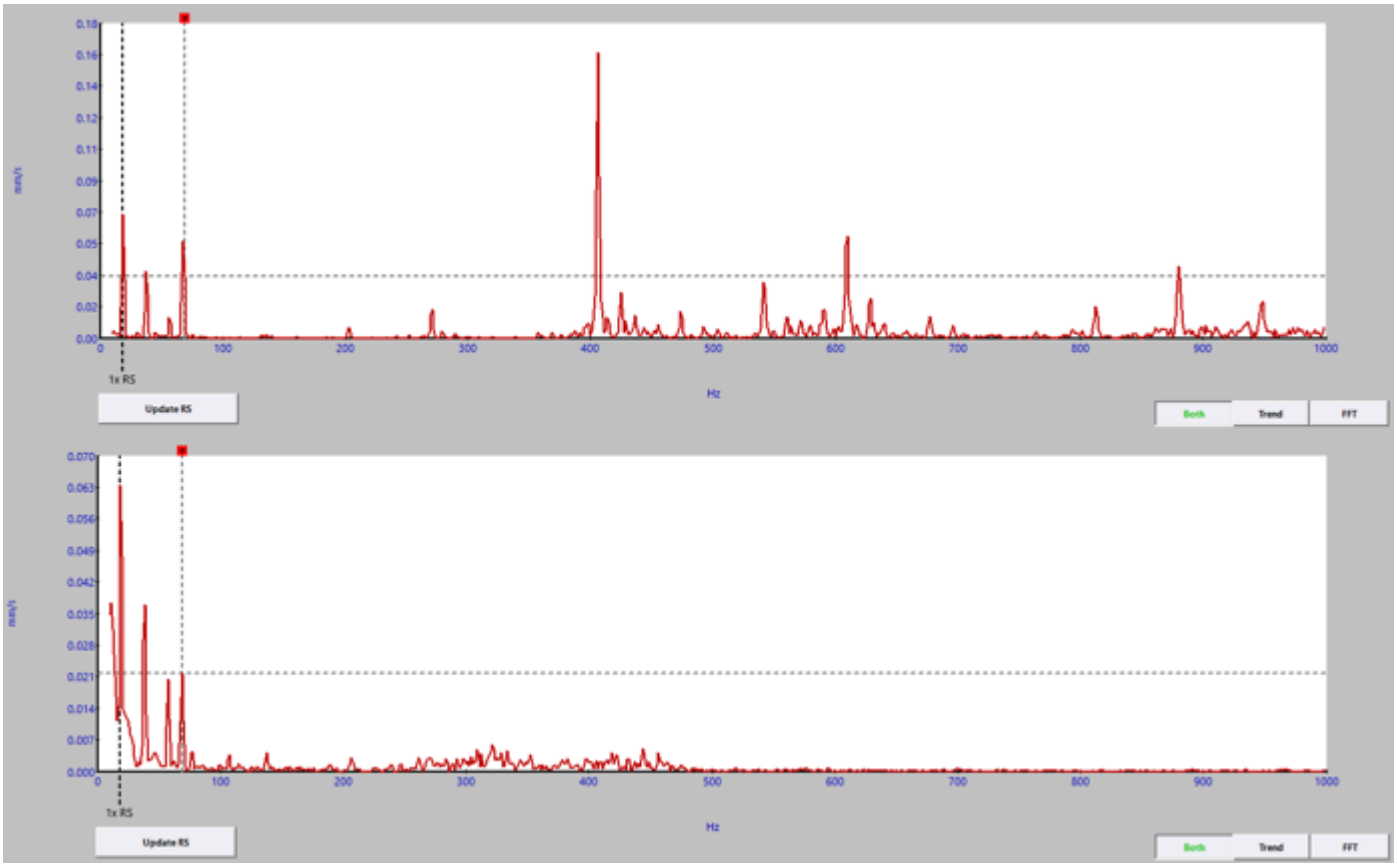

Figure 36: Frequency spectra obtained by SmartMeter for the damaged (top) and healthy (bottom) bearing.

A summary of the test results is presented in Table 4. As was the case for the results presented in section 9.3, the experimental frequencies reported in the table for SpinScope and SmartMeter are the frequencies identified in Figure 35 and Figure 36, respectively, while the reported differences in peak amplitude are the absolute differences between the same identified frequency for the healthy and damaged bearing. All other data refer to measurements involving the damaged bearing. The results demonstrate that while both SmartMeter and SpinScope consistently detect the ball pass frequency with reasonable accuracy, the error associated with SmartMeter is much greater, again owing to the coarser resolution of the frequency spectrum. SpinScope, on the other hand, is much more accurate, consistently detecting the ball pass frequency with an error less than 1%, which is superior even to the results obtained by SpinScope in section 9.3. This improvement in the performance is likely due to using a different accelerometer than the previous test, which used an accelerometer with a lower sensitivity. The accelerometer used in the current test has a higher sensitivity and a finer broadband resolution, but a smaller measurement and frequency range. Additionally, the results show that the difference in peak amplitude observed with SpinScope are very inconsistent from one trial to the next, further demonstrating that considering peak amplitude alone is insufficient to properly diagnose spindle bearings. The same metric obtained with SmartMeter is consistent between trials, by contrast; however, the same conclusion regarding peak amplitude applies equally to SmartMeter as it does to SpinScope.

Table 4: Summary of the results of trial 3 testing the differences between SpinScope and SmartMeter

	SpinScope			Smart Meter		
Parameter	Trial 1	Trial 2	Trial 3	Trial 1	Trial 2	Trial 3
Measured Shaft Speed [RPM]	1140	1130	1128	1140	1130	1128
Theoretical Ball Pass Frequency - Outer Race [Hz]	72.20	71.57	71.44	72.20	71.57	71.44
Experimental Ball Pass Frequency - Outer Race [Hz]	72.22	70.95	71.04	67.5	67.5	67.5
Max Spectral Kurtosis	2168	2570	2364	-	-	-
Difference in Peak Amplitude [m/s2?]	0.0045	0.085	0.2049	0.038	0.043	0.044
Relative Error (Ball Pass Frequency)	0.03%	0.86%	0.56%	6.51%	5.68%	5.52%
Consistency of Experimental BFPO	99.01%			100%		

9.5 Experimental Test Results of 'DMU' machining Centre at DAMRC

The experimental procedure implemented in the previous section to compare the SmartMeter and SpinScope on the custom test rig is applied to measure the health of the spindle bearings of the DMU 80T CNC machining centre. The same accelerometers and software settings as before are used for the tests with DMU machining centre, with 3 acceleration measurements each for spindle speeds of 1100, 5000, and 10,000 RPM recorded simultaneously with SmartMeter and SpinScope. The accelerometers are placed on the spindle as shown in Figure 37. Once again, 30 second measurements are taken with SpinScope, while best efforts are made to align the measurements taken with SmartMeter during a representative midpoint of the SpinScope measurement. For brevity, only the results obtained during the second trial of each spindle speed is presented here, with the other results available in appendix 13.3.

Unlike the previous tests, it is not possible to compare the kurtogram and envelope spectrum to "baseline" results as it is infeasible to disassemble the DMU machining centre and replace the spindle bearings. Therefore, conclusions about the health of the bearings must derive exclusively from calculating theoretical fault frequencies from the geometry of the bearing and comparing these frequencies with the results of the envelope analysis. Reviewing the technical drawings in the parts catalogue of the DMU 80 T (a physical copy is available at DAMRC), the bearings supporting the spindle are identified as Schaeffler angular contact ball bearings (HCB71916E.T). The required geometric parameters necessary to calculate theoretical fault frequencies can be obtained from the technical data and CAD files on the vendor's website. However, the technical data for the bearing also includes basic frequency factors that simplifies the required calculations. These frequency factors, presented in Table 5, relate a given shaft input frequency to the various fault frequencies. Although the nomenclature used in industry and academic research differs, the underlying principle is the same.

Table 5: Basic frequency factors for DMU 80 T spindle bearings [26]

Basic Frequency Factors related to 1/s for model nr. HCB71916-E-T-P4S-UL	
Over rolling frequency factor on outer ring (BPFFO)	11.3641
Over rolling frequency factor on inner ring (BPFFI)	13.6359
Over rolling frequency factor on rolling element (BSFF)	4.9457
Ring pass frequency factor on rolling element (RPFFB)	9.8914
Speed factor of rolling element set for rotating inner ring (FTFF_i)	0.4546
Speed factor of rolling element set for rotating outer ring FTFF_o)	0.5454

The kurtogram generated from acceleration measurements during the test at 1100 RPM is presented in Figure 38. The Kurtogram in the figure presents a maximum spectral kurtosis of 455 in a frequency band centered approximately at 31.5 kHz and having a bandwidth of approximately 2.7 kHz. These results are consistent with Kurtograms obtained previously for the damaged bearing in the custom test rig.

Figure 37: Accelerometer placement on the DMU.

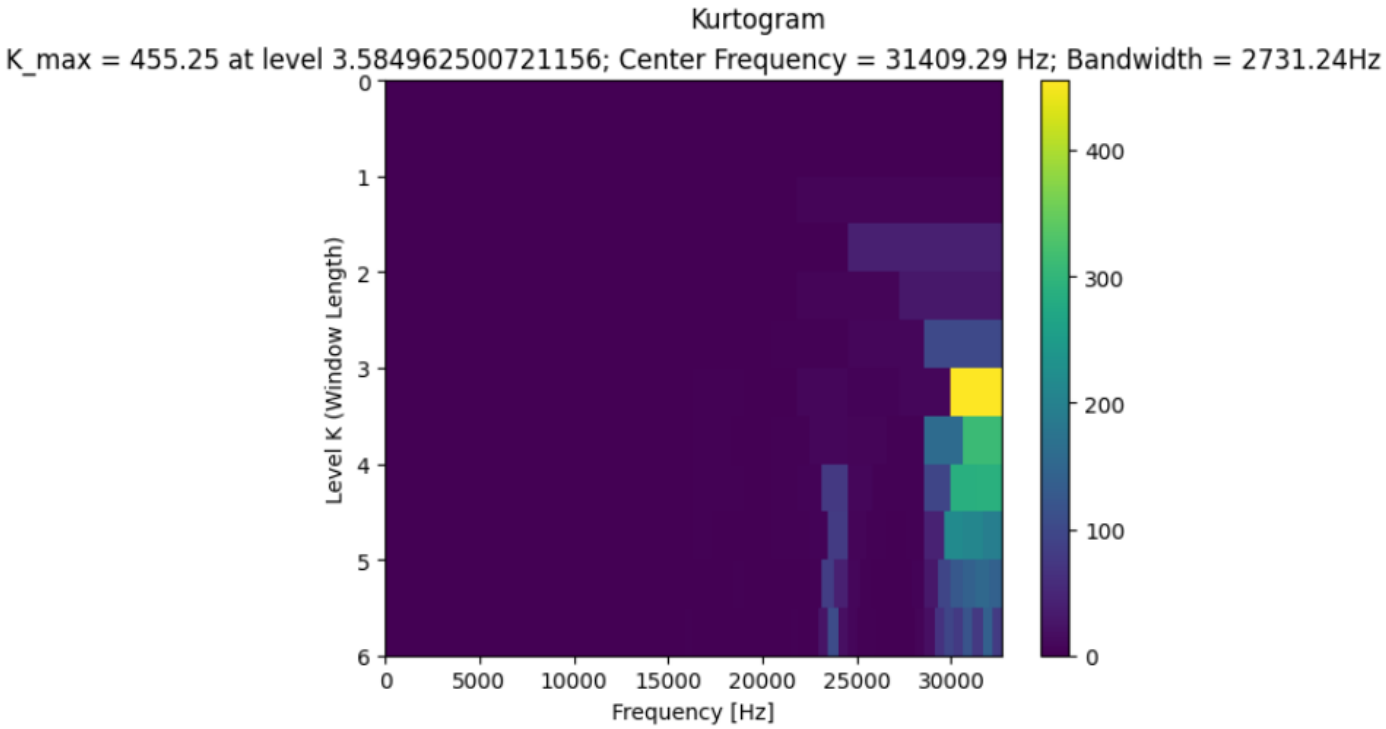

Figure 38: Kurtogram generated for trial 2 at 1100 RPM

The associated envelope spectrum is presented in Figure 39, which highlights the outer and inner race fault frequencies and their harmonics. The fault frequencies are calculated using the basic factors in Table 5. The figure shows that a main frequency peak coincides with the theoretical inner race ball passing frequency (BPFFI in the table). However, it is unclear whether the harmonics of BPFFI frequency coincide with significant frequency components since the frequencies above 250 Hz are smeared together, and any pertinent frequencies are not amplified by envelope analysis. The theoretical outer race ball passing frequency (BPFFO) is also consistent with a major frequency in the spectrum, although this frequency is not as pronounced as other low frequency content. It is therefore unclear whether the detection of the outer race frequency represents a false positive diagnosis or not. The above results are consistent with the results obtained from envelope analysis of the other two trials at 1100 RPM, which are presented in Table 6.

The raw frequency spectrum obtained from the SmartMeter is presented in Figure 40, while a detailed view of the frequency spectrum between 150 and 300 Hz is shown in Figure 41. The figures show that there are no significant frequency components aligning with either the BPFFI or BPFFO frequencies, although a main peak at 418 Hz corresponding to the second harmonic of the BPFFO frequency. Given the lack of significant frequency components at the theoretical fault frequencies, it is not clear whether the 418 Hz is related to a bearing fault or some other source, which can be said of the other major frequencies in Figure 40. These results occur consistently for all trials at 1100 RPM.

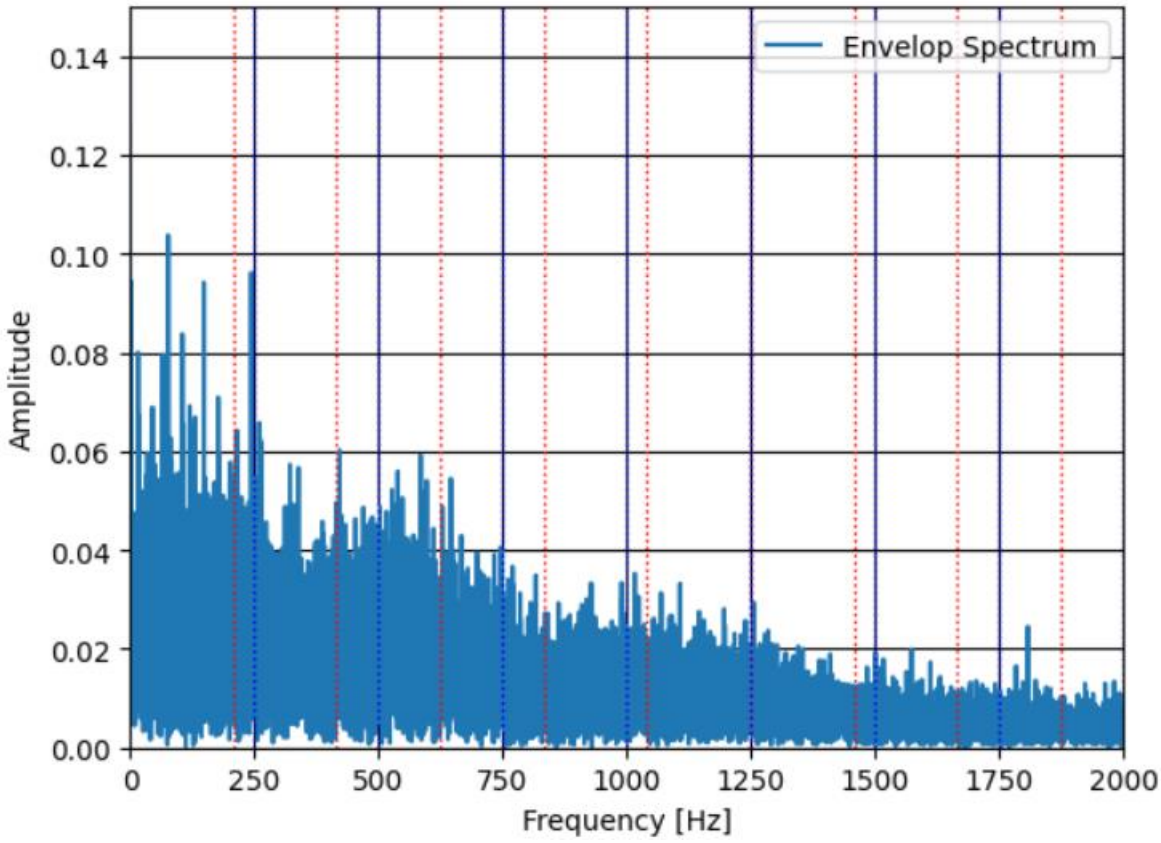

Figure 39: Envelope Spectrum generated for trial 2 at 1100 RPM. BPFO (red) and BPFI (blue) along with their harmonics are shown.

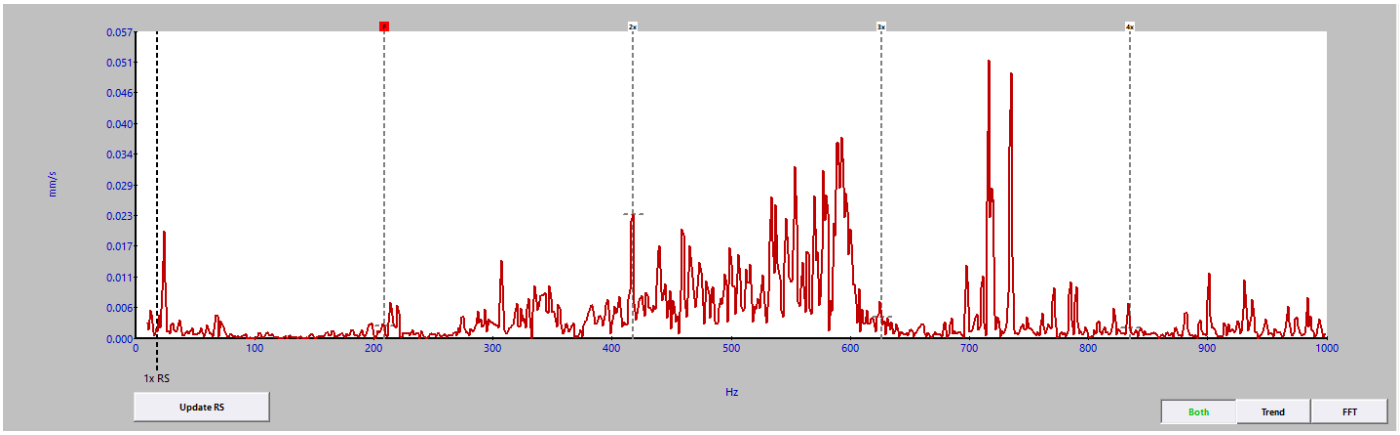

Figure 40: Raw frequency spectrum generated with SmartMeter for trial 2 at 1100RPM

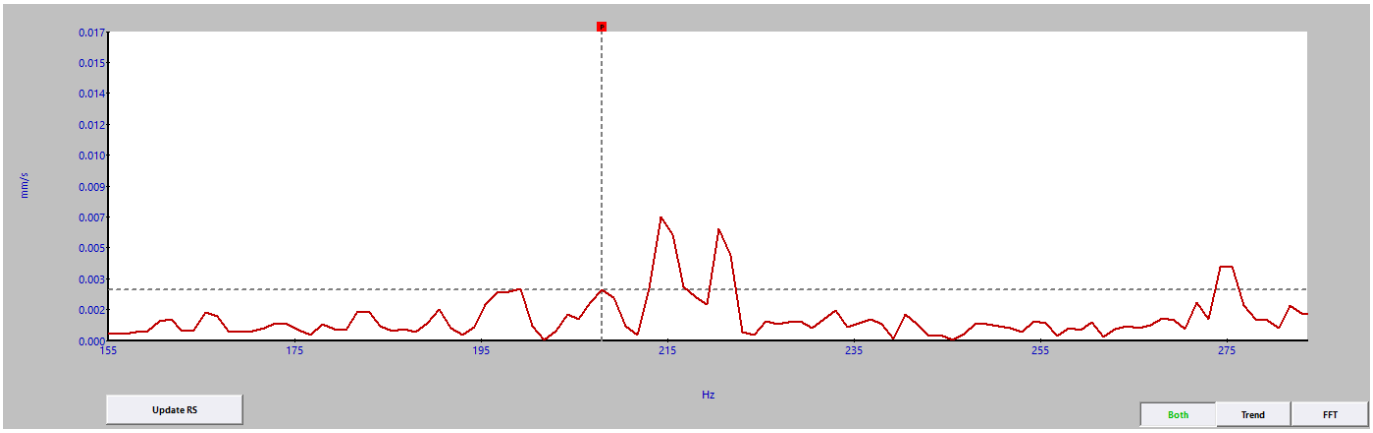

Figure 41: Detailed view of Figure 40

Table 6: Summary of envelope analysis results

Summary of DMU Test Results 1100 RPM			
Trial	**1**	**2**	**3**
Outer Race Ball Passing Frequency (BPFO) [Hz]	**208.27**	**946.67**	**1893.33**
Inner Race Ball Passing Frequency (BPFI) [Hz]	**250.07**	**1136.67**	**2273.33**
BPFO Magnitude – Envelope/SpinScope	**0.04**	**0.06**	**0.06**
BPFI Magnitude – Envelope/SpinScope	**0.08**	**0.10**	**0.10**
Maximum Spectral Kurtosis	**317.69**	**455.25**	**611.54**
Filter Central Frequency [kHz]	**31.4**	**31.6**	**31.8**
Filter Bandwidth [Hz]	**2729**	**2731**	**2729**

The kurtogram generated from acceleration measurements during the test at 5000 RPM is presented in Figure 42. The kurtogram exhibits a maximum spectral kurtosis of 50 in a frequency band centered at 31.4 kHz having a bandwidth of 2.7 kHz. These results are therefore consistent with the kurtogram obtained at 1100 RPM, with the only substantial difference being the magnitude of the maximum spectral kurtosis (455 at 1100 RPM vs 47 at 5000 RPM).

The associated envelope spectrum is presented in Figure 43, which includes the same fault frequencies as in the previous case. The figure shows that a main frequency peak coincides with the fundamental frequency of both the theoretical inner and outer race ball passing frequency, with the BPFI frequency again being more dominant. Unlike the results obtained for the trials at 1100 RPM, the higher harmonics of both BPFI and BPFO frequencies coincide with major frequency peaks between 5683 Hz (the 5th harmonic of BPFI) and 8000 Hz. The magnitudes of the frequencies corresponding with BPFI and its harmonics are higher relative to those of BPFO, possibly suggesting the presence of an inner race fault. These results are summarized in Table 7.

The raw frequency spectrum obtained from SmartMeter is shown in Figure 44, while a detailed view of the spectrum between 540 and 1960 Hz is shown in Figure 45. Similar to the results obtained for the trials at 1100 RPM, there is no evidence of major frequency peaks at the BPFI or BPFO frequencies in the SmartMeter spectrum, although dominant frequencies approximately coincide with the harmonics of BPFO but not BPFI. This seemingly contradicts the results obtained from envelope analysis; however, the results

obtained with SmartMeter warrant less confidence since the corresponding acceleration signal is unfiltered and has a coarser frequency resolution/sampling rate.

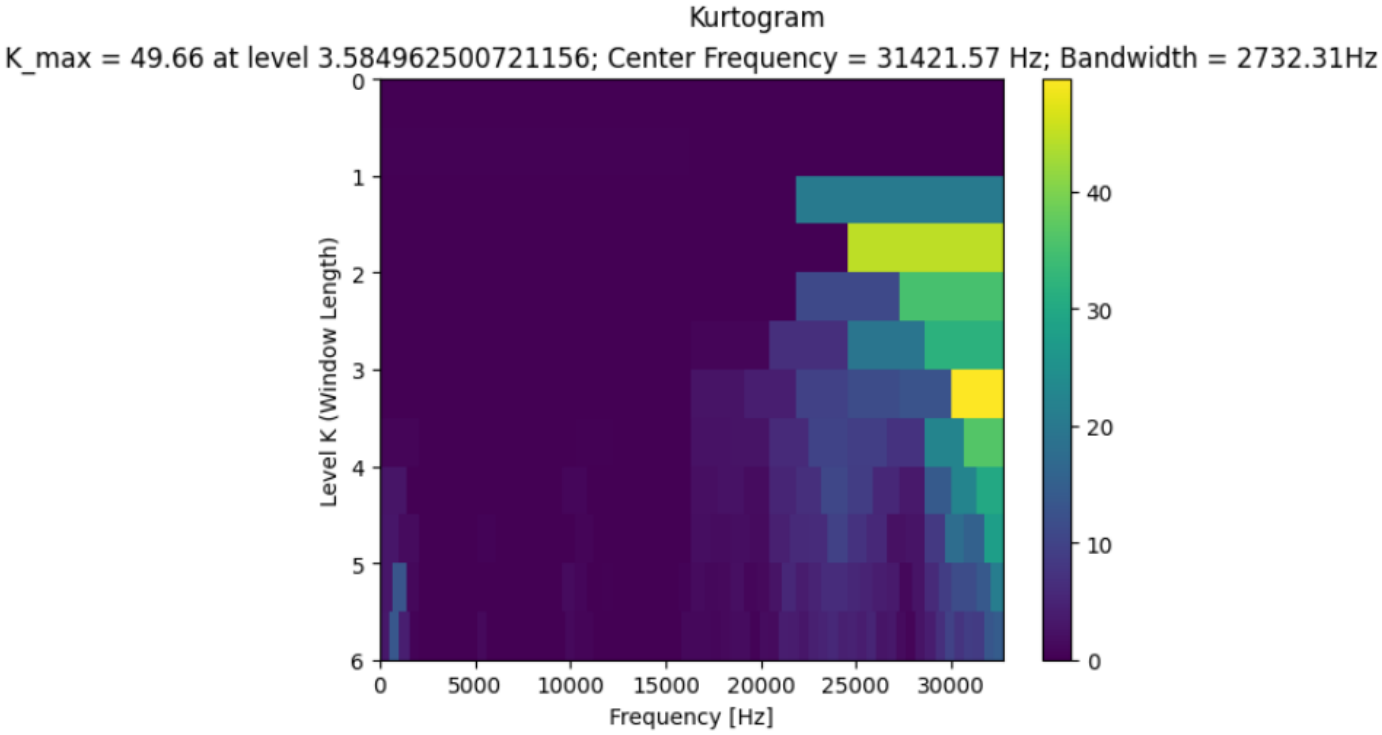

Figure 42: Kurtogram generated for trial 2 at 5000RPM

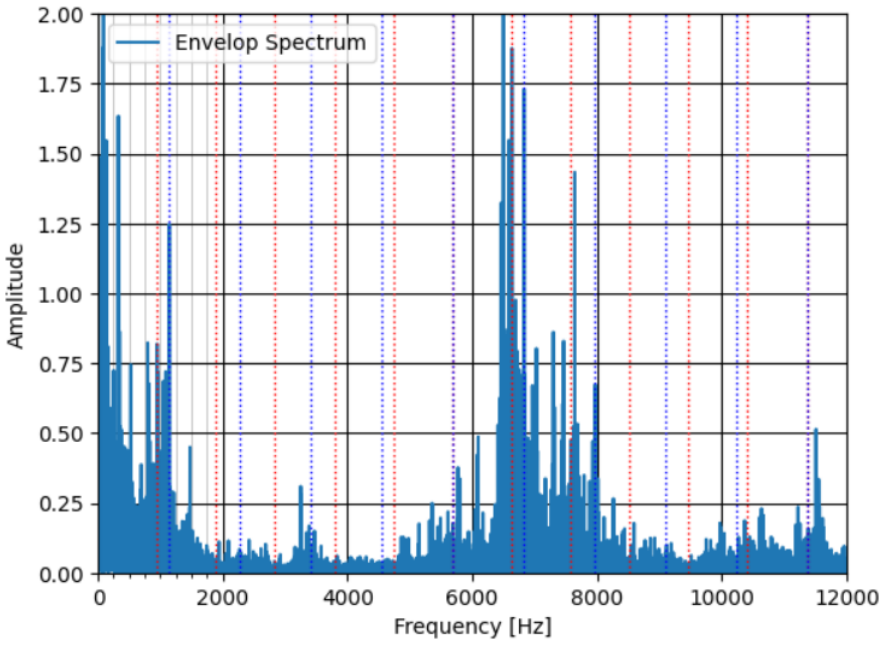

Figure 43: Envelope spectrum generated for trial 2 at 5000RPM. BPFO (red) and BPFI (blue) are shown.

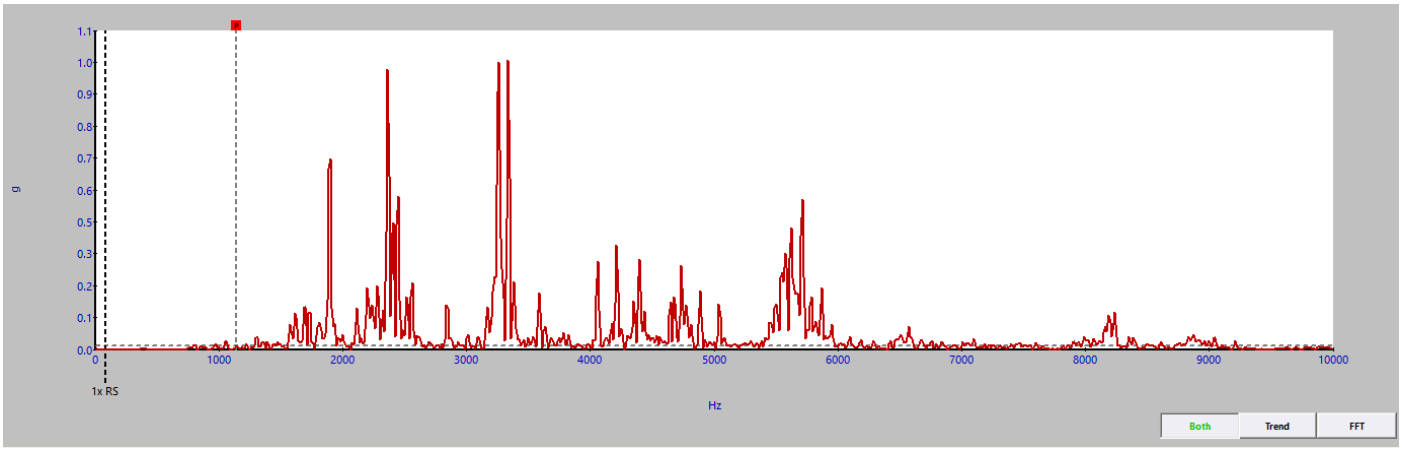

Figure 44: Raw frequency spectrum generated from SmartMeter during trial 2 at 5000RPM

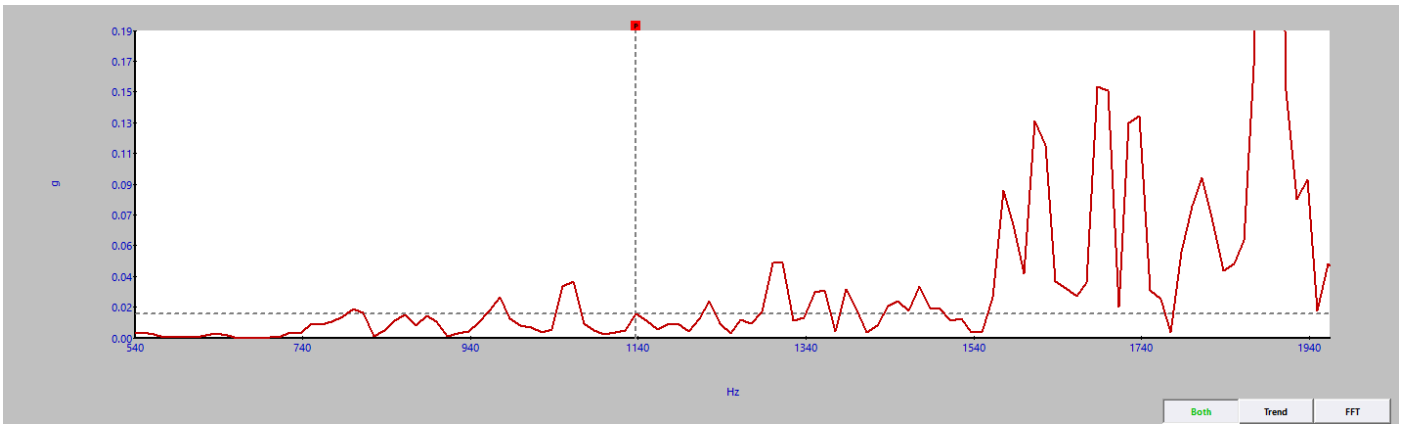

Figure 45: Detailed view of Figure 44.

Table 7: Summary of envelope analysis results

Summary of DMU Test Results 10000 RPM			
Trial	**1**	**2**	**3**
Outer Race Ball Passing Frequency (BPFO) [Hz]	**208.27**	**946.67**	**1893.33**
Inner Race Ball Passing Frequency (BPFI) [Hz]	**250.07**	**1136.67**	**2273.33**
BPFO Magnitude – Envelope/SpinScope	**0.75**	**0.80**	**0.75**
BPFI Magnitude – Envelope/SpinScope	**1.25**	**1.25**	**1.25**
Maximum Spectral Kurtosis	**45.89**	**49.66**	**42.84**
Filter Central Frequency [kHz]	**30.7**	**31.4**	**31.4**
Filter Bandwidth [Hz]	**4010**	**2732**	**2729**

The kurtogram obtained for the second trial at 10,000 RPM is presented in Figure 46, which exhibits a maximum spectral kurtosis of 2.4 in a frequency band centered at 256 Hz having a frequency bandwidth of 512 Hz. This particular kurtogram exhibits the expected characteristics of having a high maximum spectral kurtosis (in the numerical case studies presented in section 9.2, the spectral kurtosis for the healthy bearing was less than 1), a narrow bandwidth and high frequency resolution, but defies expectations by having a low center frequency. However, the figure also presents higher spectral kurtosis at a higher

frequency, approximately 27.5 kHz with the same window length. The difference in spectral kurtosis between these two candidate filtering parameters is not precisely known, but it is clear from the gradient in the figure the difference is on the order of 0.1 or less. It is not clear how significant such a difference is, but it is possible that subsequent results will be affected by using suboptimal filtering parameters.

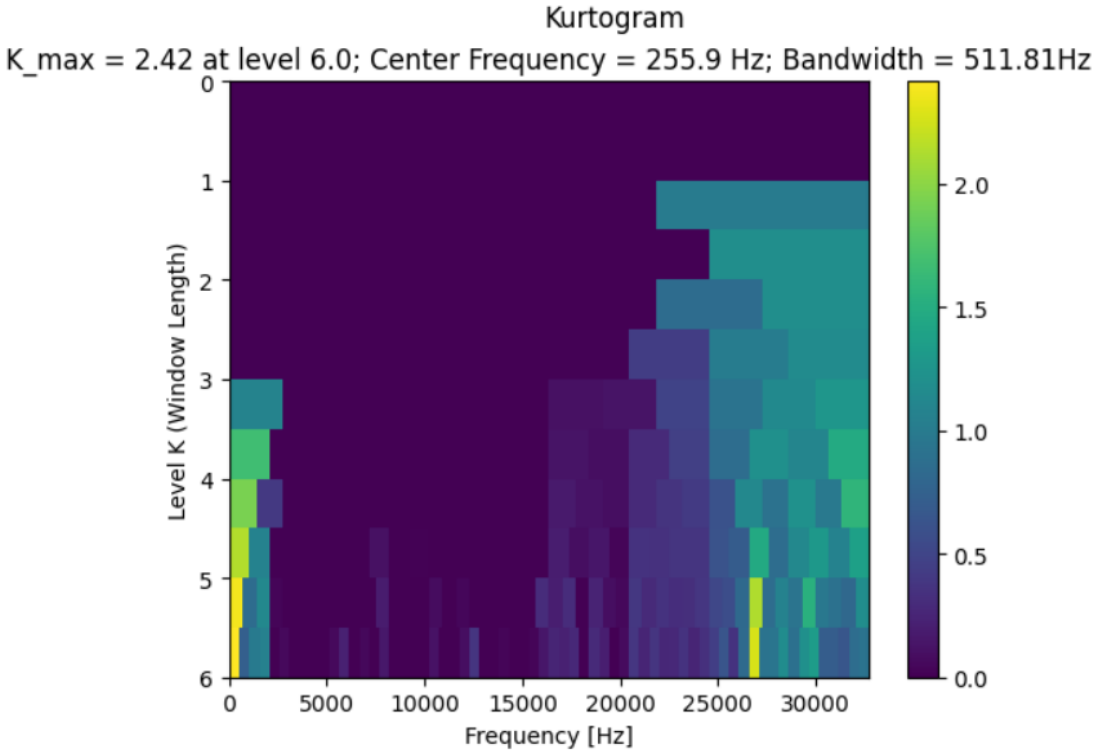

Figure 46: Kurtogram generated during trial 2 at 10,000RPM

The resulting envelope spectrum is presented in Figure 47, which again highlights the BPFI and BPFO frequencies and their harmonics. The figure shows that a major frequency peak coincides with the fundamental BPFO frequency and its harmonics, whereas there is no such correlation for BPFI below 6000 Hz. These results are inconsistent with those obtained in the other trials, in which a maximum SK of less than 1 was obtained at a centre frequency of approximately 29.7 kHz and the results from the envelope analysis were less conclusive. However, the results obtained with SmartMeter, presented in Figure 48Figure 49 and which are consistent across all trials, supports the results in the envelope spectrum of Figure 47. Figure 48 indicates that a major frequency peak is present approximately at the BPFO and its first two harmonics. Table 8 summarizes the results obtained at 10,000 RPM, while Table 9 compares selected results for all three spindle speeds.

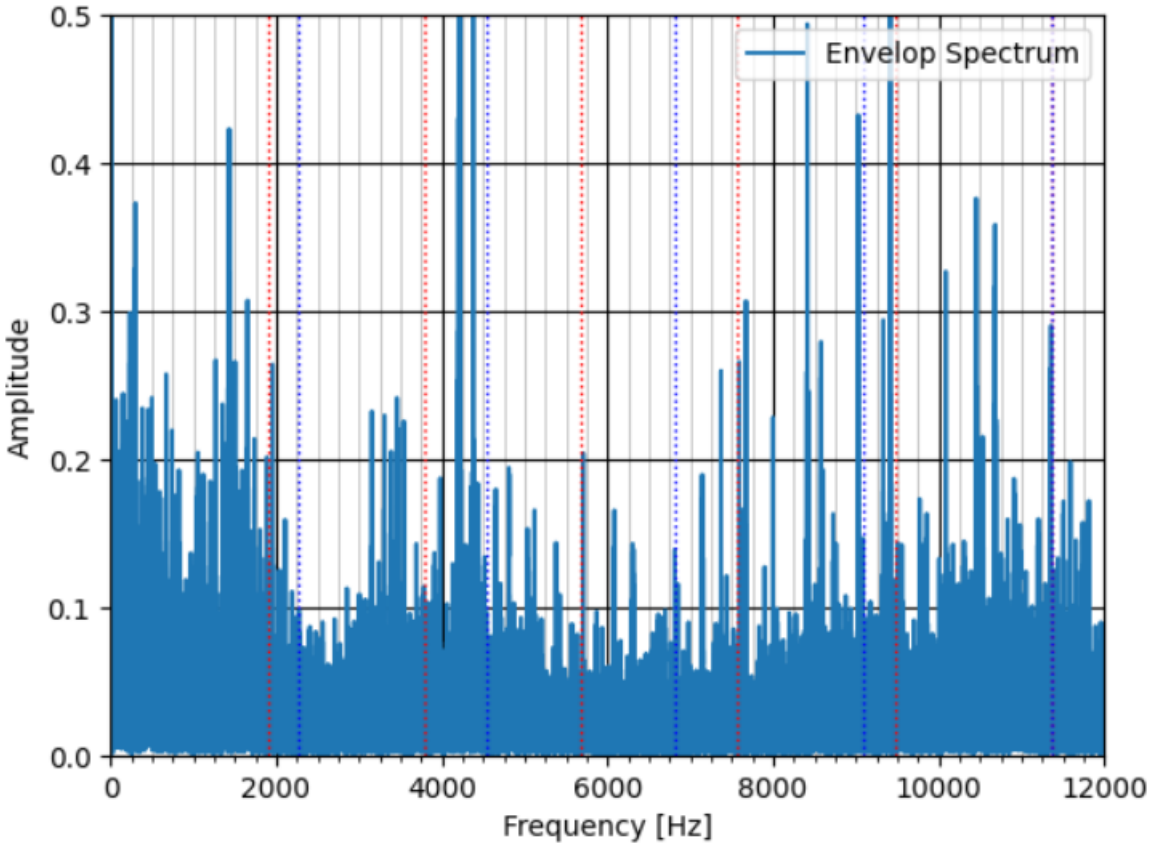

Figure 47: Envelope spectrum generated during trial 2 at 10,000RPM. BPFO (red) and BPFI (blue) are shown.

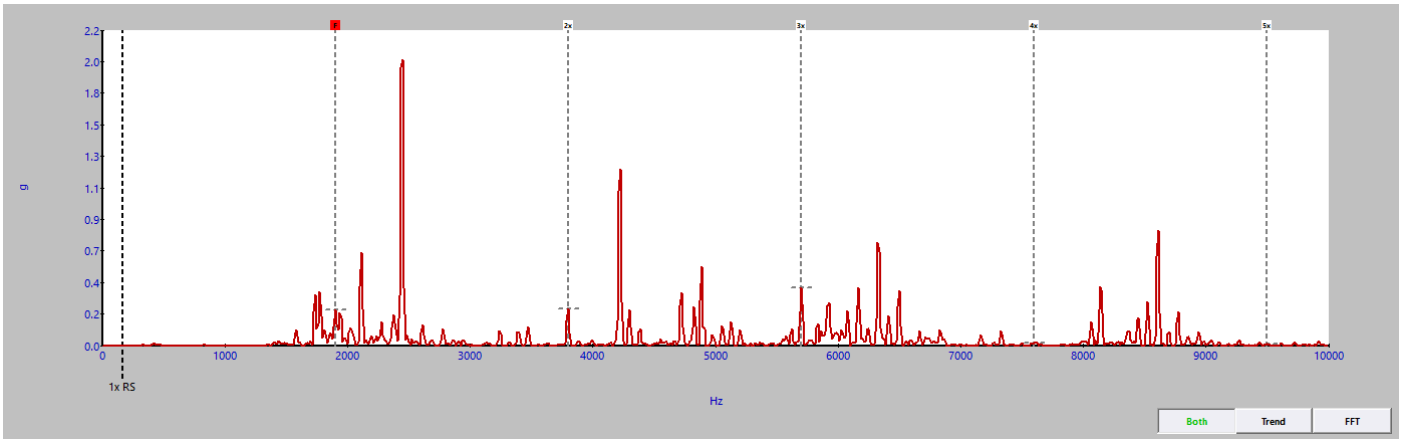

Figure 48: Raw frequency spectrum generated with SmartMeter during trial 2 at 10,000RPM

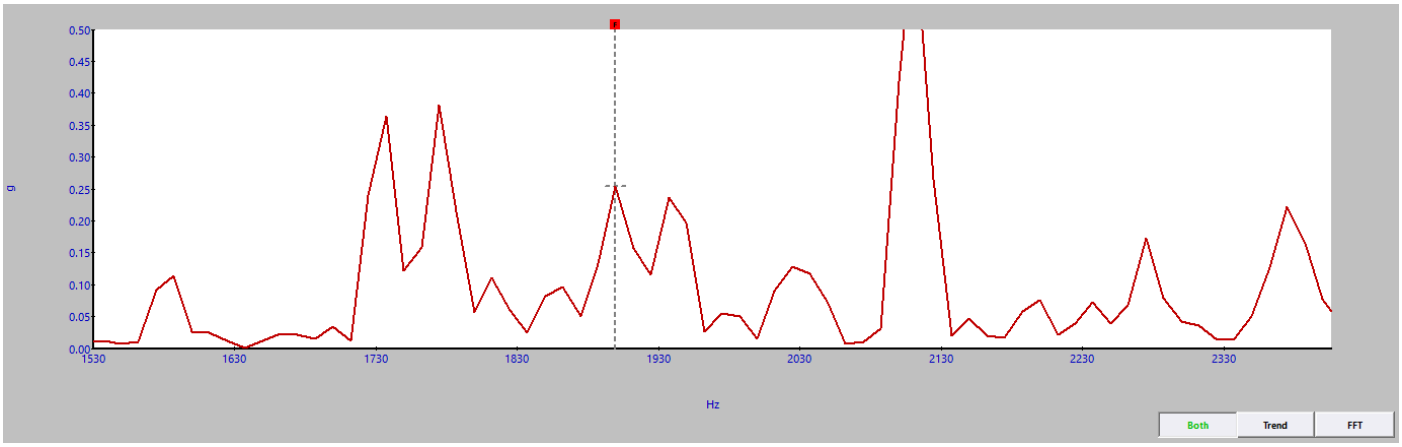

Figure 49: Detailed view of Figure 48

Table 8: Summary of envelope analysis results

Summary of DMU Test Results 10000 RPM			
Trial	1	2	3
Outer Race Ball Passing Frequency (BPFO) [Hz]	208.27	946.67	1893.33
Inner Race Ball Passing Frequency (BPFI) [Hz]	250.07	1136.67	2273.33
BPFO Magnitude – Envelope/SpinScope	0.15	0.125	0.18
BPFI Magnitude – Envelope/SpinScope	0.175	0.1	0.225
Maximum Spectral Kurtosis	1.71	2.42	1.91
Filter Central Frequency	29.7	0.26	29.7
Filter Bandwidth	683	512	682

Table 9: Summary of envelope analysis results

Summary of DMU Test Results for trial 2 of all spindle speeds			
Spindle Speed [RPM]	1100	5000	10000
Outer Race Ball Passing Frequency (BPFO) [Hz]	208.27	946.67	1893.33
Inner Race Ball Passing Frequency (BPFI) [Hz]	250.07	1136.67	2273.33
BPFO Magnitude – Envelope/SpinScope	0.065	0.80	0.275
BPFI Magnitude – Envelope/SpinScope	0.095	1.25	0.1
Maximum Spectral Kurtosis	455.25	49.66	2.42
Filter Central Frequency	31.4	31.4	0.256
Filter Bandwidth	2731	2732	512

9.6 Conclusion on the Test Results

The SpinScope software augmented with envelope analysis capabilities developed in python were tested in numerical case studies and empirical tests involving both a custom test rig in which the developed analysis methods were validated against expected theoretical results. These capabilities were later applied to tests of the spindle bearings of the DMU 80 T machining centre. The validation tests demonstrated that

SpinScope combined with envelope analysis could correctly diagnose damage of the inner and outer bearing damage and that metrics characteristic of damaged and undamaged bearing were consistent across trials and case studies.

Specifically, damage of both the inner and outer races were characterized by higher spectral kurtosis, relatively high ratio of the bandpass filter center frequency to filter bandwidth, and high amplitude of the fault frequency in the resulting envelope spectrum. However, caution should be exercised when diagnosing bearing damage from a single metric. For example, it was observed in the numerical case studies that SK for the healthy bearings never exceeded 1, while SK between 2 and 3 or higher was associated with bearing damage; however, the first empirical tests involving healthy bearings also yielded an SK of about the same magnitude. Therefore, a holistic approach should be taken when diagnosing bearings. In general, however, damaged bearings were characterized by SK greater than 3, central filter frequency greater than 10 kHz, filter bandwidth less than 3000 Hz, and fault frequency magnitude equal to or greater than 0.1.

These characteristics were observed when testing the bearings in the DMU machining center when the spindle was operating at 1100, 5000, and 10000 RPM, suggesting that the bearings are damaged or significantly worn. This is to be expected as the DMU is an old and heavily used machine. However, diagnosing the specific type of bearing damage was more difficult than in the previous case studies due to the complex results obtained in the envelope spectra, where both significant BPFO and BPFI frequencies were detected.

This difficulty can be attributed to a number of factors. First, unlike the damaged bearing used in the validation tests, any damage in the DMU bearings would have developed organically over time resulting in more complicated failure effects including distributed faults, affecting the quality of the measured impact impulses. Second, the DMU tests obviously better resemble real-world test scenarios than the custom test rig. As a result, the recorded vibration measurements would contain frequencies from other machine components, for example gear mesh or other mechanical parts. The envelope analysis and corresponding results are particularly vulnerable to the effect of these other frequencies since only a ‘minimal’ analysis method was developed as discussed in section 9.1. Finally, it was observed that the results contained in the envelope analysis were sensitive to the spindle speed, suggesting that speed dependent properties of the bearings and/or spindle must be taken considered. It is possible that test results were affected by running the spindle at a suboptimal speed. The performance of SmartMeter was also tested on both the validation test rig and the DMU machine. However, the limitations of the resulting unprocessed frequency spectra (due to limited sampling rate/frequency resolution, sampling period, lack of analysis options) made it difficult to diagnose the type of bearing damage, although SmartMeter does feature useful metrics (for example, bearing damage units or BDU) to quantify excessive vibration levels.

10. Discussion

The planned work packages and bearing tests were adapted to the operational needs of the project. These changes were made to reflect the limitations in the SpinScope software that were not accounted for in planned work activities. As discussed in sections 7.4 and 8.1, these limitations rendered the SpinScope software usable only for data acquisition as the connected spindle software modules were unusable. Work was therefore done to develop the analysis methods needed to extract meaningful diagnostic information from the frequency spectra of measured acceleration signals, and greater emphasis was placed on validating these new methods in the experiments and numerical simulations Comparative tests of measurements obtained from different CNC machines were not done in favour of extensive testing with a

custom assembled test rig and a single case study involving the DMU 80 T machining center. Consequently, planned tests of the KUKA robot, CNC lathe, and newer CNC milling machines were not completed.

To see why these changes were necessary, consider the frequency spectrum in Figure 50 obtained from the raw, unprocessed acceleration signal measured with SpinScope during the second trial of the DMU tests at 5000 RPM. The figure shows that bearing fault frequencies clearly identified with envelope analysis in Figure 43 are non-existent. Detailed inspection of the spectrum (see Figure 51) reveals that there are minor frequency peaks approximately aligned with the expected bearing fault frequencies; however, the magnitudes of these frequencies are similar to those obtained during tests of healthy bearings. This is more clearly demonstrated in Figure 52 and Figure 53, which show the raw SpinScope frequencies of the damaged and healthy bearings, respectively, presented in section 9.4. From these figures, it can be seen that the expected fault frequency for the damaged bearing, while noticeable, is in fact smaller in magnitude than noise appearing in the healthy bearing spectrum. It is therefore clear from these results that envelope analysis greatly amplifies bearing fault frequencies, rendering them easier to detect and, more significantly, reduces the nontrivial risk of obtaining false positive test results if the only raw frequency spectrum is used instead.

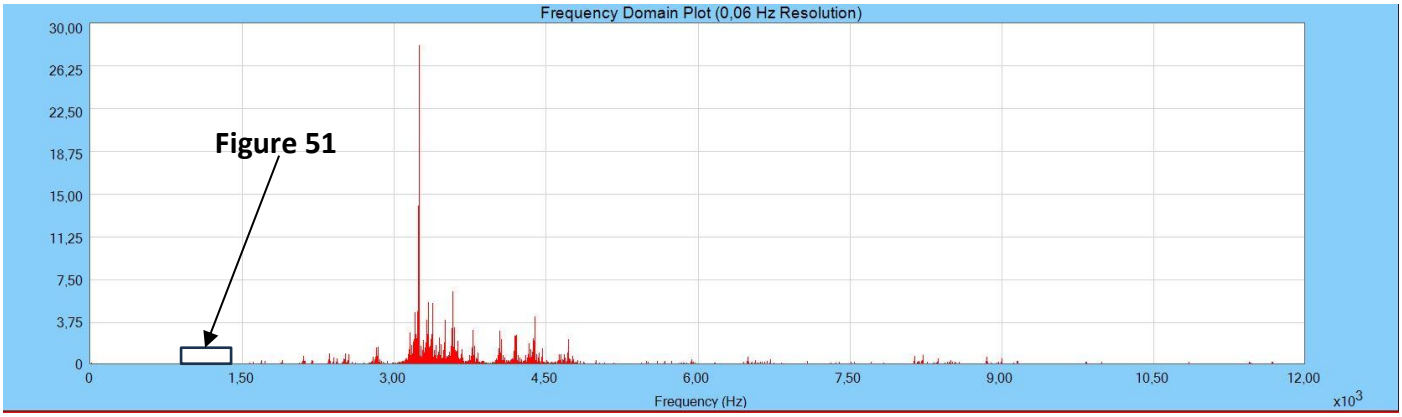

Figure 50: Raw frequency spectrum obtained with SpinScope during Trial 5 (5000 RPM) of the DMU Tests

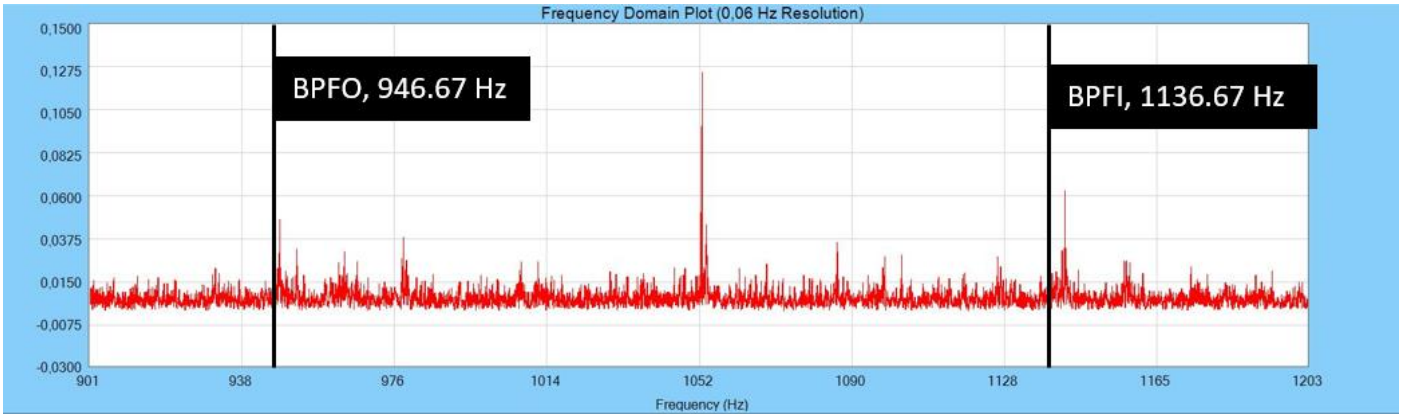

Figure 51: Detailed view of Figure 50

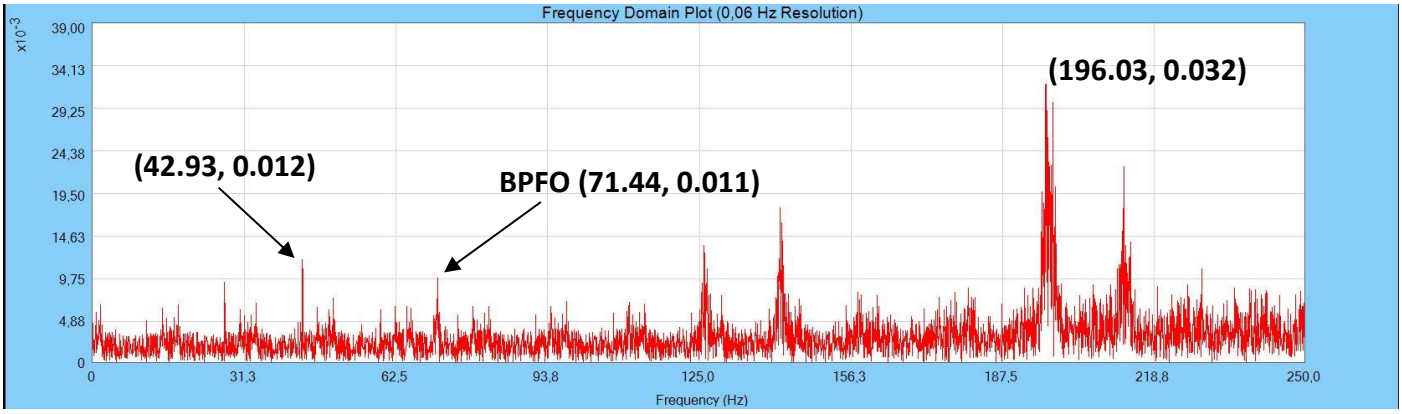

Figure 52: Raw SpinScope frequency spectrum from trial 3 of the damaged bearing in section 9.4.

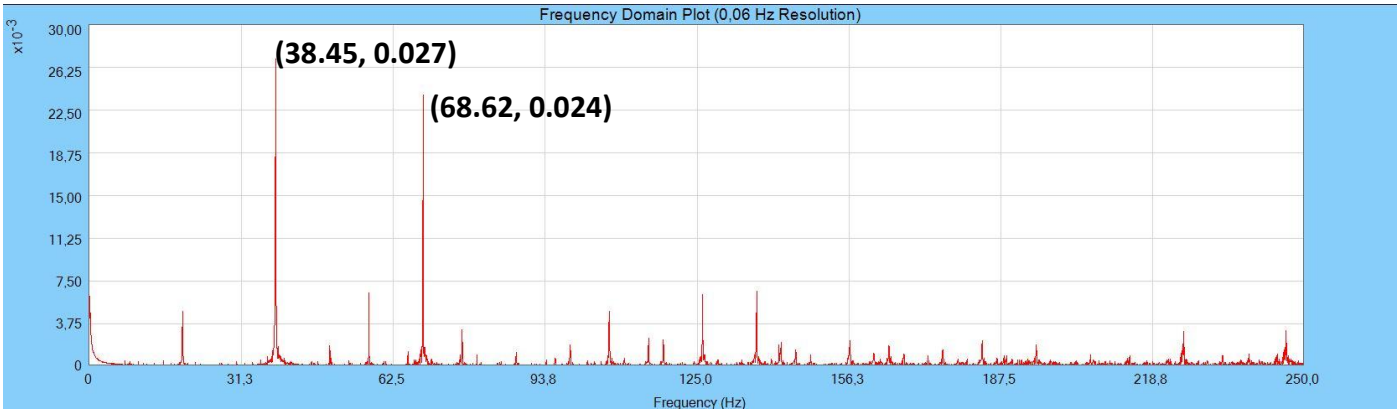

Figure 53. Raw SpinScope frequency spectrum from trial 3 of the healthy bearing in section 9.4.

11. Conclusion

After performing a literature review and an analysis of the existing technologies at DAMRC, analysis methods generating the envelope spectrum of an acceleration signal were implemented to augment the capabilities of SpinScope and SmartMeter. These new methods were tested and validated against known healthy and damaged bearings using a purpose-built test bench (as well as numerical simulations) before being applied in a case study involving the DMU 80 T CNC machining center. The results of all these tests show that localized inner or outer race faults in bearings can be diagnosed by detecting the theoretical fault frequency in the resulting envelope spectrum. This was achieved by analysing the acceleration signals measured with SpinScope, and it is expected, but has not yet been verified, that the same could be achieved by analysing measurements exported from SmartMeter.

Envelope analysis yielded the expected fault frequencies consistently across all trials for a given set of testing conditions with the exception of the case study using the DMU machining center, in which potential complex or distributed bearing wear, and the influence other machine components and speed-dependent bearing stiffness affected the analysis. Even then, the consistency between trials only broke down for tests of the DMU at higher spindle speeds (10,000 RPM). The project can therefore be considered a success as SpinScope augmented with envelope analysis were able to diagnose bearing health correctly, and the

results obtained with both SpinScope and SmartMeter met the consistency criteria stated in the project application.

However, this success was primarily achieved during the controlled tests using the test rig. The envelope spectra obtained from the DMU, while consistent, were affected by speed-dependent dynamics of the bearing, the frequencies arising from other machine components, and complex bearing wear, yielding fault frequencies associated with both the inner and outer race. It is therefore highly recommended that additional insights and experience testing and diagnosing spindle bearings in real CNC machines be acquired.

This experience can be obtained both by implementing the technology in industry and by continuing internal testing, for example in an R&D project. An R&D project would have the benefit of having negligible costs and substantial potential upside. There be no costs associated with consuming workpiece material or tools in the spindle tests, and the supplemental analysis methods and test bench have already been implemented. Meanwhile, further competency in the field of bearing/spindle health, insights into optimal test procedures/test conditions, potential advancement of the state of the art, and experience with internal and third-party technologies may be realized to the mutual benefit of DAMRC and Danish industry. Therefore, continuing the project, either as a R&D project or in another format, is highly recommended.

12. Dissemination

Insights from the project have not yet been disseminated – however planned at the first coming technical seminar.

13. Appendix

13.1 Experimental Data for Preliminary Test (Section 9.3)

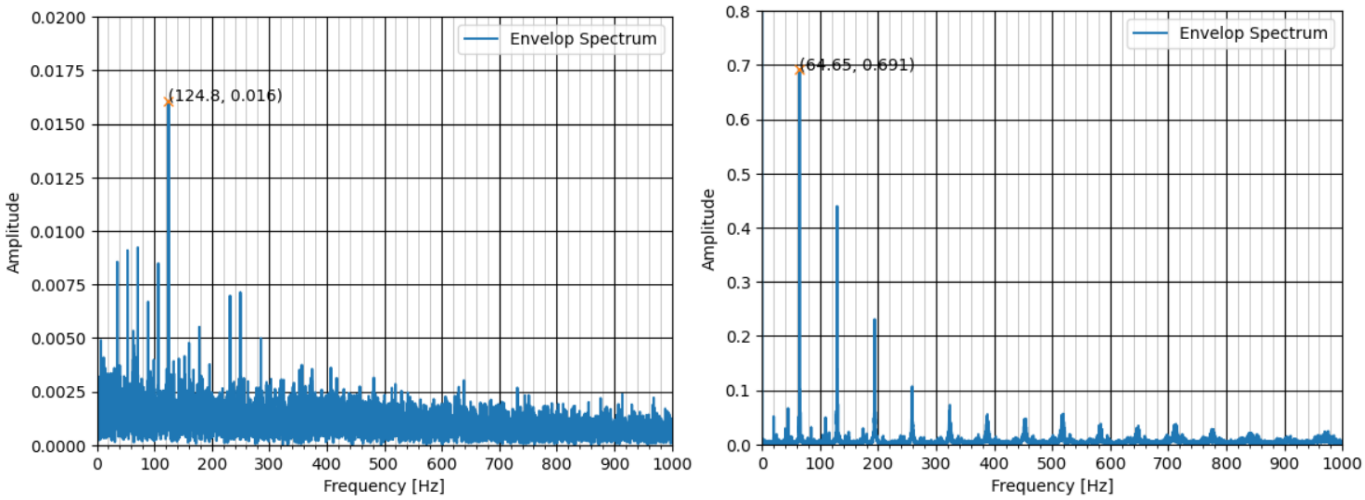

Figure B-1: Results from trial 1. Left: healthy bearing; Right: faulty bearing

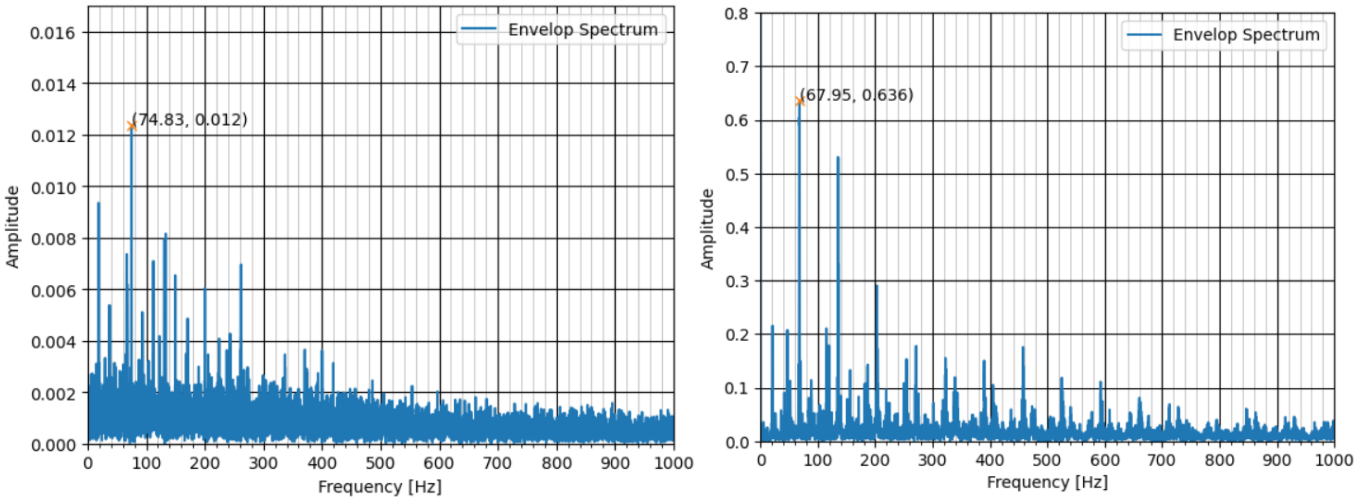

Figure B-2: Results from trial 2. Left: healthy bearing; Right: faulty bearing

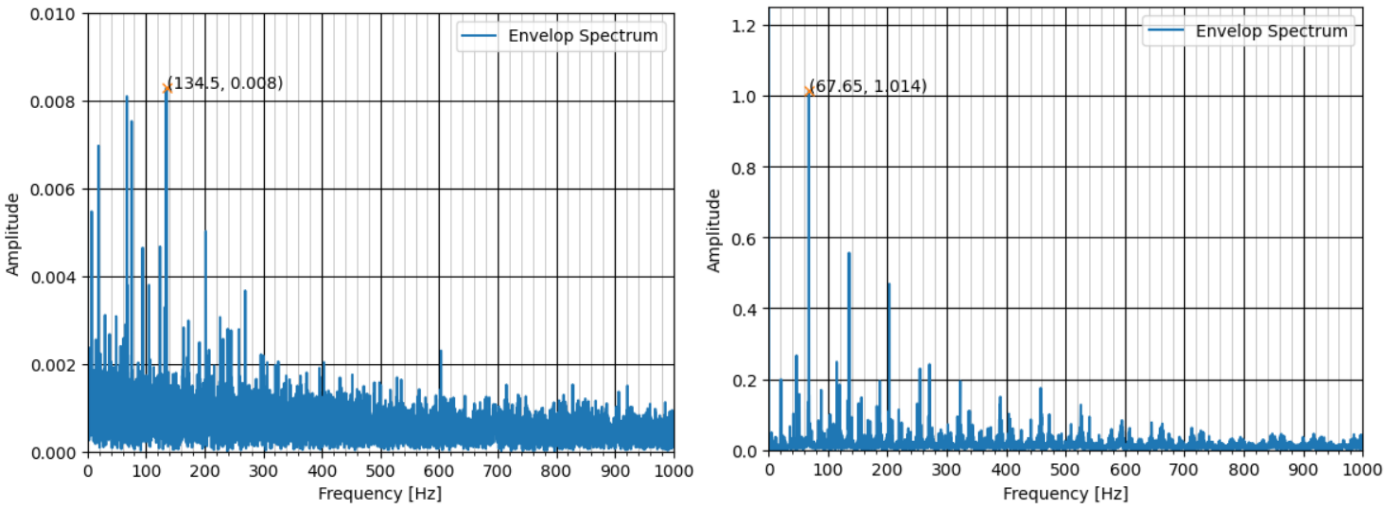

Figure B-3: Results from trial 3. Left: healthy bearing; Right: faulty bearing

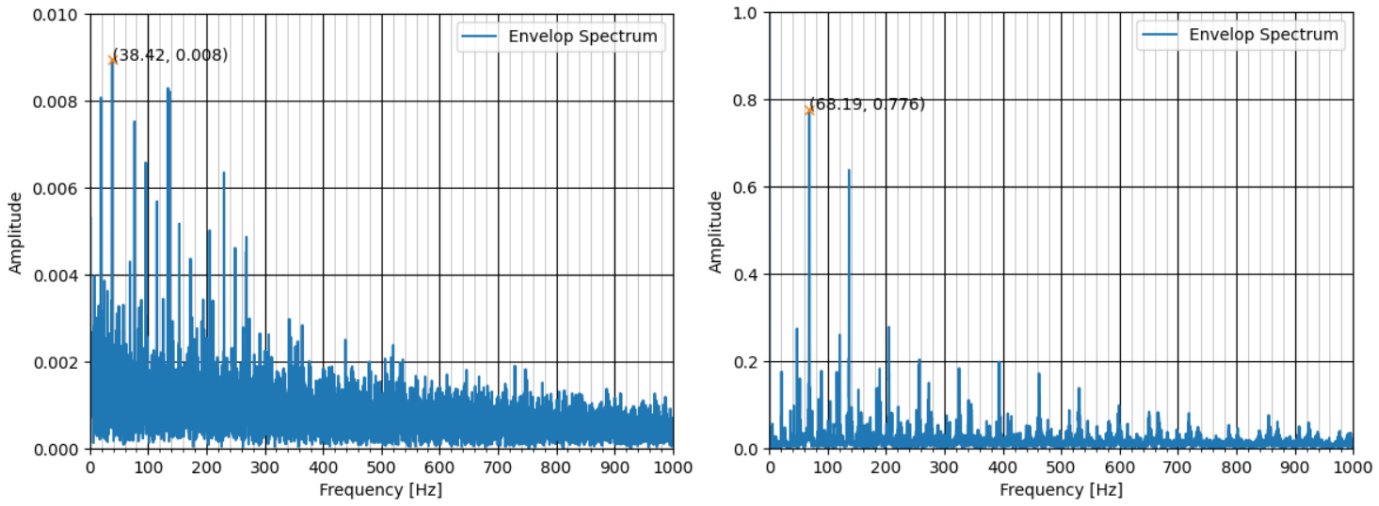

Figure B-4: Results from trial 4. Left: healthy bearing; Right: faulty bearing

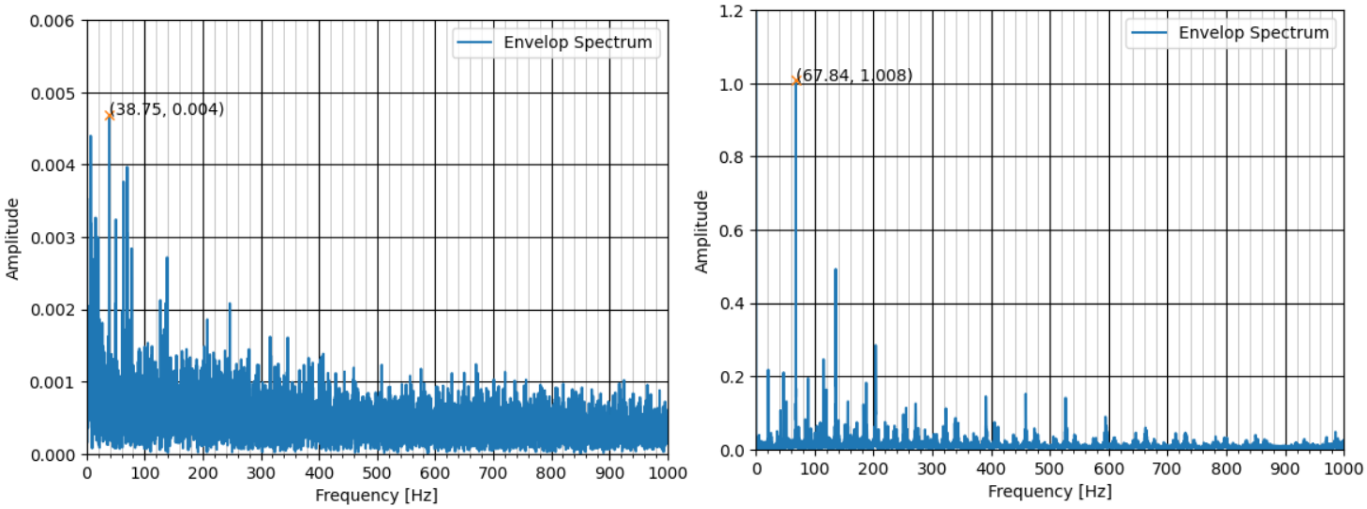

Figure B-5: Results from trial 5. Left: healthy bearing; Right: faulty bearing

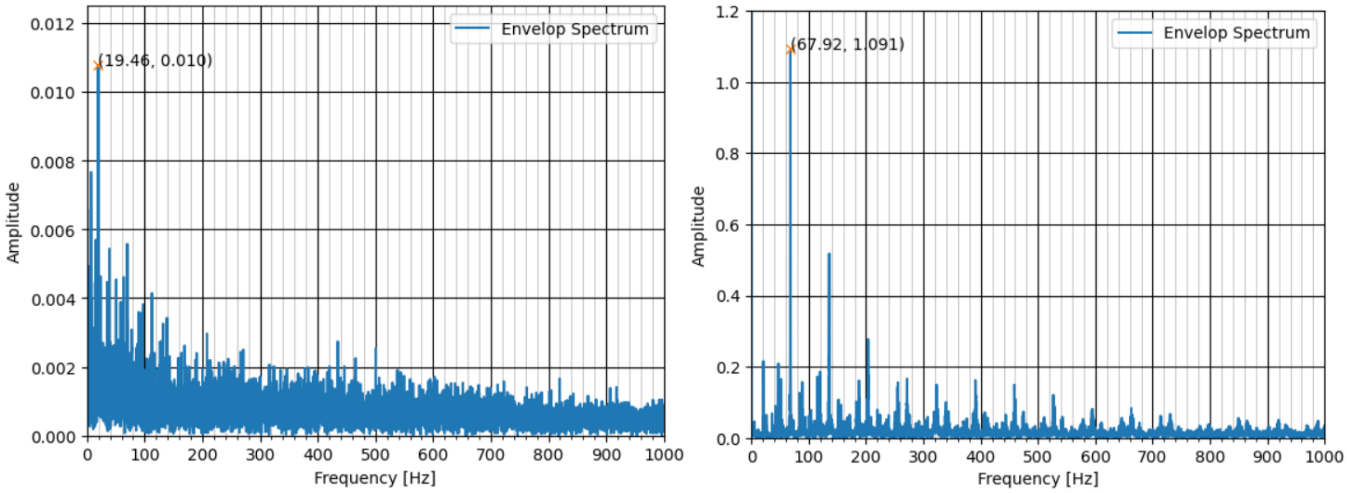

Figure B-6: Results from trial 6. Left: healthy bearing; Right: faulty bearing

13.2 Experimental Data for Comparative Test of SpinScope/SmartMeter (Section 9.4)

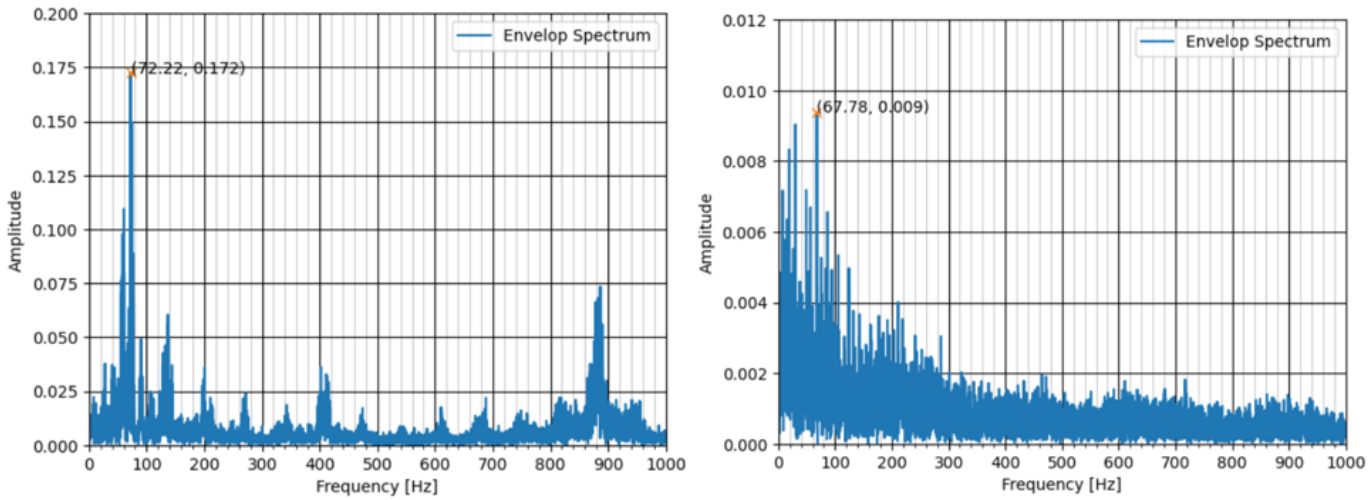

Figure B-7: Results from SpinScope trial 1. Left: faulty bearing; Right: healthy bearing (Trial 1 and 4)

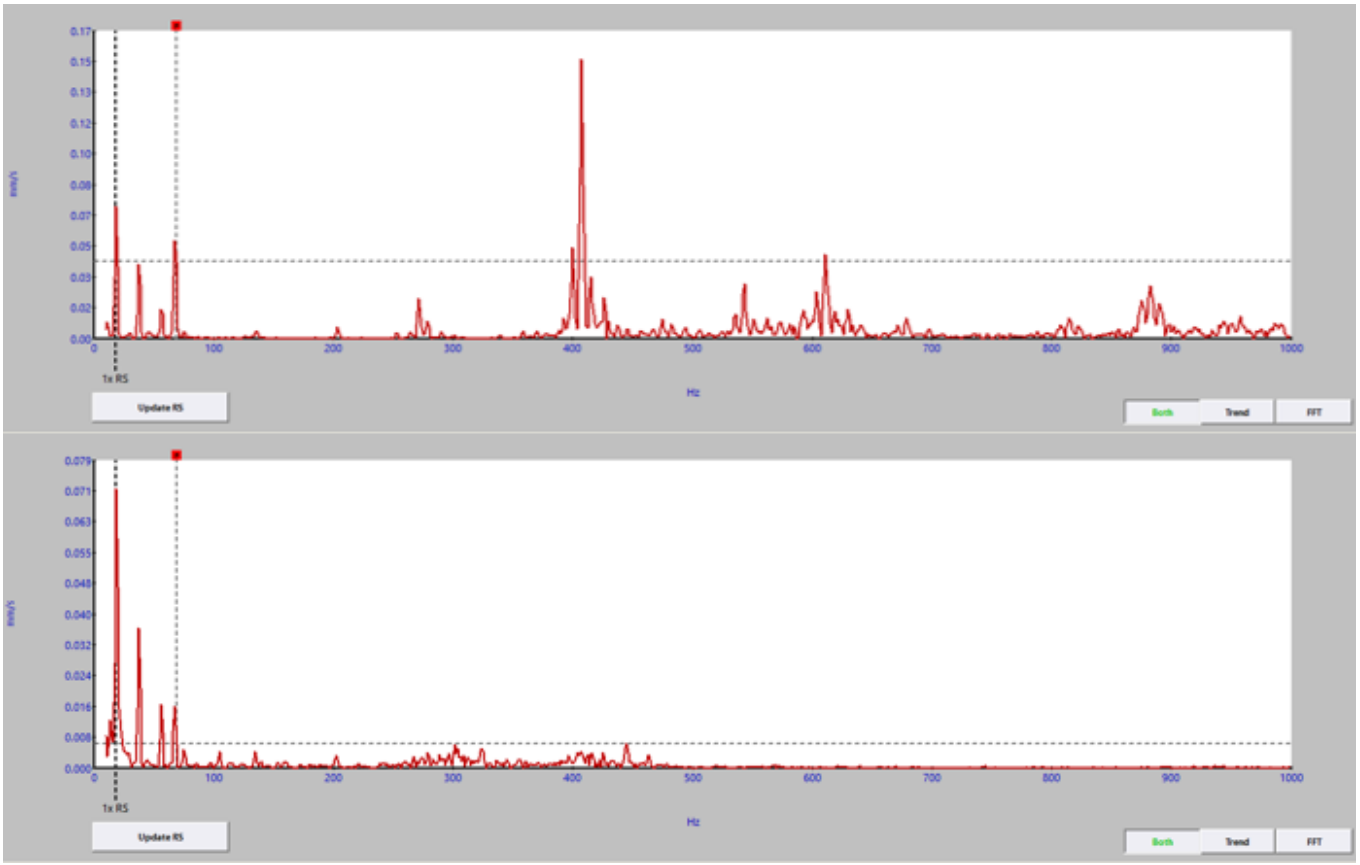

Figure B-8: SmartMeter Trial 1. Top: damaged bearing; Bottom: healthy bearing (Trial 1 and 4)

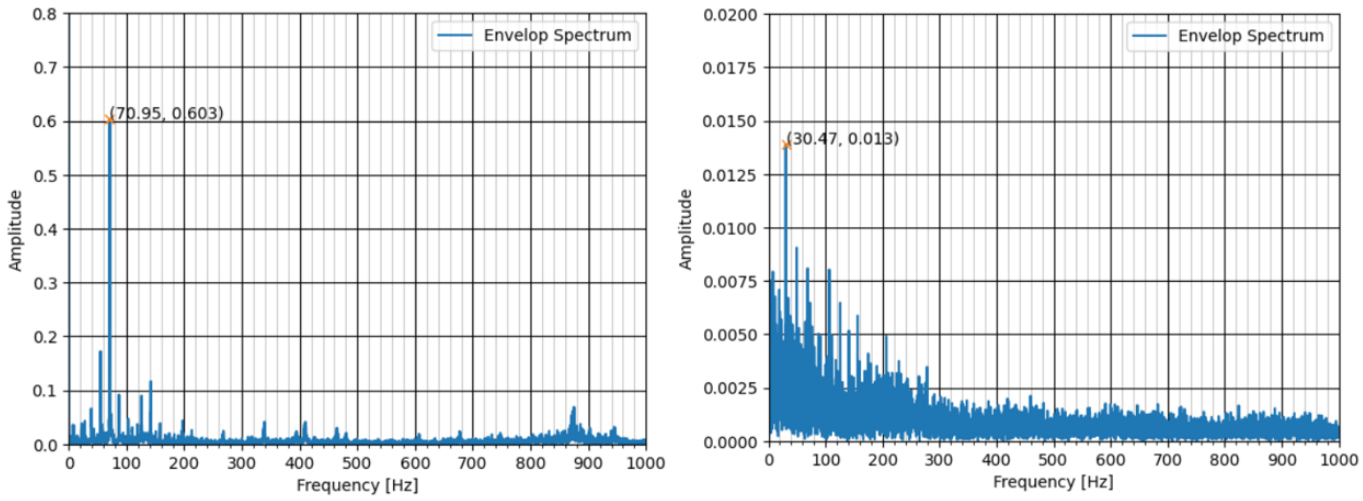

Figure B-9: Results from SpinScope trial 2. Left: faulty bearing; Right: healthy bearing (Trial 2 and 5)

Figure B 10: Results from SmartMeter trial 2. Top: faulty bearing; Bottom: healthy bearing (Trial 2 and 5)

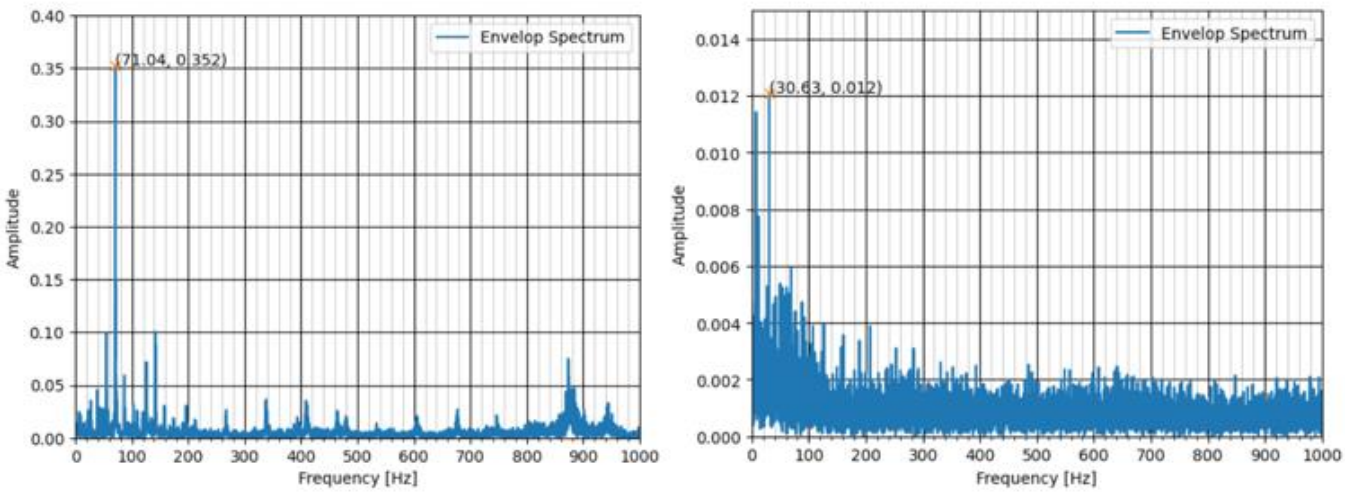

Figure B-11: Results from SpinScope trial 3. Left: faulty bearing; Right: healthy bearing (Trial 3 and 6)

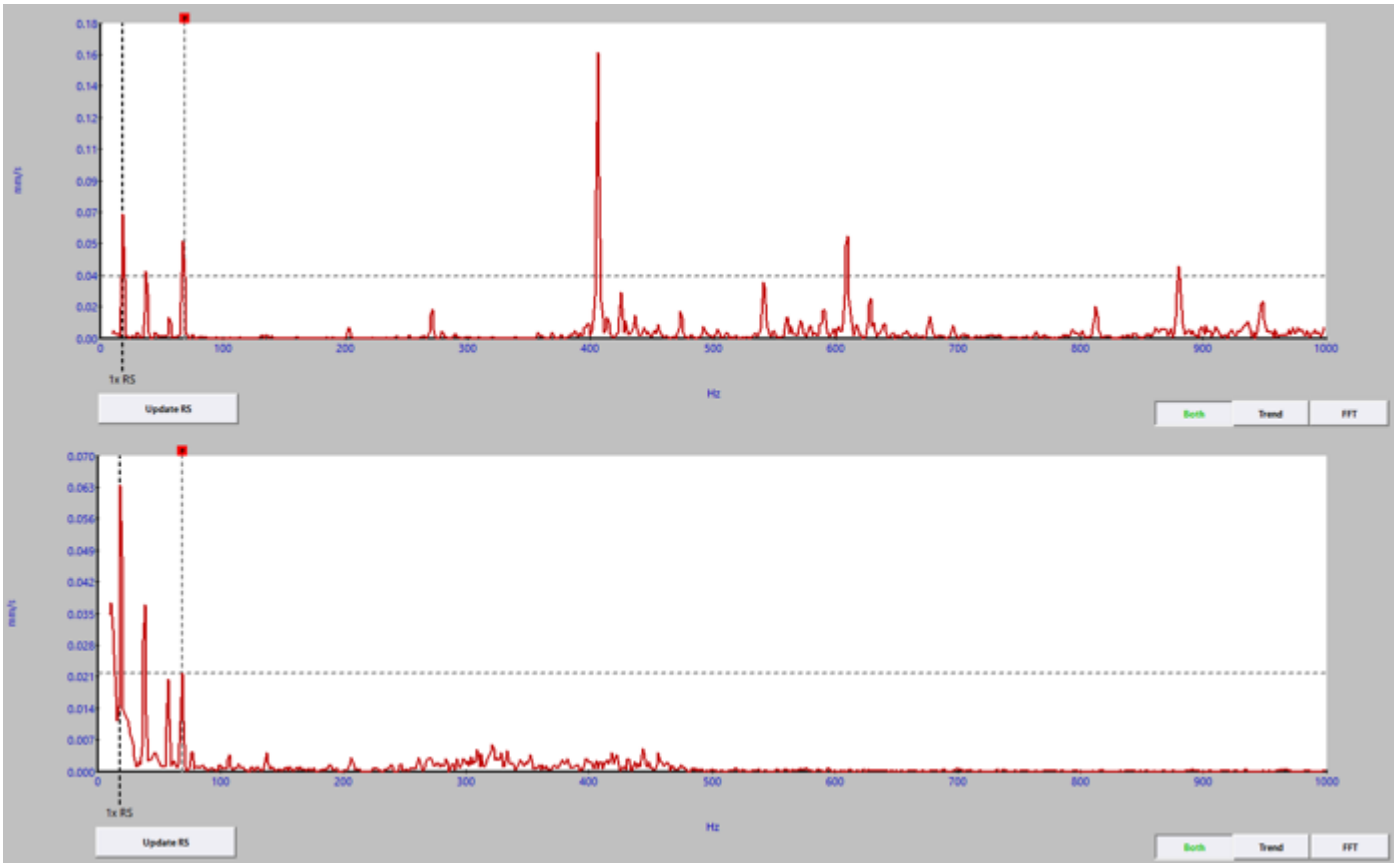

Figure B-12: Results from SmartMeter trial 3. Top: faulty bearing; Bottom: healthy bearing (Trial 3 and 6)

13.3 Appendix B3: Experimental Data for Bearing Diagnosis Test on DMU (Section 9.5)

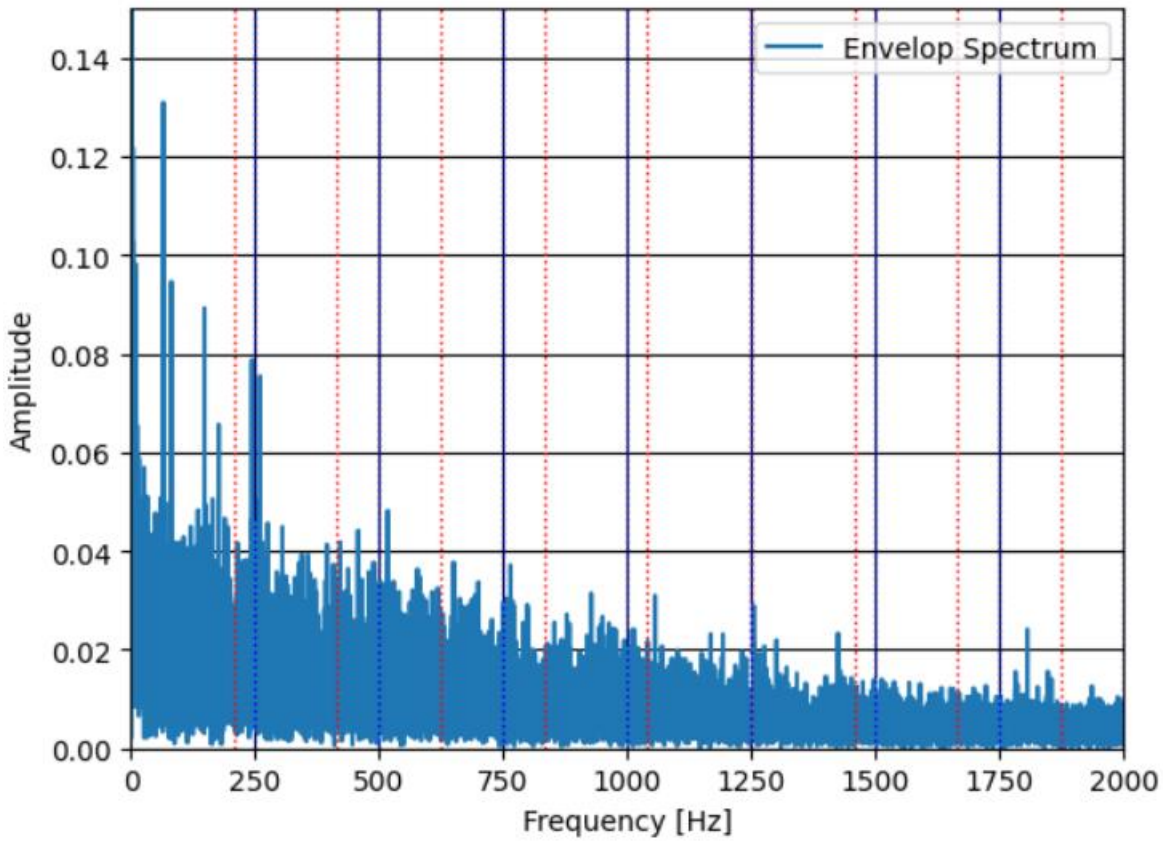

Figure B-13: Results from SpinScope for trial 1 of DMU tests.

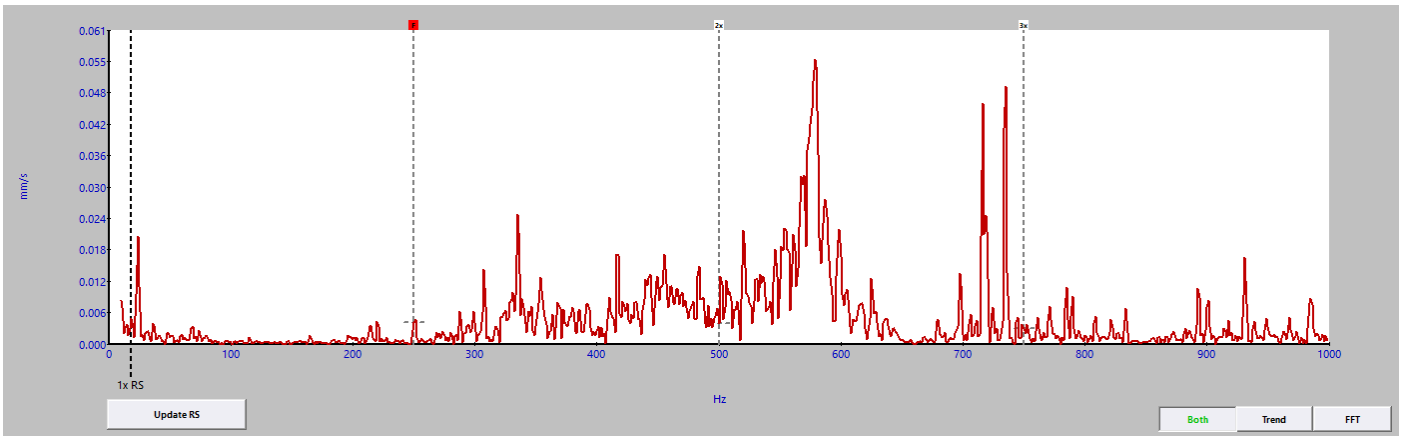

Figure B-14: Results from SmartMeter for trial 1 of DMU tests

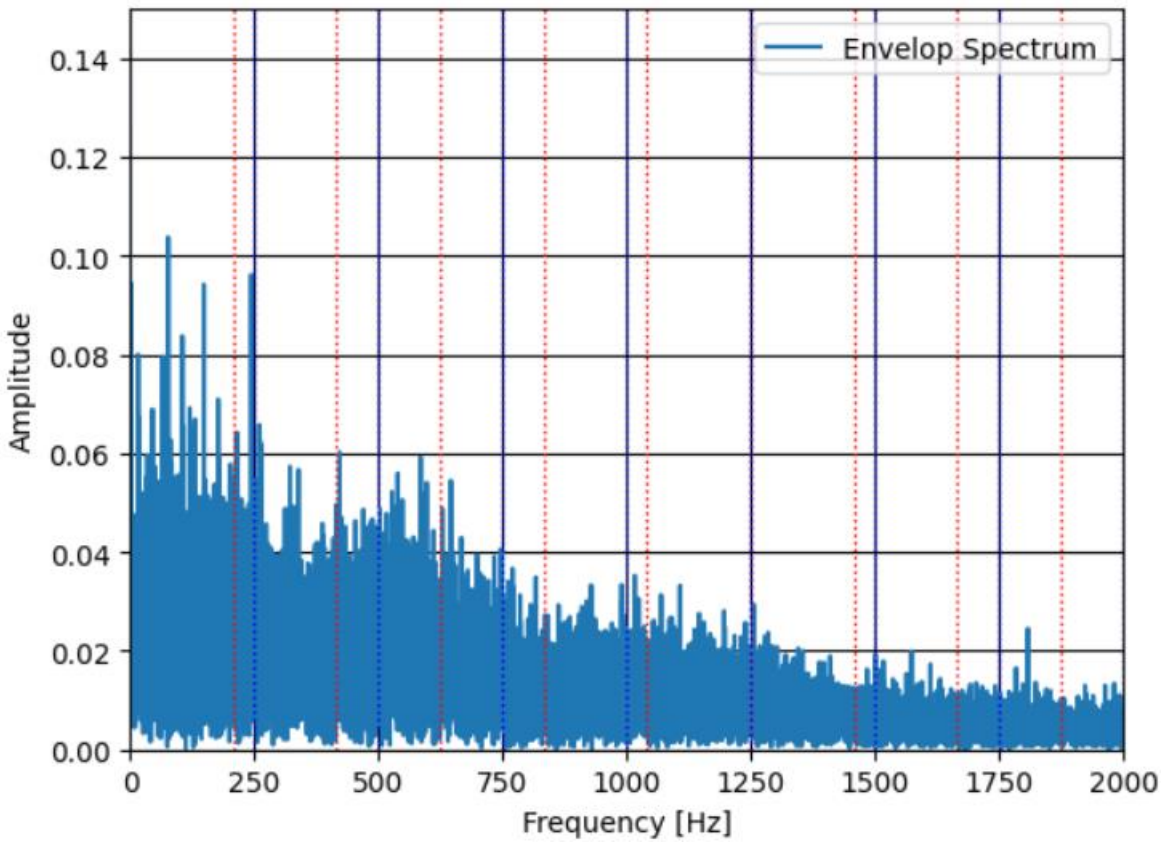

Figure B-15: Results from SpinScope for trial 2 of DMU tests.

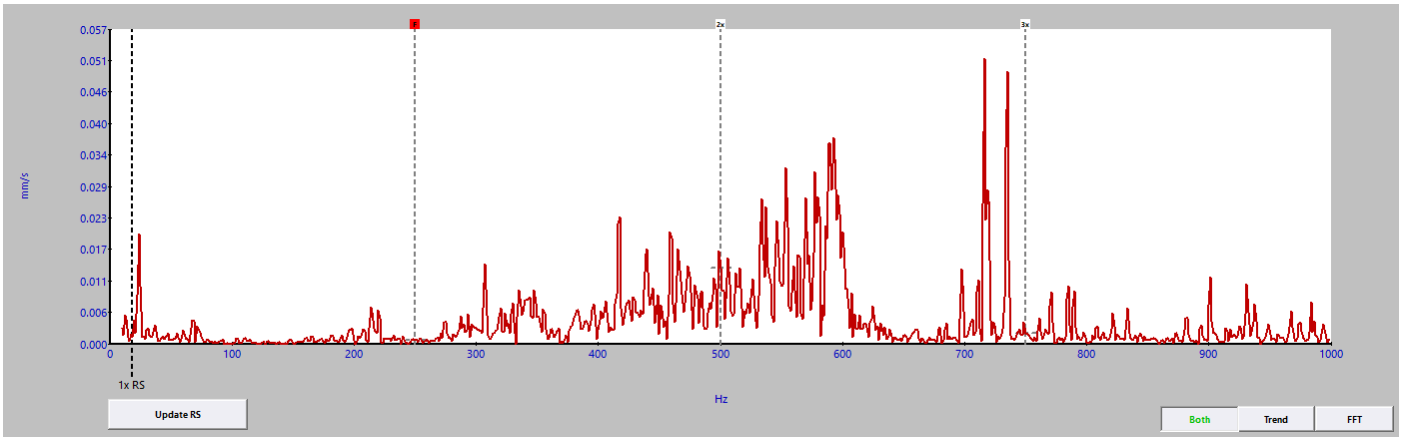

Figure B-16: Results from SmartMeter for trial 2 of DMU tests

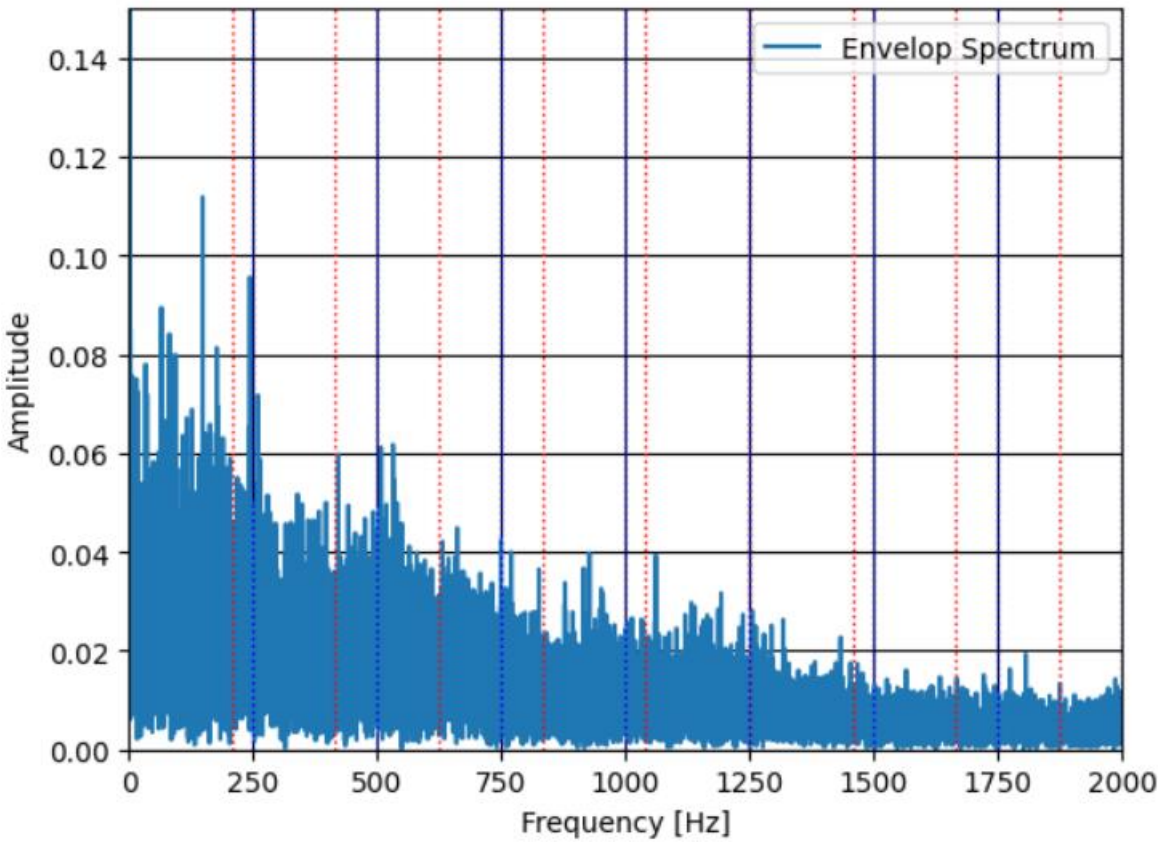

Figure B-17: Results from SpinScope for trial 3 of DMU tests.

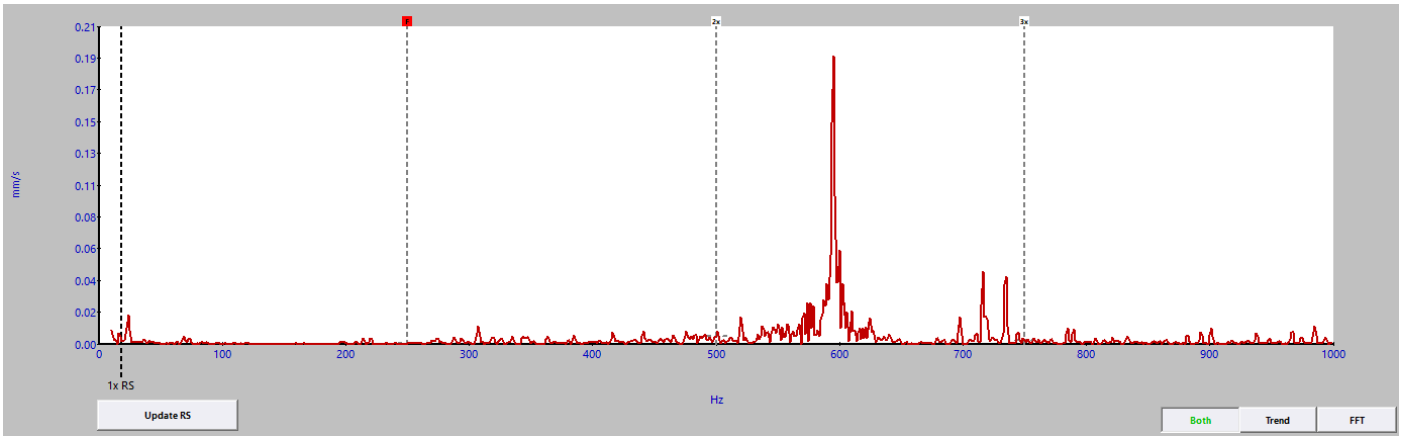

Figure B-18: Results from SmartMeter for trial 3 of DMU tests

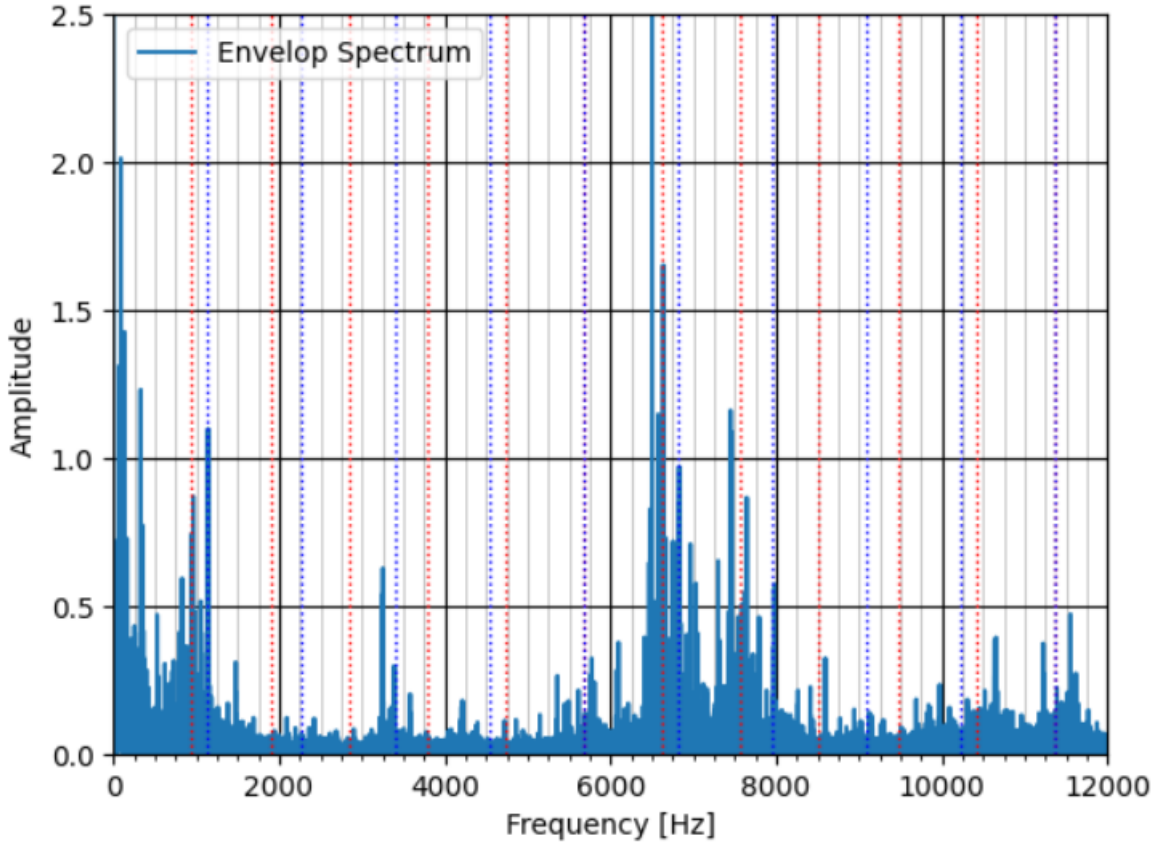

Figure B-19: Results from SpinScope for trial 4 of DMU tests.

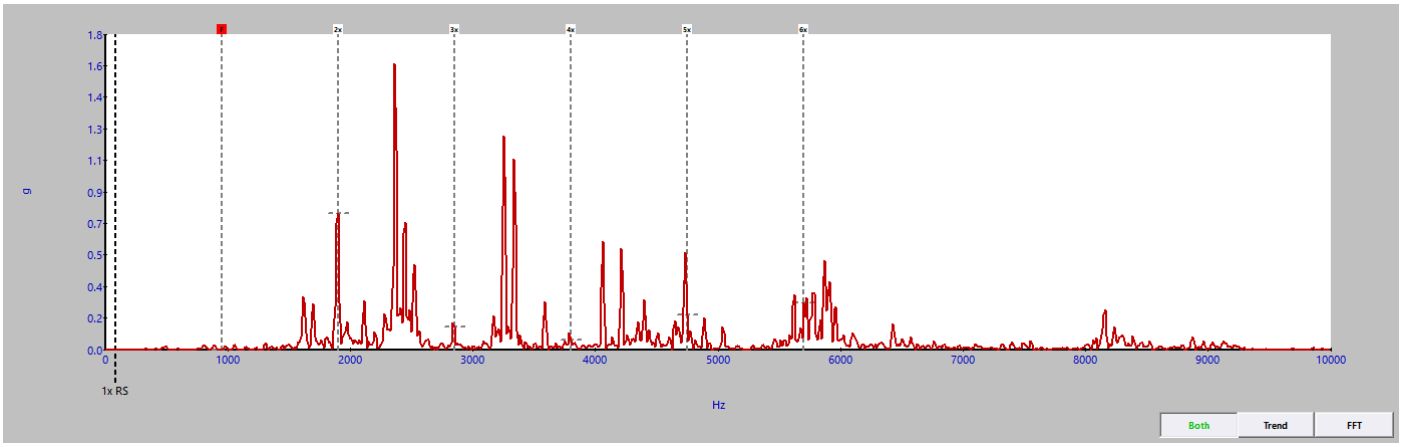

Figure B-20: Results from SmartMeter for trial 4 of DMU tests

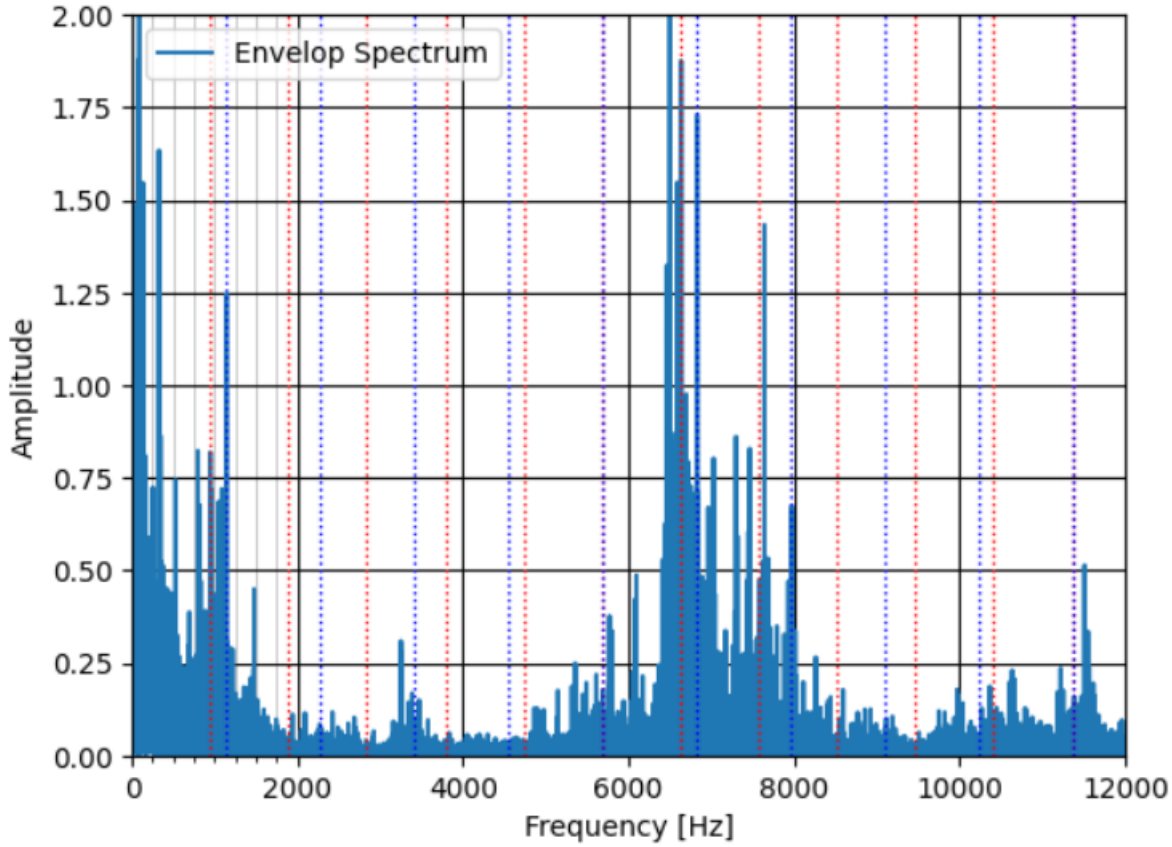

Figure B-21: Results from SpinScope for trial 5 of DMU tests.

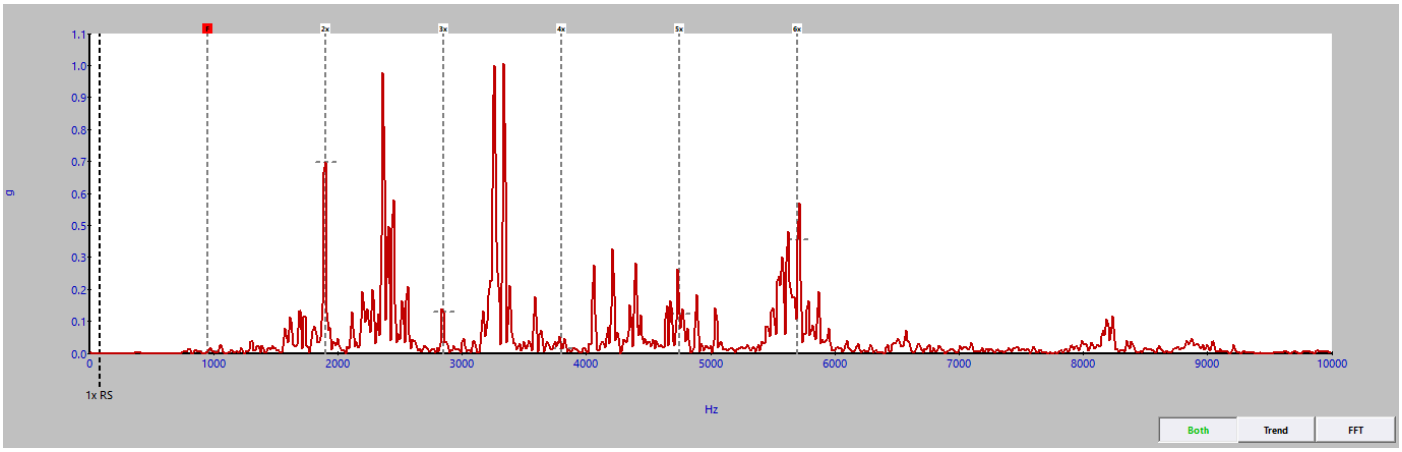

Figure B-22: Results from SmartMeter for trial 5 of DMU tests

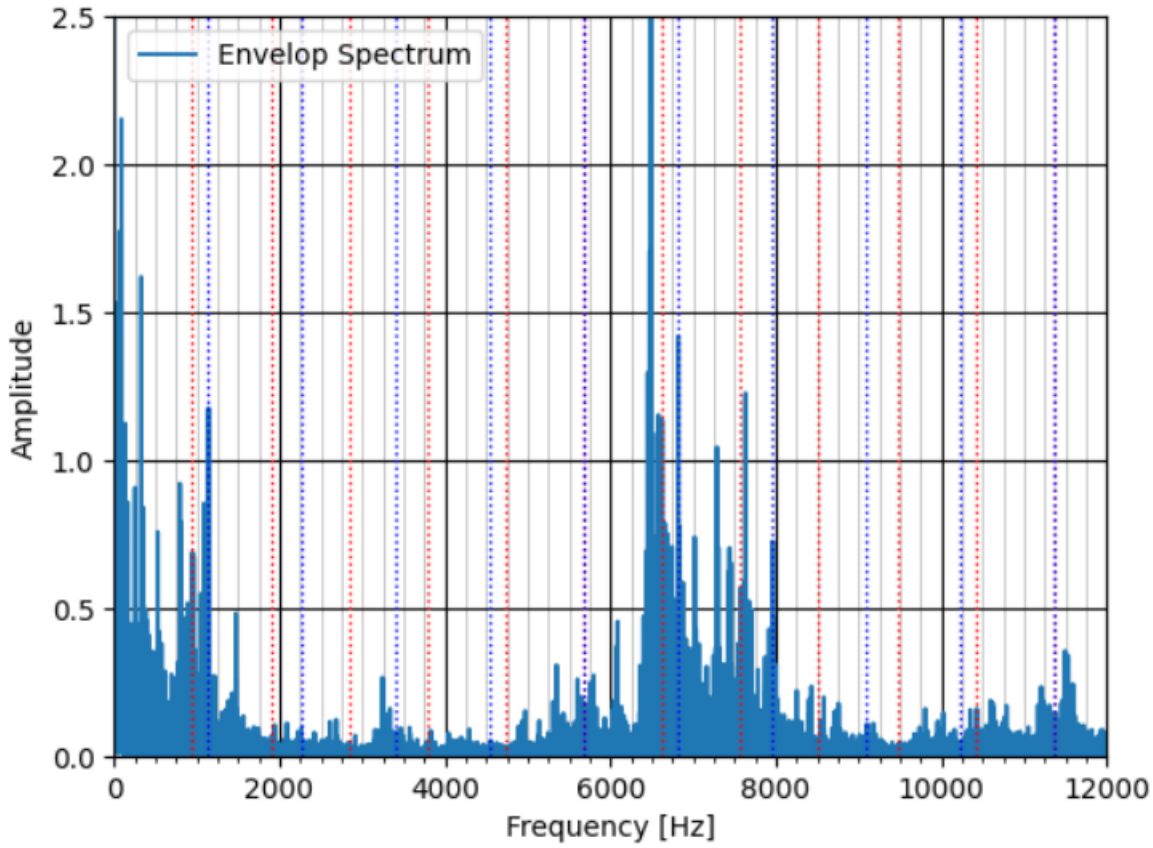

Figure B-23: Results from SpinScope for trial 6 of DMU tests.

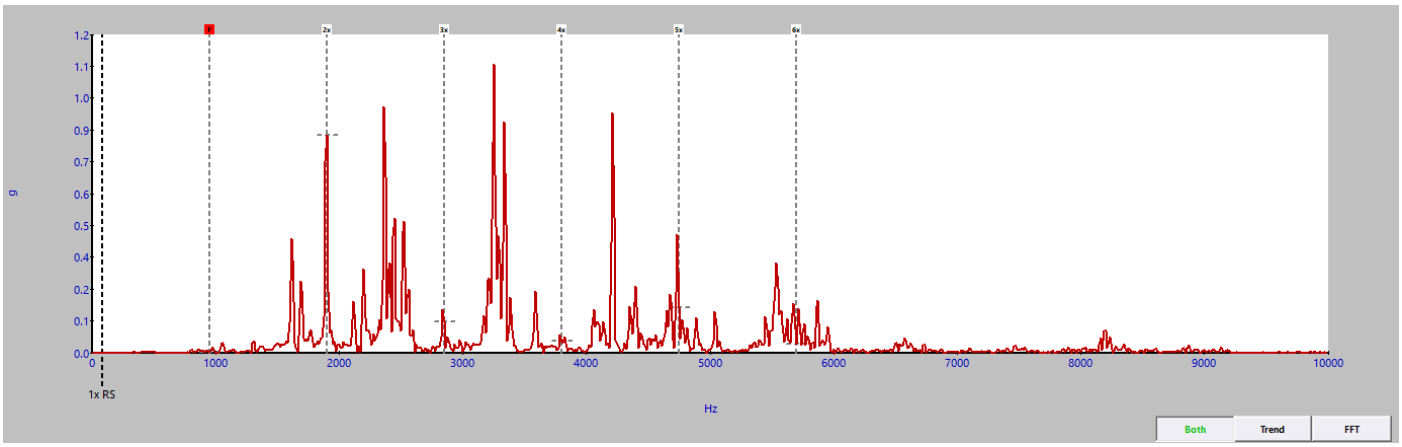

Figure B-24: Results from SmartMeter for trial 6 of DMU tests

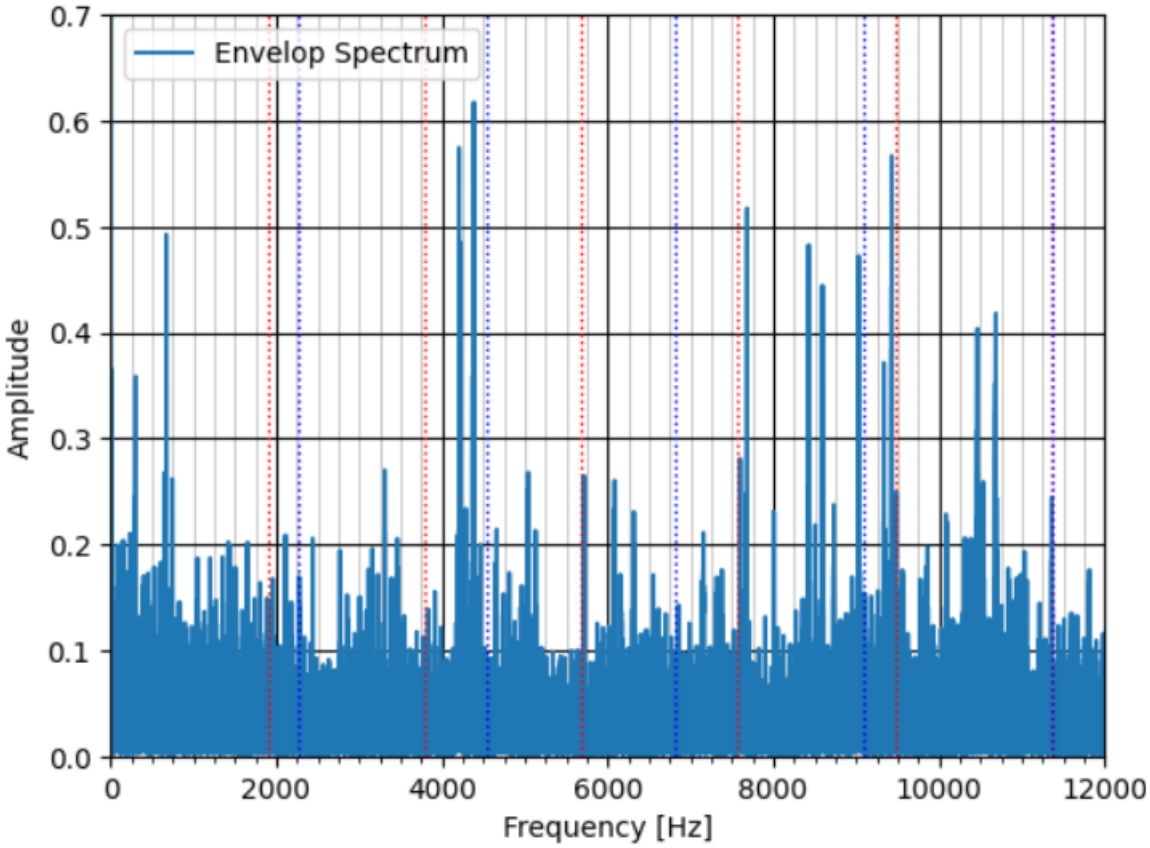

Figure B-25: Results from SpinScope for trial 7 of DMU tests.

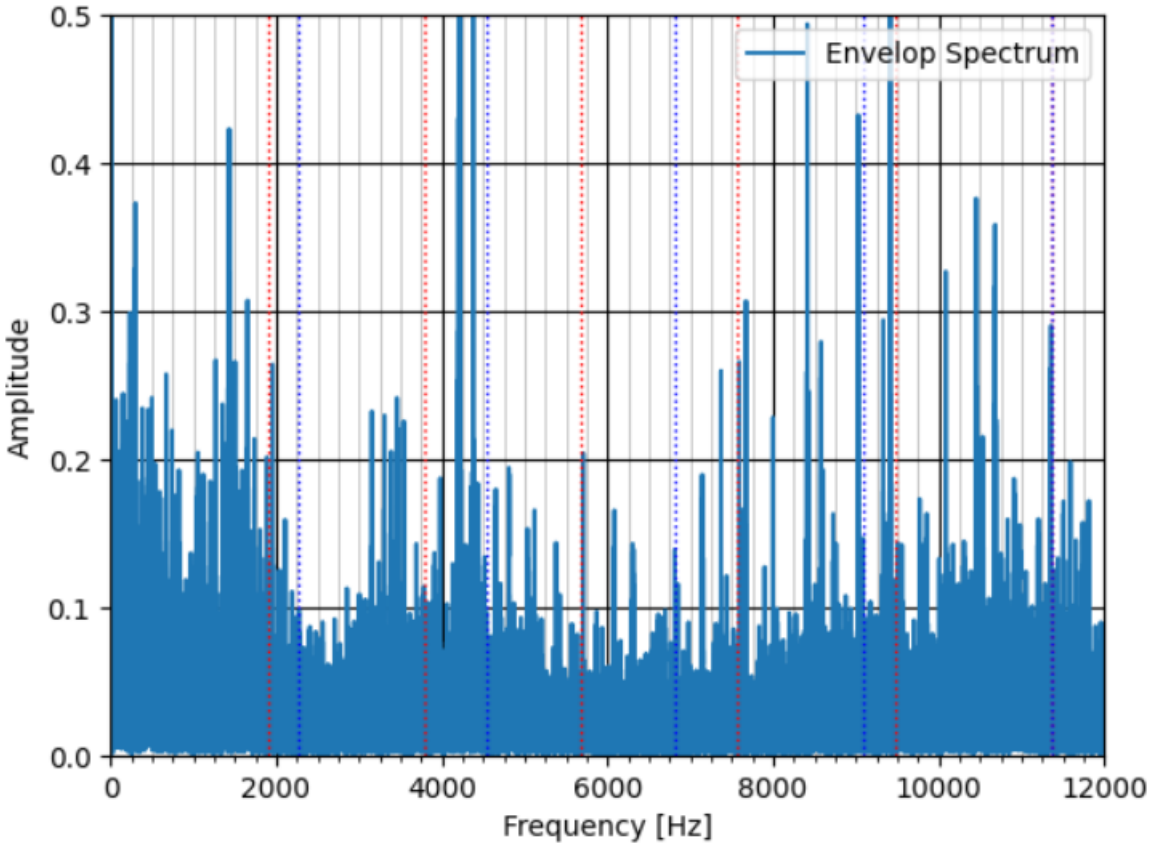

Figure B-26: Results from SpinScope for trial 8 of DMU tests.

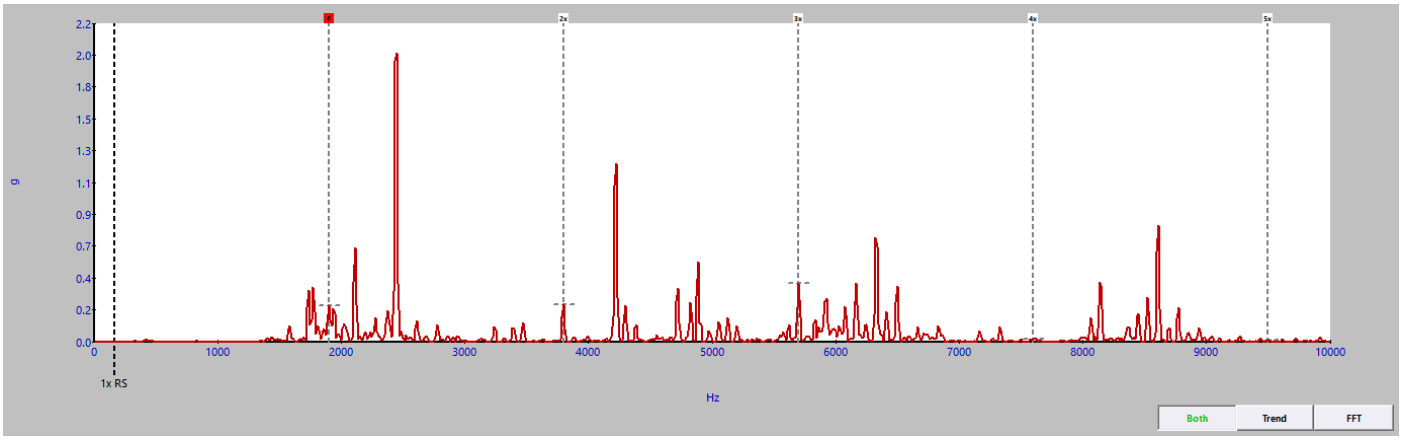

Figure B-27: Results from SmartMeter for trial 8 of DMU tests

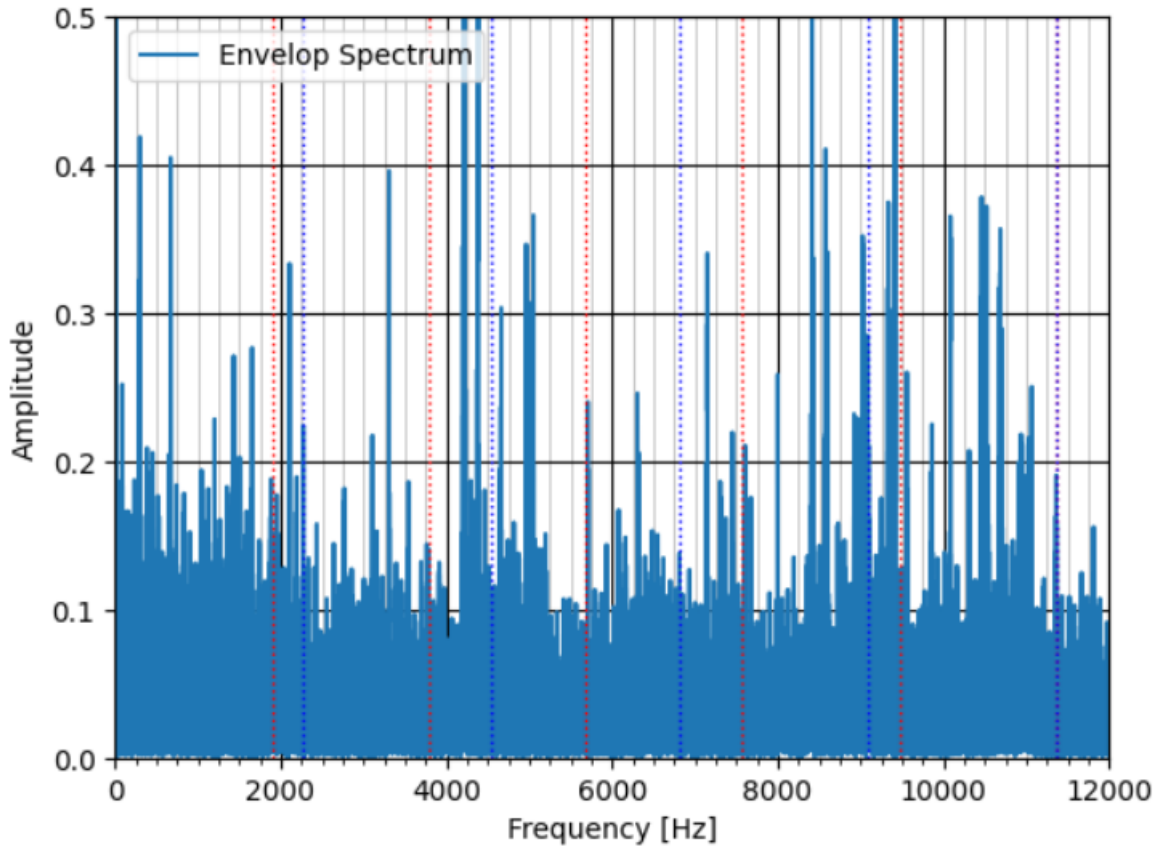

Figure B-28: Results from SpinScope for trial 9 of DMU tests.

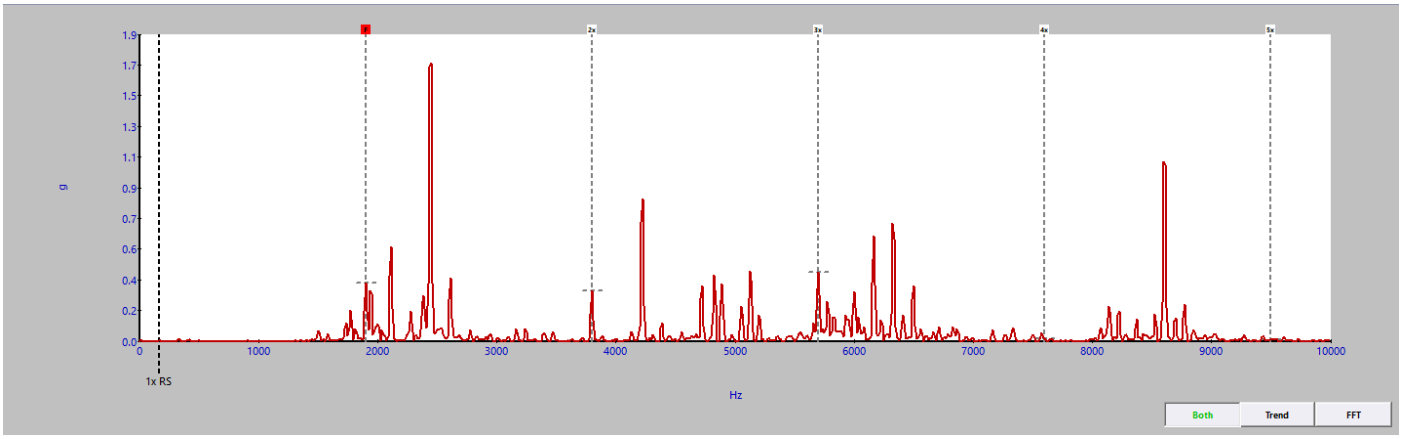

Figure B-29: Results from SmartMeter for trial 9 of DMU tests

14. References

[1] Y. A. C. B. E. Abele, “Machine Tool Spindle Units,” *CIRP Annals - Manufacturing Technology,* 2010.

[2] Ox tool, “25K RPM Bridgeport Mill,” 11 October 2012. [Online]. Available: https://oxtool.blogspot.com/2012/10/25k-rpm-bridgeport-mill.html. [Accessed 20 Febuary 2024].

[3] Norton, Machine Design.

[4] S. K. P.P Kharche, “Review of Fault Detection in Rolling Element Bearing,” *International Journal of Innovative Research in Advanced Engineering,* 2014.

[5] J.-O. A. B. G. P. N. M. Rantatalo, “Milling machine spindle analysis usingFEM and con-contact spindle excitation and response measurement,” *International Journal of Machine Tools and Manufacture,* vol. 47, 2007.

[6] J. G. Q. H. F. L. Y. L. J. Z. S. Lu, “A novel contactless angular resampling method for motor bearing fault diagnosis under variable speed,” *IEEE transactions on instrumentation and measurement,* 2016.

[7] J. Z. K. Y. J. H. M. Y. W. B. Fang, “A comprehensive study on the speed-varying stiffness of ball bearing under different load conditions,” *Mecanism and Machine Theory,* 2019.

[8] J. A. R.B. Randall, “Rolling Element Bearing Diagnostics - A Tutorial,” *Mechanical Systems and Signal Processing,* 2011.

[9] D. T. GK Chaturvedi, “Bearing Fault detection using adaptive noise cancelling,” *ASME Paper 81-DET-7,* 1981.

[10] N. Tandon, “A comparison of some vibration parameters for the condition monitoring of rolling element bearings,” *Measurement ,* 1994.

[11] B. D. S. Braun, “Analysis of ball/roller bearing vibrations,” *ASME Paper 77-WA/DE-5,* 1986.

[12] N. K. T. Y. Y. U. K. Mori, “Prediction of spalling on a ball bearing by applying the discrete wavelet transform to vibration signals.,” *Wear,* 1996.

[13] M. J. B. H. CJ Li, “Bearing condition monitoring by pattern recognition based bicoherence analysis of vibrations,” in *Proceedings of the institution of mechanical engineers, Part C: Journal of mechanical*

engineering science, 1996.

[14] F. A. B. W. LD Meyer, "An analytic model for ball bearing vibrations to predict vibration response to distributed defects," *ASME Journal of Mechanical Design,* 1980.

[15] Y. S. Y.T. Su, "On the detectability of roller bearing damage by frequency analysis," in *Proceedings of the institution of mechanical engineers, part C: journal of mechanical engineering science*, 1996.

[16] A. F. A. Moshrefzadeh, "The Autogram: an effective approach for selecting the optimal demodulation band in rolling element bearings diagnosis," *Mechanical Systems and Signal Processing,* 2018.

[17] D. M. A Morhain, "Bearing defect diagnosis and acoustic emission," *Proceedings of the Institution of Mechanical Engineers, Part J: Journal of Engineering Tribology,* 2003.

[18] Y. K. S. L. T. K. S. D. J Shiroishi, "Bearing Condition Diagnostics via vibration and acoustic emission measurements," *Mechanical systems and signal processing ,* 1997.

[19] J. M. L. C. A.-R. A. V.-I. G. D. A. A Sio-Sever, "Improved estimatio of end-milling parameters from acoustic emission signals using a microphone array assisted by AI modelling," *Sensors,* 2022.

[20] J. Antoni, "Fast computation of the kurtogram for the detection of transient faults," *Mechanical Systems and Signal Processing ,* no. 21, pp. 108-124, 2007.

[21] J. Antoni, "Fast Kurtogram (version 1.0.0)," [Online]. Available: https://se.mathworks.com/matlabcentral/fileexchange/48912-fast-kurtogram. [Accessed 14 August 2023].

[22] J. Antoni, "The spectral kurtosis: a useful tool for characterizing non-stationary signals," *Mechanical Systems and Signal Processing ,* no. 20, pp. 282-307, 2006.

[23] R. R. Jerome Antoni, "The spectral kurtosis: application to the vibratory surveillance and diagnostics of rotating machines," *Mechanical Systems and Signal Processing,* no. 20, pp. 308-331, 2006.

[24] Technology, Society for Machinery Failure Prevention, "Fault Data Sets," [Online]. Available: https://www.mfpt.org/fault-data-sets/. [Accessed 14 August 2023].

[25] MathWorks, “Rolling Element Bearing Fault Diagnosis,” [Online]. Available: https://se.mathworks.com/help/predmaint/ug/Rolling-Element-Bearing-Fault-Diagnosis.html. [Accessed 14 August 2023].

[26] Schaeffler, “HCB71916-E-T-P4S-UL Spindle Bearing,” [Online]. Available: https://medias.schaeffler.dk/en/product/rotary/rolling-and-plain-bearings/super-precision-bearings/radial-super-precision-bearings/spindle-bearings/hcb71916-e-t-p4s-ul/p/363456#Product%20Information. [Accessed 13 March 2024].